National Library of Canada
Bibliothèque nationale du Canada

Canadian Theses Service
Service des thèses canadiennes

Ottawa, Canada
K1A 0N4

NOTICE

The quality of this microform is heavily dependent upon the quality of the original thesis submitted for microfilming. Every effort has been made to ensure the highest quality of reproduction possible.

If pages are missing, contact the university which granted the degree.

Some pages may have indistinct print especially if the original pages were typed with a poor typewriter ribbon or if the university sent us an inferior photocopy.

Previously copyrighted materials (journal articles, published tests, etc.) are not filmed.

Reproduction in full or in part of this microform is governed by the Canadian Copyright Act, R.S.C. 1970, c. C-30.

AVIS

La qualité de cette microforme dépend grandement de la qualité de la thèse soumise au microfilmage. Nous avons tout fait pour assurer une qualité supérieure de reproduction.

S'il manque des pages, veuillez communiquer avec l'université qui a conféré le grade.

La qualité d'impression de certaines pages peut laisser à désirer, surtout si les pages originales ont été dactylographiées à l'aide d'un ruban usé ou si l'université nous a fait parvenir une photocopie de qualité inférieure.

Les documents qui font déjà l'objet d'un droit d'auteur (articles de revue, tests publiés, etc.) ne sont pas microfilmés.

La reproduction, même partielle, de cette microforme est soumise à la Loi canadienne sur le droit d'auteur, SRC 1970, c. C-30.

NL-339 (r. 88/04)

Canada

THE UNIVERSITY OF ALBERTA

A Determination of the Load Position Causing Maximum Fillet Stress in Helical Gear Teeth Using Three-Dimensional Finite Elements

by

Matthew Eisentraut

A THESIS

SUBMITTED TO THE FACULTY OF GRADUATE STUDIES AND RESEARCH IN PARTIAL FULFILMENT OF THE REQUIREMENTS FOR THE DEGREE OF Master of Science

Mechanical Engineering

EDMONTON, ALBERTA

Fall 1988

Permission has been granted to the National Library of Canada to microfilm this thesis and to lend or sell copies of the film.

The author (copyright owner) has reserved other publication rights, and neither the thesis nor extensive extracts from it may be printed or otherwise reproduced without his/her written permission.

L'autorisation a été accordée à la Bibliothèque nationale du Canada de microfilmer cette thèse et de prêter ou de vendre des exemplaires du film.

L'auteur (titulaire du droit d'auteur) se réserve les autres droits de publication; ni la thèse ni de longs extraits de celle-ci ne doivent être imprimés ou autrement reproduits sans son autorisation écrite.

ISBN 0-315-45499-7

THE UNIVERSITY OF ALBERTA

RELEASE FORM

NAME OF AUTHOR Matthew Eisentraut

TITLE OF THESIS A Determination of the Load Position Causing Maximum Fillet Stress in Helical Gear Teeth Using Three-Dimensional Finite Elements

DEGREE FOR WHICH THESIS WAS PRESENTED Master of Science

YEAR THIS DEGREE GRANTED Fall 1988

Permission is hereby granted to THE UNIVERSITY OF ALBERTA LIBRARY to reproduce single copies of this thesis and to lend or sell such copies for private, scholarly or scientific research purposes only.

The author reserves other publication rights, and neither the thesis nor extensive extracts from it may be printed or otherwise reproduced without the author's written permission.

(SIGNED) Matthew Eisentraut

PERMANENT ADDRESS:

107 FRASER AVE.
FORT McMURRAY, AB.
T9H 1Y9

DATED October 10 1988

THE UNIVERSITY OF ALBERTA

FACULTY OF GRADUATE STUDIES AND RESEARCH

The undersigned certify that they have read, and recommend to the Faculty of Graduate Studies and Research, for acceptance, a thesis entitled A Determination of the Load Position Causing Maximum Fillet Stress in Helical Gear Teeth Using Three-Dimensional Finite Elements submitted by Matthew Eisentraut in partial fulfilment of the requirements for the degree of Master of Science.

.....J.R. Colbourne.....
Supervisor

.....T. Dinsdale.....

.....A. Craggs.....

.....Garry Faulkner.....

Date.....Oct.10,.1988.....

Dedicated to my two sons, Nathan and Paul.

Abstract

Involute helical gears are widely used for the transmission of mechanical power. During the design of a pair of helical gears careful attention must be given to the maximum tensile stress expected in the fillets of the gear teeth. As a pair of teeth goes through the cycle of engagement the load transmitted from the driving tooth to the driven tooth varies in both magnitude and point of application. In this study the relationship between load position and load magnitude is systematically analyzed for a variety of helical gear pairs. The variety in gear pairs is generated primarily by varying the helix angle, the numbers of teeth, and the face width of the gears. Three-dimensional finite element analysis is used to calculate the fillet stress caused by loads at various positions. The load position causing maximum fillet stress is determined. It is shown that for most helical gear pairs the position causing maximum fillet stress is the position that maximizes the total load on the gear tooth. Circumstances that create exceptions to this generalization are found and the practical consequences of these exceptions are evaluated. In the last part of the study results from the finite element analysis show that the three-dimensional model gives a significantly more complex picture of the stress distribution in the fillet than can be obtained from a two-dimensional model.

Acknowledgement

The completion of this thesis gives the author great satisfaction. There are many people who have played a role in this project to whom the author is truly grateful.

The author would like to thank his advisor, Dr. J.R. Colbourne, for his encouragement and patience. Over the years the author has developed a very high respect for Dr. Colbourne's judgement and integrity. The author regards himself as being very fortunate to have had Dr. Colbourne as his adviser.

The author is thankful for the time and effort given by Dr. Craggs, Dr. Faulkner, and Dr. Hrudey to the task of critically reading this thesis. The author would like to offer a general thanks to the professors and staff in the Department of Mechanical Engineering for the friendly and supportive environment they have created over the last several years. The author especially appreciates the efforts on his behalf of Dr. Bellow and then Dr. Faulkner as they took in turn the position of Chairman of the department.

The topic of this thesis required a large amount of work with the University's computer. The author is grateful for the enthusiastic and friendly help received from Computing Services. In particular the author would like to thank Ron Torgerson, Eva Wong and Denise Thornton.

This thesis would certainly not have been finished this Fall without the help of two of the author's former students, Debbie Westman and Charlene Petroskey. Debbie and Charlene took generous amounts of time from their busy schedules to do time-consuming tasks for the author. Many other people at Keyano College went out of their way to help the author finish this thesis. To all of these people the author offers his thanks.

Since the author commuted regularly between Fort McMurray and Edmonton, he is appreciative of the efforts people made to provide food, shelter, and transportation. In this connection the author would like to thank Joyce Halferdahl, Geoff Halferdahl, Stew and Rita Kennedy, and Ivan DeFaveri. A special debt of gratitude is owed to Stew Kennedy for his patience in listening to the author chatter about this project and for his comforting words.

Finally, the author would like to thank his wife Sue Halferdahl for the enormous amount of work she has done as a consequence of this thesis and for the support she has given him. The author hopes that someday in the future he will be able to help her in a similar way to complete a graduate degree.

Table of Contents

Chapter 1: Introduction.....1

Chapter 2: Typical Spur and Helical Gears

2.1 Spur Gears.....11

2.2 Helical Gears.....22

2.3 Fillet Stresses in Spur and Helical Gears.....29

Chapter 3: Detailed Analysis of Helical Gear Pairs

3.1 $m_c \leq 2$.....34

3.2 $2 - m_p < m_f \leq m_p - 1$.....42

3.3 $m_p - 1 \leq m_f < 1$.....47

3.4 $1 \leq m_f$.....51

3.5 The Position Causing Maximum Fillet Stress.....61

Chapter 4: The Finite Element Programs

4.1 Introduction.....76

4.2 Introduction to the Mesh Generation Program.....77

4.3 The Mesh Generation Subroutines.....85

4.4 The Finite Element Program.....98

4.5 Creating the Constrained Stiffness Matrix.....101

4.6 The Stress Output Programs.....103

Chapter 5: Evaluation and Results of the Finite Element Programs

5.1 Assessing the Performance of the Finite Element Programs.....104

5.2 Results of the Finite Elements Programs.....115

5.3 Conclusion.....121

Bibliography.....123
Appendix A: Additional Information on Figures.....125
Appendix B: An Algorithm for the Formation of the Global
Stiffness Matrix.....129

List of Figures

Figure 1.1. Transverse section of two gears in mesh.....2

Figure 1.2. Transverse section of Tooth A' driving Tooth A.....3

Figure 1.3. A progression showing Tooth A' drive Tooth A.....5

Figure 1.4. Transverse section of Tooth A showing applied loads 6

Figure 2.1. Oblique drawings of (a) a spur gear tooth and (b) a helical gear tooth.....12

Figure 2.2. Transverse section showing two pairs of teeth in contact.....14

Figure 2.3. A sequence of contact regions for a pair of spur gears.....16

Figure 2.4. Maximum stress for a spur gear tooth with a constant tooth load as a function of S.....20

Figure 2.5. Contact region for a typical pair of helical gears in the corner loading position..23

Figure 2.6. A contact region for a pair of helical gears showing the relationship between the contact ratios.....26

Figure 2.7. A summary of some important definitions and relationships.....32

Figure 3.1. Contact regions for helical gears with $m_c < 2$ and $m_c = 2$ 35

Figure 3.2. Fillet stress parameters versus load position for $m_c < 2$ 37
Figure 3.3. Contact regions for a pair of helical gears with $m_c > 2$ and $m_t < m_p - 1$ 43
Figure 3.4. Fillet stress parameters versus load position for $m_c > 2$ and $m_t < m_p - 1$ 46
Figure 3.5. Contact region for a pair of helical gears with $m_c > 2$ and $m_p - 1 < m_t < 1$ 48
Figure 3.6. Fillet stress parameters versus load position for $m_c > 2$ and $m_p - 1 < m_t < 1$ 50
Figure 3.7. Contact region for a pair of helical gears with $m_t = 1$ 52
Figure 3.8. Contact region for a pair of helical gears for $1 < m_t \leq m_p$ 54
Figure 3.9. Contact region for a pair of helical gears with $m_p < m_t \leq 2$ 56
Figure 3.10. Contact regions for helical gears with large face contact ratios 59
Figure 3.11. Fillet stress versus load position for different helix angles 64
Figure 3.12. Fraction of the load versus load position for different face contact ratios with a helix angle of 20° 70
Figure 3.13. Fraction of the load versus load position for different face contact ratios with a helix angle of 2.5° 71
Figure 3.14. Critical values of F_L and S 74

Figure 4.1. A 3D drawing of a finite element mesh for a spur gear.....78
Figure 4.2. A 3D drawing of a finite element mesh for a rectangular cantilever beam.....79
Figure 4.3. Side views of the 3D meshes shown in Figure 4.1 and Figure 4.2.....81
Figure 4.4. A basic element structure used for a gear tooth with a large face width.....82
Figure 4.5. A basic element structure used for a gear tooth with a small face width 83
Figure 4.6. Data created by MSHGNR for rectangular cantilever beams.....86
Figure 4.7. Data created by MSHGNG for the gear tooth mesh shown in Figure 4.1.....87
Figure 4.8. A curvilinear daughter element and its parent.....91
Figure 4.9. The boundary between elements of different size 94
Figure 5.1. A mesh used for the 2D finite element analysis of a rectangular bar with circular shoulder fillets.....108
Figure 5.2. A mesh used for the 2D finite element analysis of a spur gear.....110
Figure 5.3. Maximum fillet stress along the face width for a spur gear with different values of Poisson's ratio.....116

Figure 5.4. Maximum fillet stress along the face width for a helical gear with different values of Poisson's ratio.....118
Figure 5.5. Maximum fillet stress along the face width for a helical gear at different load positions.....120

Nomenclature

F	Face width.
F_L	Fraction of the load on contact line A.
F_{LC}	Critical value of F_L.
F_{LM}	Maximum value of F_L.
F_{LT}	Value of F_L when $S = S_{max}$.
$[k]$	Element stiffness matrix.
$[K]$	Global stiffness matrix.
L	Length of a contact line.
L_{max}	Maximum value of L_{tot}.
L_{min}	Minimum value of L_{tot}.
L_{tot}	Total length of the contact lines.
m_c	Total contact ratio.
m_f	Face contact ratio.
m_n	Normal module.
m_p	Profile contact ratio.
p_a	Axial pitch.
p_b	Transverse base pitch.
$\{q\}$	Nodal displacements.
$\{Q\}$	Nodal loads.
R_σ	Ratio of σ at $S = S_{max}$ to σ at S corresponding to F_{LM}.
S	Distance from pitch point to contact point.
S_c	Critical value of S.
S_{max}	Value of S corresponding to a tip load for a spur tooth and a corner load for a helical tooth.

S_{min}	Minimum value of S.
S_{tot}	Length of the path of contact.
V_σ	Decrease in σ_w/σ_T as S decreases from S_{max} to 0.
u_i, v_i, w_i	Displacements of node i in the directions of the x, y, and z axes respectively.
W	Load being transmitted from the driving gear to the driven gear.
W_i	Load intensity along the contact lines.
x, y, z	Global coordinate axes.
x_i, y_i, z_i	Global coordinates of element node i.
ϵ, ρ, η	Coordinate axes for the parent element.
ν	Poisson's ratio.
σ	Maximum tensile fillet stress caused by load W being transmitted from the driving gear to the driven gear.
σ_T	Maximum tensile fillet stress caused by having the entire load W applied to the tooth in the corner loading position.
σ_w	Maximum tensile fillet stress caused by having the entire load W applied to the tooth.
ϕ_i	Shape function corresponding to node i.
ϕ_n	Operating pressure angle measured in a normal section.
ϕ_t	Operating pressure angle measured in a transverse section.
ψ	Helix angle measured on pitch cylinder.
ψ_b	Helix angle measured on base cylinder.

Chapter 1: Introduction

In this thesis finite element analysis is used to explore and answer some questions concerning root stresses in spur and helical gear teeth. A more precise description of the questions considered in this study will be easier after a brief review of some gear geometry. This review will be extremely limited and will not include much of the basic information about gear geometry that would be required to fully comprehend this study. A more complete description of the geometry of gears may be found in any of a number of books and articles on the subject. The reader will find several of these books and articles listed in the bibliography [4,7,11,12]*.

Figure 1.1 shows a transverse section of two gears in mesh. The view is said to be transverse because the section is perpendicular to the axes about which the gears rotate. In Figure 1.1 Gear 2 is driving Gear 1 in the indicated direction. Two teeth are specifically labeled. These two teeth are shown by themselves in Figure 1.2. Tooth A and Tooth A' touch each other at the contact point. As the gears rotate the location of the contact point will change. The locus of these points is called the path of contact. The majority of gears in the world today are based on the geometry of the involute. For involute gears the path of contact is a segment of a straight line. The point of

---

*Numbers in square brackets designate entries in the Bibliography.

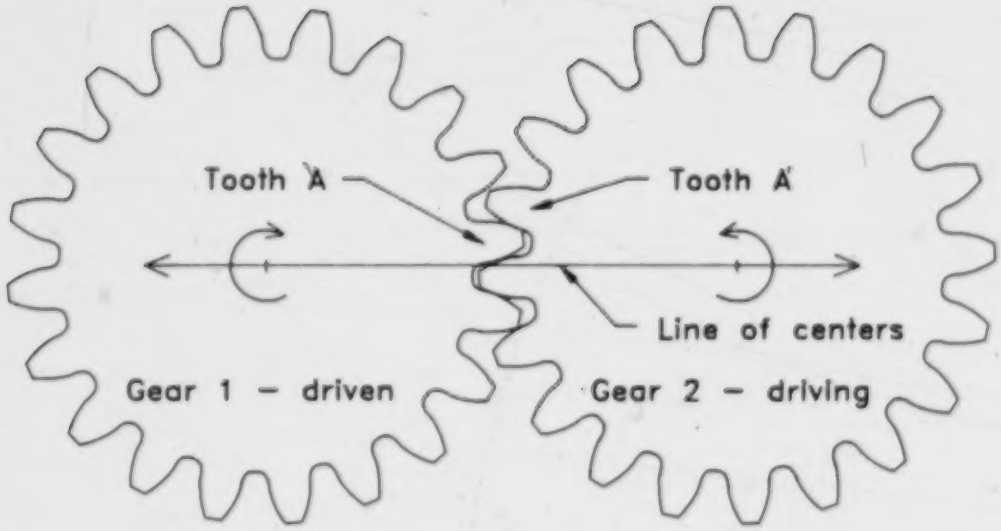

Figure 1.1. Transverse section of two gears in mesh.

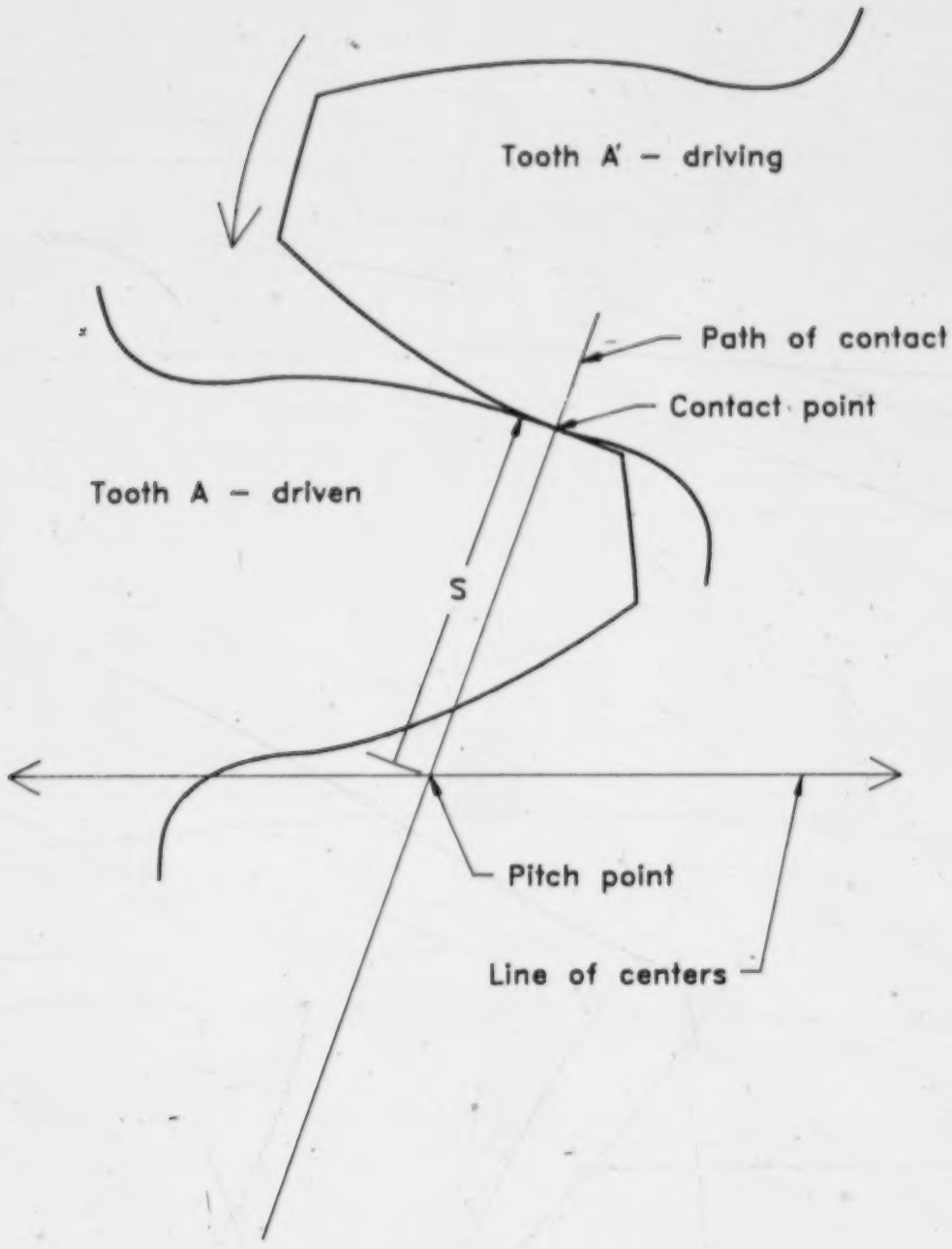

Figure 1.2. Transverse section of Tooth A' driving Tooth A.

intersection between the path of contact and the line joining the centers of the gears is called the pitch point. The distance from the pitch point to the contact point will be defined as S. By convention the value of S in Figure 1.2 will be positive. If the contact point is on the other side of the pitch point then S will be negative.

Figure 1.3 is a sequence of pictures showing Tooth A again being driven by Tooth A'. In Figure 1.3a a pair of teeth is shown just before they come into contact with one another. Figure 1.3b shows the position where the teeth first come into contact. The value of S in Figure 1.3b is a maximum and will be called S_{max}. Figure 1.3c shows an intermediate position where the value of S happens to be zero. Finally, Figure 1.3d shows the last position in which the pair of teeth are in contact. In this figure the value of S is a minimum and will be called S_{min}. With these definitions the total length of the path of contact, S_{tot}, is equal to $S_{max} - S_{min}$. The reader may have noticed the statement $S > S_{max}$ in Figure 1.3a and object that since no contact point exists, S is undefined. The sense of the statement $S > S_{max}$ will become clear in the next chapter.

The value of S defines the positions of the gear teeth and therefore the location of the load being transmitted from one tooth to the other. Figure 1.3 clearly shows how the load on Tooth A moves from its tip towards its root as the teeth rotate. In Figure 1.4 Tooth A is shown by itself

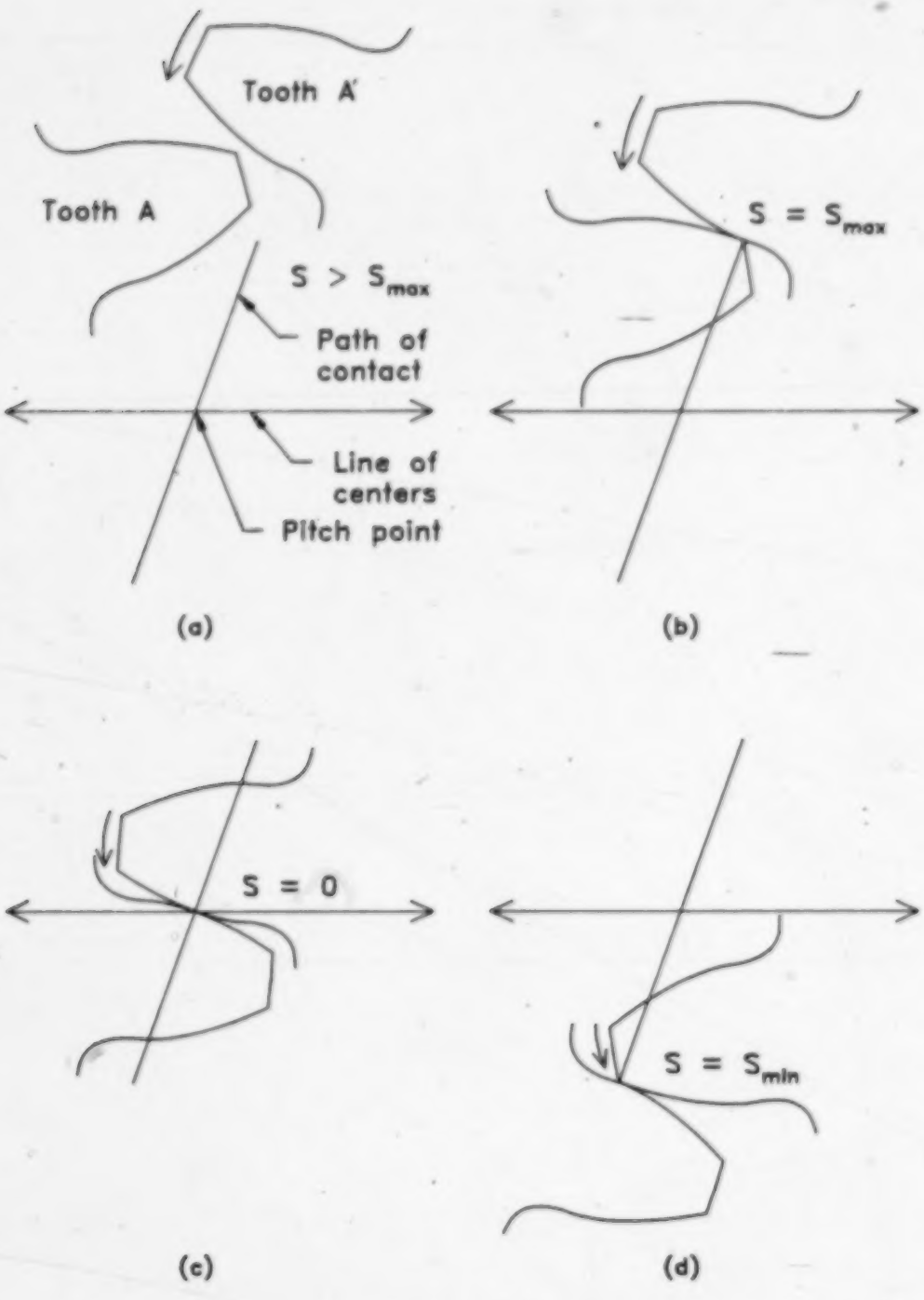

Figure 1.3. A progression showing Tooth A' drive Tooth A.

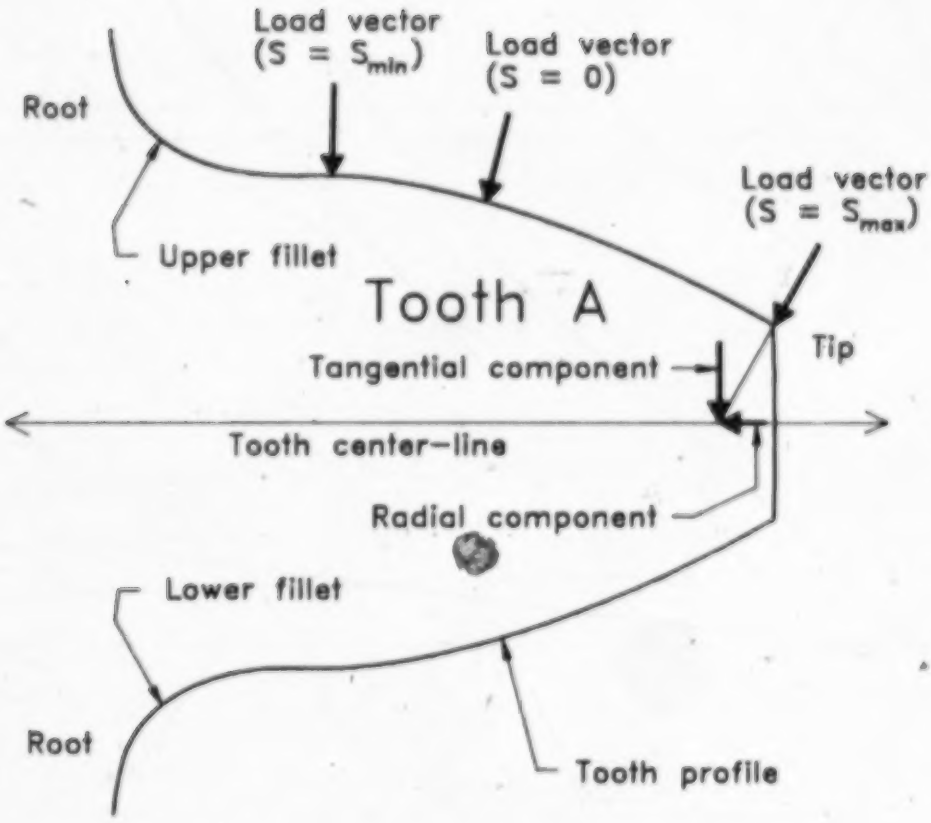

Figure 1.4. Transverse section of Tooth A showing applied loads.

with load vectors applied to the surface of the tooth. These load vectors are normal to the surface of the tooth. As indicated, the positions of the load vectors can be specified with the variable S. The load vector at the tip has been slid down its line of action so that its point of application is on the center-line. The figure shows the components of this load vector acting on the center-line. The component that points at the center of the gear is known as the radial component. The component that is perpendicular to the center-line is known as a tangential component.

The process of sliding the load vector to the center-line and then resolving it into components could have been done with any of the load vectors. If Tooth A is regarded as a short cantilever beam it is obvious that the radial component will produce a radial compressive stress and the tangential component will cause bending stresses. If the bending is considered by itself, one would expect a tensile stress in the upper fillet and a compressive stress in the lower fillet. The addition of the radial compressive stress would cause a relatively small reduction of the tensile stress in the upper fillet and a corresponding increase in the compressive stress in the lower fillet. The magnitude of these root stresses will depend upon the magnitude and location of the load.

The subject matter of this thesis has evolved from the following questions: At what position of engagement will the

tensile stresses in the root be a maximum? What is the magnitude and location of this maximum tensile stress? The scope of these questions is limited by a number of assumptions. For example, it is assumed the gears are accurately cut involute gears, the total load transmitted from one gear to the other is constant, and the loading condition is static and of such a magnitude that linear elastic behavior can be assumed. Helical gears will be the primary focus of this study though spur gears also receive some attention.

Since the value of S specifies the relative positions of a pair of teeth, the first question stated above can be answered in terms of a value of S. The value of S that results in maximum tensile stress in the fillet will be called the critical value of S, S_c.

The concern with tensile rather than compressive stresses results from the fact that it is the tensile stresses that cause failure. As explained above, the maximum compressive stress is somewhat larger than the maximum tensile stess. However, from the standpoint of failure due to fatigue this fact is irrelevant. Unless otherwise indicated, future references to stresses in this study can be assumed to refer to tensile stresses along the upper fillet.

It will be demonstrated in Chapter 3 that for most pairs of helical gears the critical value of S can be

confidently predicted without having to actually obtain the value of any stresses. However, there exists a small class of helical gears for which S_c is not obvious. For these cases it is necessary to obtain stresses as a function of S and then choose the value of S that causes the largest stress. All of this ground has already been covered by Colbourne [5], who calculates stresses using a method based on the ideas found in AGMA 218.01 [1]. In contrast to Colbourne this study relies on finite element analysis as a means to calculate stresses. The conclusions of this study regarding the orientation which causes the maximum stress confirm to a large degree the conclusions reached by Colbourne. The form in which these conclusions are stated are different and somewhat more concise than Colbourne's. It will become obvious in later sections that this difference in form can be attributed to the influence of using finite elements rather than AGMA 218.01.

The main body of this thesis consists of five chapters. Chapter 2 continues the introduction of basic concepts begun in Chapter 1. A detailed discussion of two spur gears in mesh is included to serve as an introduction to the somewhat more complex case of helical gears. Basic concepts relevant to the analysis of helical gears are defined and the meshing of a typical helical gear pair is discussed. Finally, Chapter 2 outlines two basic approaches to finding root stresses in spur and helical gears, and presents the method by which helical gears will be analyzed in greater detail in

this study. Chapter 3 consists of a detailed discussion of helical gears. The question of which loading position produces the maximum tensile root stress is explored and to a large extent answered. Much of the information in Chapter 3 depends on results from the finite element programs. Chapter 4 is devoted to giving a description of the finite element programs. Most of this description is quite general though some aspects of the programming are described in detail. An evaluation of the performance of the finite element programs is found in the first part of Chapter 5. This last chapter continues with a presentation and discussion of the results of the finite element programs.

Chapter 2: Typical Spur and Helical Gears

2.1 Spur Gears

All of the figures in Chapter 1 showed two-dimensional transverse sections of gears and gear teeth. Real gears are three-dimensional. Figure 2.1 shows oblique drawings of a spur gear tooth and a helical gear tooth. The width of a tooth in the axial direction is called the face width F. The thickness of the tooth is indicated in Figure 2.1a. Two parameters that are widely used and representative of tooth thickness are diametral pitch and module. In this study, the normal module m_n, which has units of length, will be used as an indicator of tooth thickness.

Figure 2.1 illustrates how a single tooth will be positioned within a cartesian coordinate system. The z axis coincides with the axis of rotation of the gear. The near side of the gear is located in the plane z = 0 and the far side is in the plane z = -F. The x axis lies along the tooth center-line in the z = 0 plane. The y axis is chosen so that the system is right-handed.

It is clear in Figure 2.1 that when the third dimension is added the contact point becomes a contact curve. For spur gears this curve will be a straight line segment that runs parallel to the tip of the tooth. Every transverse section of a spur gear tooth will show the load at the same position. Therefore, the value of S is independent of where the transverse section cuts the z axis. In the case of

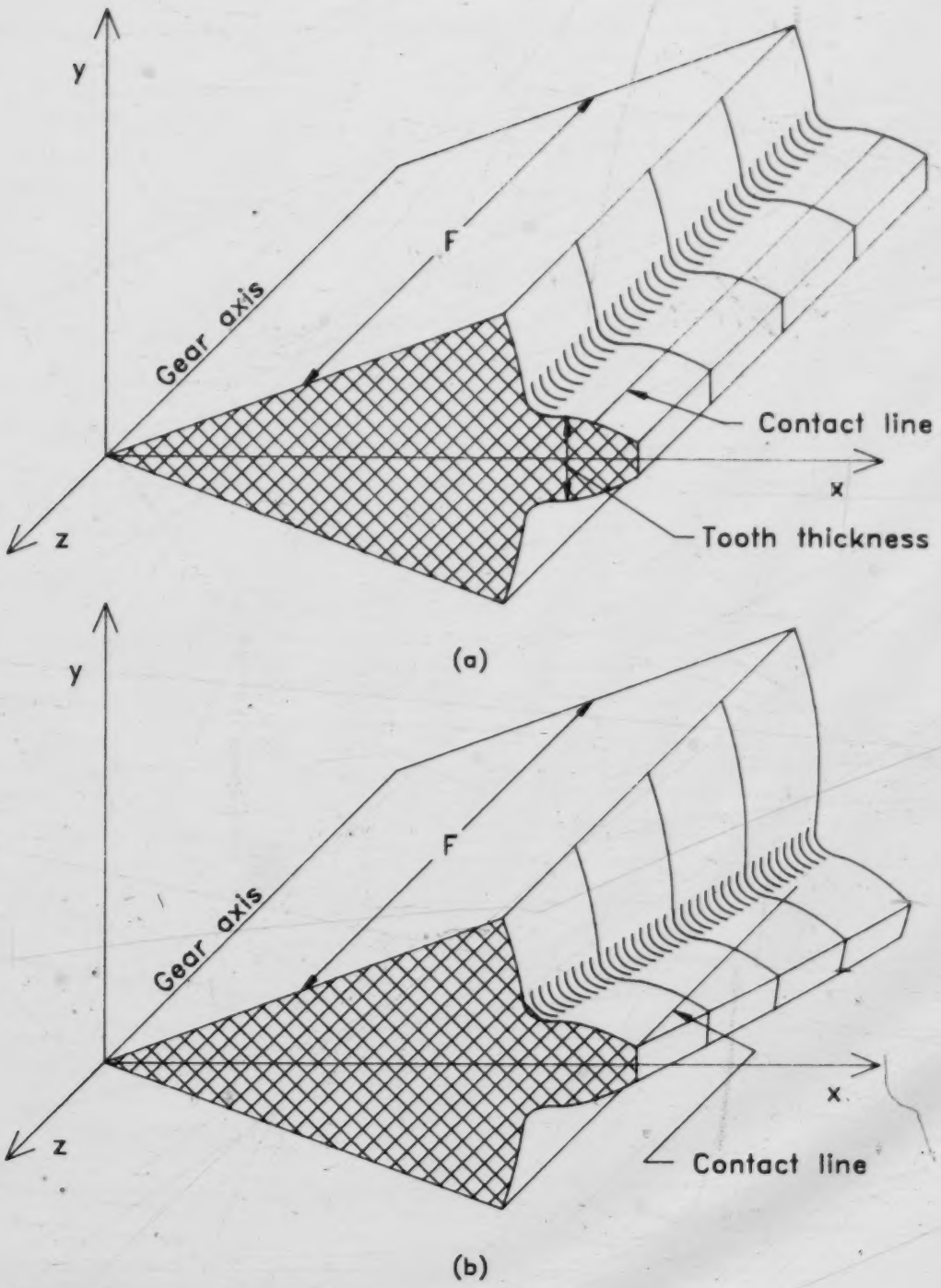

Figure 2.1. Oblique drawings of (a) a spur gear tooth and (b) a helical gear tooth.

involute helical gears it can be shown that the contact curve is also a segment of a straight line. However, as shown in Figure 2.1b, the contact line runs at an oblique angle across the tooth. The contact line is a generator of the involute helicoid surface. Unlike spur gears, the position of the load in a transverse section of the helical tooth will depend on where the section cuts the z axis. In the transverse plane z = 0 the load is at the tip of the tooth and S is equal to S_{max}. As the transverse plane is moved along the negative z axis the value of S decreases until it reaches S_{min} and the contact line ends. A transverse section at z = -F would show no load being applied.

The path of contact exists in a transverse section such as that shown in Figure 2.2. The angle the path of contact makes with a line perpendicular to the line of centers is called the operating pressure angle ϕ_t. For helical gears this angle may be measured in the normal section, in which case it is denoted ϕ_n.

Figure 2.2 demonstrates that two pairs of teeth may be in contact at the same time. The distance between the contact points is equal to the transverse base pitch p_b. The ratio of S_{tot} to p_b is the profile contact ratio m_p. A consequence of this definition is that S_{tot} may be replaced with the product $m_p p_b$. For the gears considered in this study the profile contact ratio is always a number between 1 and 2. A pair of spur gears each having twenty teeth will

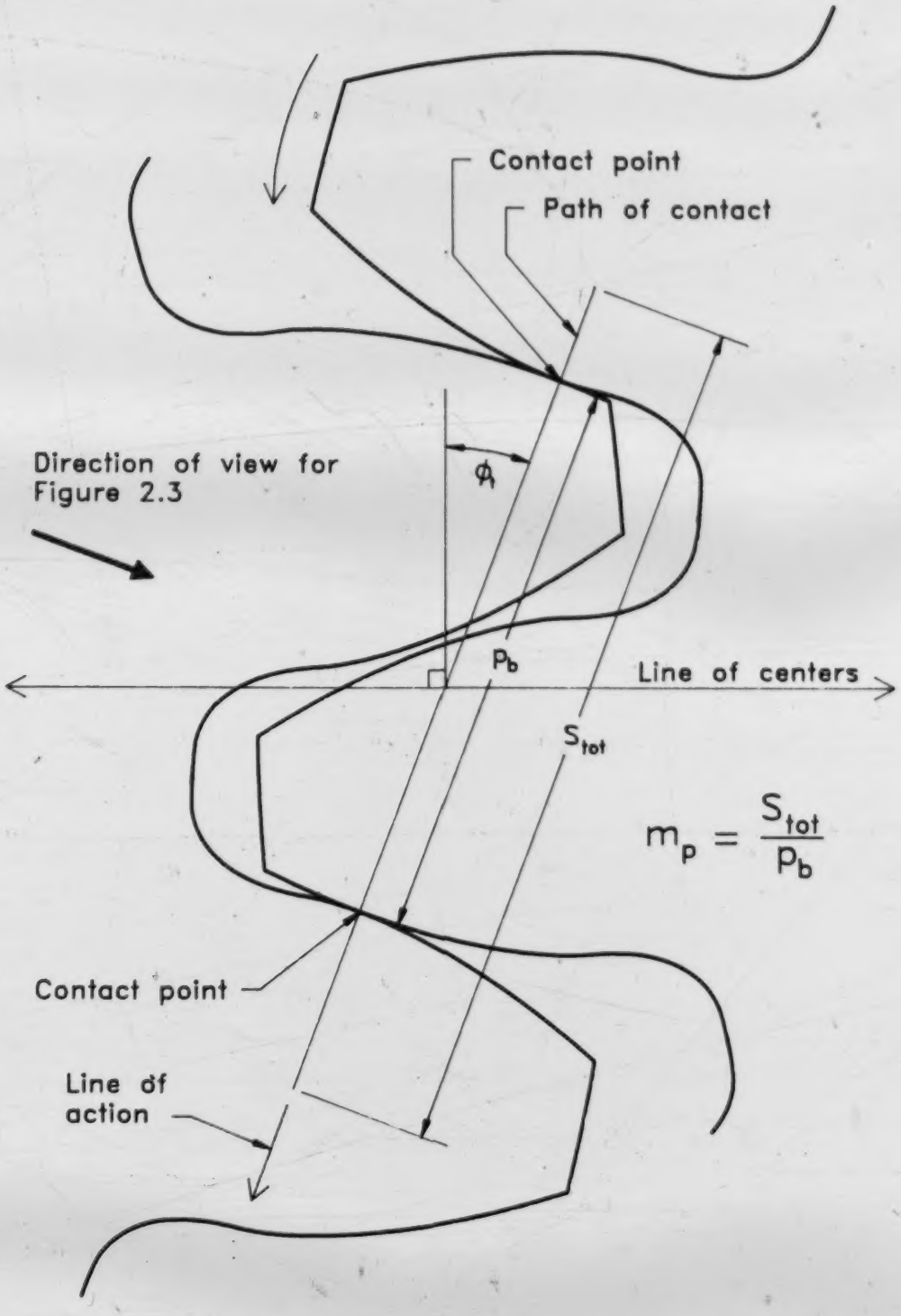

Figure 2.2. Transverse section showing two pairs of teeth in contact.

have a profile contact ratio of about 1.5. A pair of spur gears each having eighty teeth will have a profile contact ratio of about 1.75. The value of m_p is less for helical gears. Increasing helix angle tends to reduce the profile contact ratio.

The path of contact is a segment of a line which is called the line of action. The line of action is the common tangent to the base circles of the gears. With the addition of the third dimension, lines become planes just as points become lines. The path of contact becomes a contact region within a plane called the plane of action. The plane of action is the common tangent plane to the base cylinders of the gears. It is useful to rotate one's point of view so the contact region in the plane of action can be seen. The direction of the required point of view is indicated in Figure 2.2.

Figure 2.3 is a sequence of pictures showing contact regions for a pair of spur gears as the gears rotate. The contact region is the rectangle KLMN whose sides have lengths S_{tot} and F. The two horizontal sides, KN and LM, are parallel to the z axis. The z axis lies along the the gear axis (see Figure 2.1) and would not be seen in the plane of action. However, an indication of the direction of the z axis is given in Figure 2.3 and the values of the z coordinates are shown for the vertical sides of the contact region.

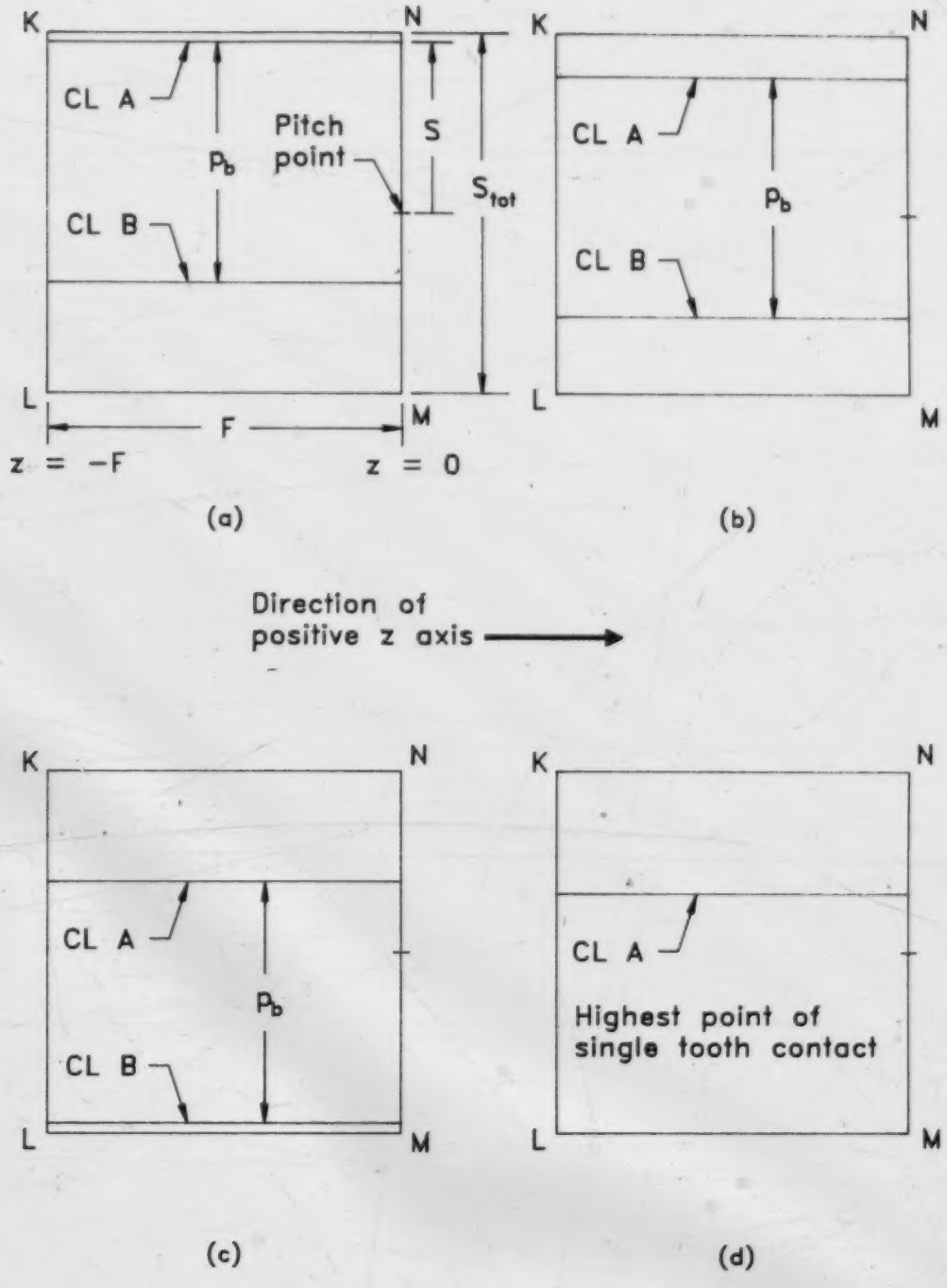

Figure 2.3. A sequence of contact regions for a pair of spur gears.

In Figure 2.3a the presence of two contact lines, CL A and CL B, reflects the fact that two pair of teeth are in contact at the same time. The contact regions in Figure 2.3 are drawn with $m_p = 1.5$. Figure 2.3a has the pitch point indicated on the side MN. The pitch point has not been extended into a line across the contact region simply to avoid clutter in the drawing. The value of S for CL A is also indicated.

The contact line CL A is near the top of the contact region in Figure 2.3a. This means the contact line is near the tip of the driven tooth and near the root of the driving tooth. We will limit our concern to the driven tooth. A small rotation of the gears will cause the contact lines to move downward to the position shown in Figure 2.3b. Such a rotation will be called a positive rotation. A positive rotation causes the load on the driven tooth to move towards the root and the value of S to decrease. As the gears rotate the lines of contact continue to move downwards across the contact region. In Figure 2.3c CL B is shown to be very close to the bottom edge of the contact region. With a slight positive rotation CL B leaves the contact region and the corresponding pair of teeth cease to be in contact. Figure 2.3d shows the contact region just after CL B has passed out of the contact region. For obvious reasons this situation is called the highest point of single tooth contact. As the gears continue to rotate CL A will continue to move downward. Eventually a new contact line will appear

at the top of the contact region and the cycle that started in Figure 2.3a will repeat itself.

A gear tooth can be thought of as a short cantilever beam. As the tooth goes through the cycle of engagement (see Figure 1.3 and 1.4) the load on the driven tooth moves from the tip towards the root. If the load is held constant, it would be expected that the stress in the root would be a maximum when the load is at the tip ($S = S_{max}$). As the gears rotate in the positive direction, the load moves towards the root, S decreases, and the stress in the root should decrease. Figure 2.3 shows that during the meshing cycle the total load is transmitted through either two pairs of teeth (two contact lines) or just one pair of teeth (one contact line). In Figure 2.3a, b, and c the load is shared by two pairs of teeth. Figure 2.3d is the position where the load along CL A abruptly increases since CL B has just passed out of the contact region. The stress in the teeth touching along Cl A would also increase abruptly. As the gears continue to rotate the load on the driven tooth would move towards the root and the stress would decrease.

It should be clear from the preceding paragraph that a graph of root stress versus S should show two local maximums - one at $S = S_{max}$ and another at the value of S corresponding to the highest point of single tooth contact. The question for the gear designer is which of these local maximums is the absolute maximum. If the gears are accurately cut it is

assumed that the load is shared evenly when two contact lines exist in the contact region. In this case it is uncontroversial that the maximum root stress occurs at the point of highest single tooth contact. The graph in Figure 2.4 helps to show why this is true. A typical graph of the variation of fillet stress due to a constant load is shown as a function of the position of the load on the tooth. In this study σ_w is used to denote the fillet stress when the entire load W is placed on a single tooth. By multiplying σ_w by $m_n F/W$ a dimensionless variable for stress is created. Likewise, dividing S by S_{max} yields a dimensionless variable for position. The effect of load sharing between more than one pair of teeth means for accurately cut spur gears that the load at the tip will be half as much as the load at the highest point of single tooth contact. If the load at the tip is to cause the absolute maximum fillet stress, then the curve shown in Figure 2.4 must fall by more than 50% as S decreases from S_{max} to the value at the highest point of single tooth contact. Clearly this is not the case.

For gears that are not accurately cut it cannot be assumed the load is evenly shared or shared at all. A conservative designer would assume the load is always transferred through a single pair of teeth and would therefore place the total load at the tip of the tooth for the calculation of maximum root stress.

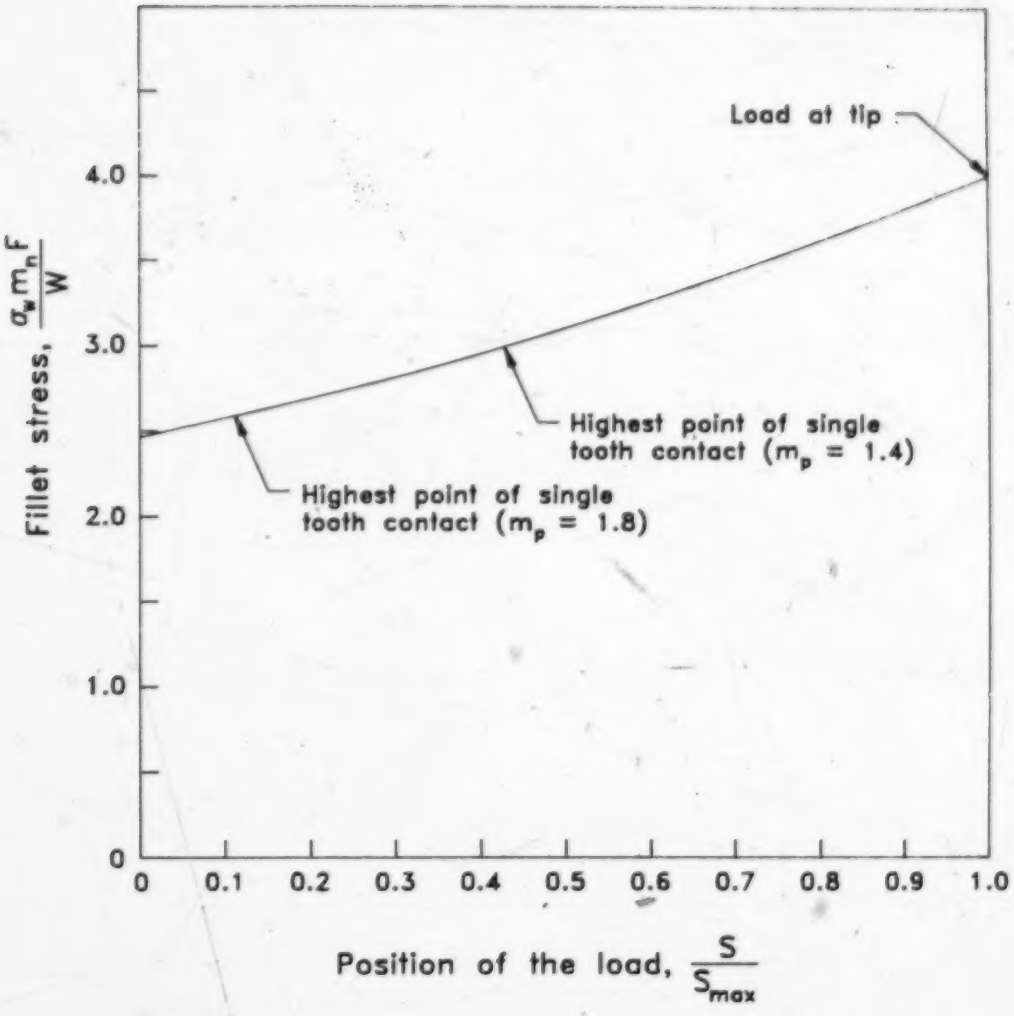

Figure 2.4. Maximum stress for a spur gear tooth with a constant tooth load as a function of S.

The preceding discussion has concerned itself with a pair of spur gears. The next section moves on to the focus of this thesis, helical gears. Before moving to helical gears one point about spur gears needs to be emphasized. Nowhere in the discussion of spur gears was the face width of importance. Changing the face width would not, for example, change the location of the highest point of single tooth contact. It will be seen in the following sections that in the case of helical gears the face width becomes a parameter of primary importance.

2.2 Helical Gears

Figure 2.5 shows two drawings of the contact region for a pair of helical gears. Again, the difference between helical and spur gears is apparent. The contact lines for the spur gears run horizontally across the contact region while those of the helical gear are oblique. The angle a contact line makes with the z axis is constant and equal to the base helix angle ψ_b.

The contact region in Figure 2.5b is basically the same as that in Figure 2.5a. However, in Figure 2.5b CL C has been extended beyond the boundary of the contact region and a contact line labelled CL D has been drawn which does not pass through the contact region at all. It is only that part of a contact line that lies within the contact region that represents actual contact between a pair of teeth. Those parts of a contact line outside of the contact region are, in a sense, imaginary and are drawn as a convenience. When counting the number of contact lines only those passing through the contact region are counted.

Figure 2.5b shows the transverse base pitch p_b and a new quantity called the axial pitch p_a. The ratio of the face width to the axial pitch is called the face contact ratio m_f. A consequence of this definition is that F may be replaced with the product $m_f p_a$. The value of m_f is a measure of the number of pairs of teeth in contact as a result of the teeth having width. The special importance of the face

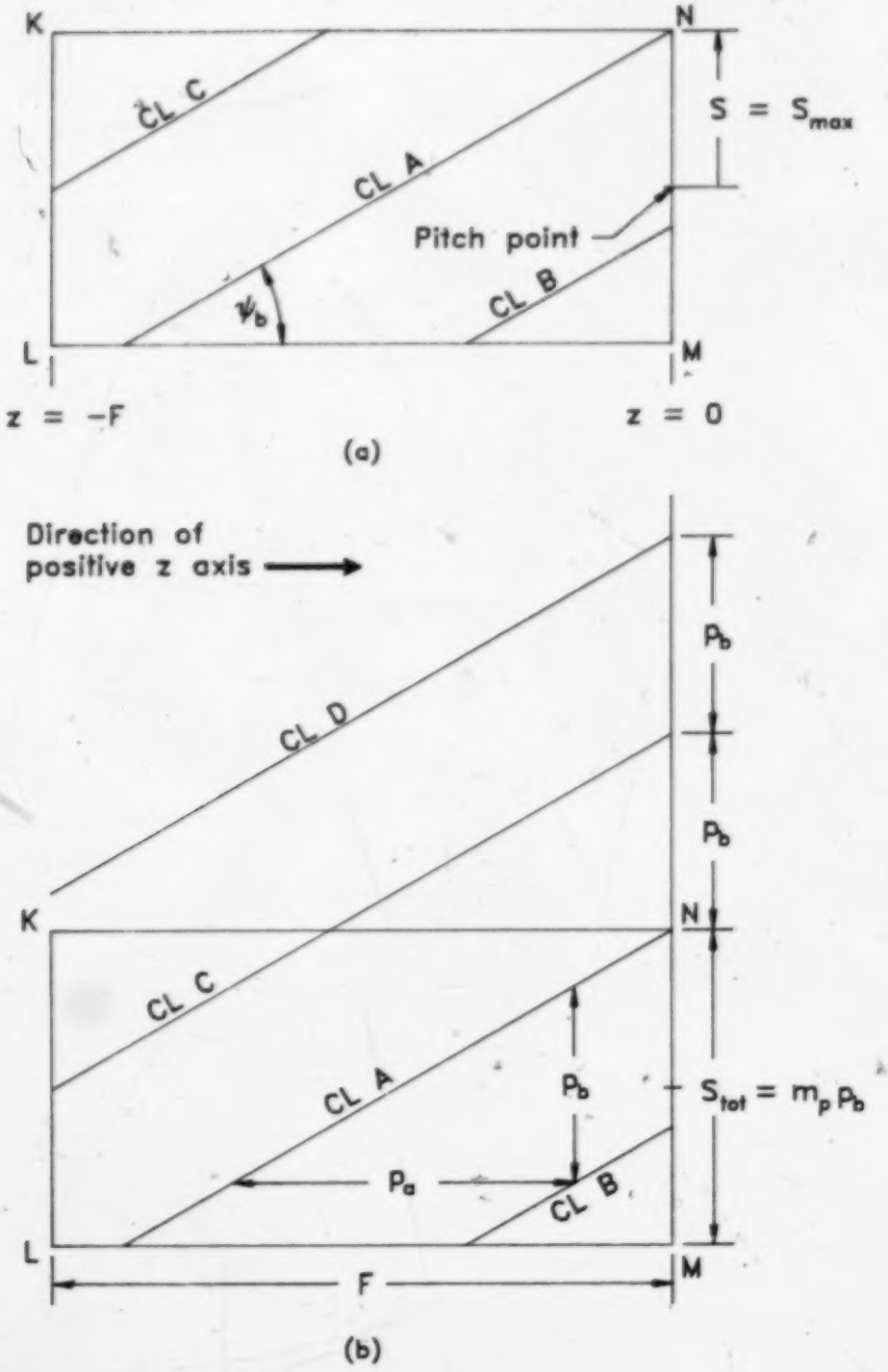

Figure 2.5. Contact region for a typical pair of helical gears in the corner loading position.

width of helical gears is now easily seen. Whereas a change in F will not affect the number of contact lines for spur gears, a change in F can change the number of contact lines for helical gears. In Figure 2.5 a significant reduction in F would cause CL C to no longer pass through the contact region. Consequently, the total load would no longer be shared by the pair of teeth meeting along CL C. If instead F were increased sufficiently, CL D would pass through the corner of the contact region; another pair of teeth would share the load.

The variable S was defined previously as the distance from the pitch point to the point of contact measured in a transverse section (see Figure 1.2). Since all transverse sections of spur gears are identical, S is uniquely defined for spur gears. In the case of helical gears, every transverse section is different so the question arises as to which section S is being measured in. The primary purpose for creating S was to provide a means of unambiguously quantifying the relative positions of a pair of teeth and therefore the location of the contact line. This purpose can be accomplished by agreeing to measure S in the transverse plane $z = 0$. The value of S can be given for any of the contact lines shown in the plane of action. In this study the contact line of importance will always be CL A and S will usually refer to its location. When reference is made to stresses in a gear tooth, the tooth in question will always be the driven tooth that is being loaded along CL A.

Inspection of the helical tooth in Figure 2.1b and the contact regions in Figure 2.5 show that these two figures are compatible with one another in the sense that the contact line in Figure 2.1b can be identified with CL A in Figure 2.5. The contact line in Figure 2.1b passes through the corner of the tooth in the plane z = 0. Likewise, in Figure 2.5 CL A passes through the upper corner of the contact region at z = 0. Also, in neither Figure 2.1b nor 2.5 does the contact line extend across the entire width of the tooth. The situation depicted in both these figures is known as a corner loading. Figure 2.5a indicates that a corner loading occurs when S is equal to S_{max}.

If the pair of gears creating the contact region shown in Figure 2.5 were given a positive rotation, the contact lines would move downward across the contact region. As the gears rotated, CL D would eventually enter the contact region. Figure 2.6 shows the position where CL D is just about to enter the contact region. The lower part of Figure 2.6 shows why the distance NQ is equal to the product $m_p p_b$. The total contact ratio m_c is defined as the sum of the profile contact ratio and the face contact ratio, $m_c = m_p + m_f$. Figure 2.6 shows that the total contact ratio can also be interpreted as the ratio of distance QM to the transverse base pitch p_b. The total contact ratio indicates the average number of pairs of teeth in contact as the gears rotate.

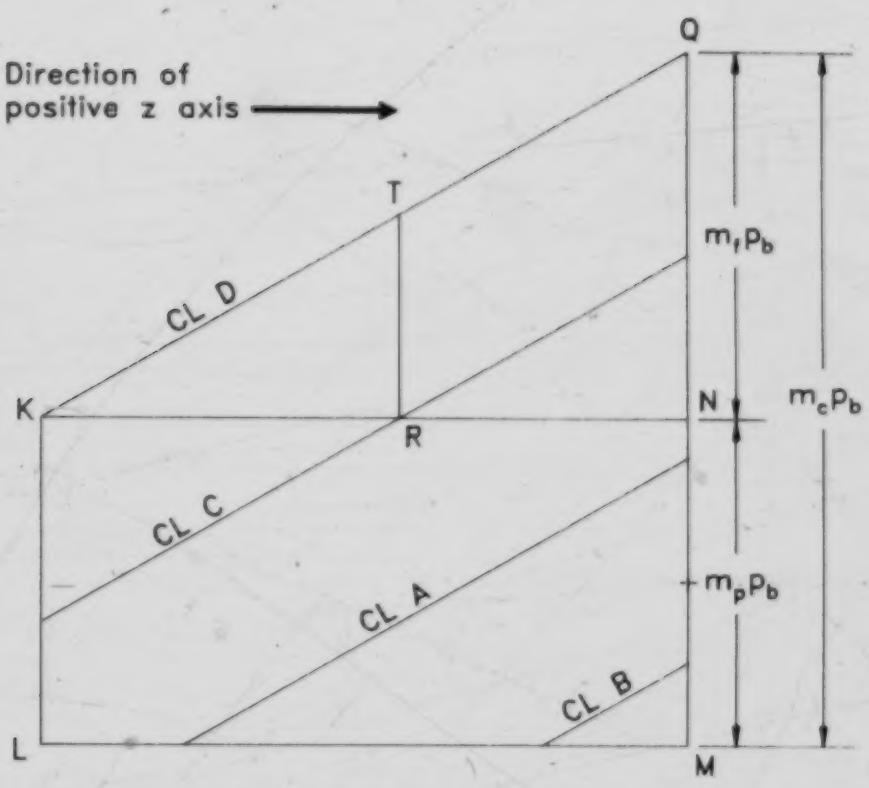

Triangle QKN is similar to triangle TKR

$$\frac{X}{F} = \frac{P_b}{P_a} \quad \Longrightarrow \quad X = \frac{F}{P_a} P_b = m_f P_b$$

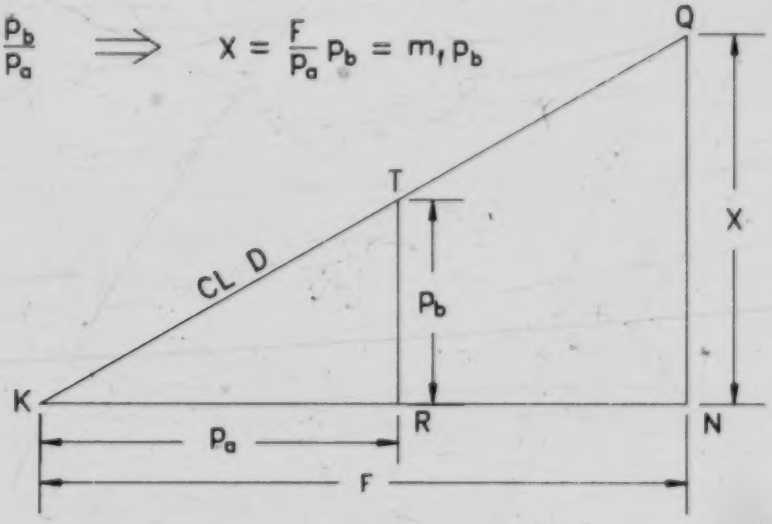

Figure 2.6. A contact region for a pair of helical gears showing the relationship between the contact ratios.

The length of a contact line, L, will be defined as the length of the contact line bounded in the contact region. The lengths of contact lines CL A, CL B, and CL C will be denoted L_A, L_B, and L_C respectively. According to this definition the length of CL D shown in Figure 2.6 is zero ($L_D = 0$), because it does not pass through the contact region. The sum $L_A + L_B + L_C + \ldots$ will be called the total length of the contact lines L_{tot}. A contact line that becomes longer as the gears rotate a small positive amount will be said to be entering the contact region. If the contact line becomes shorter then it will be said to be leaving the contact region. In Figure 2.6 CL C and CL D are entering while CL A and CL B are leaving the contact region. Though no examples are shown in the figure it is possible that the length of a contact line will remain constant as a result of a small positive rotation. Such a line would be neither entering nor leaving the contact region. Because the contact lines are parallel and a constant distance apart, the rate at which a contact line entering the contact region becomes longer will be exactly equal to the rate at which a contact line leaving the contact region becomes shorter. In Figure 2.6, two contact lines are entering the contact region and two are leaving. For a small positive rotation the increase in L_D and L_C will be matched by the decrease in L_A and L_B and therefore L_{tot} will not change. It is assumed in this study that the total load W on a gear will be distributed evenly over the contact lines. Therefore, the

load intensity W_i, defined as W/L_{tot}, will be constant along the contact lines. As the gears rotate the lengths of the contact lines will change. The total length of the contact lines may or may not change depending on the value of the face contact ratio. Since L_{tot} does usually change as the gears rotate it is useful to define L_{max} and L_{min} as the maximum total length and minimum total length respectively. A consequence of the definition of W_i and the assumption that W is constant is that when $L_{tot} = L_{max}$ the load intensity will be a minimum and when $L_{tot} = L_{min}$ the load intensity will be a maximum. The ratio of L_A to L_{tot} will be called the fraction of the load F_L. Given the previously stated assumption of uniform load intensity, F_L gives the fraction of the total load that is being applied along CL A. The fraction of the load F_L has been defined specifically with reference to CL A because it is the stresses in the driven tooth being loaded by CL A which are of interest. As the gears rotate F_L will vary from zero to some maximum value and then back to zero. The nature of this variation will depend partly upon the face contact ratio.

2.3 Fillet Stresses in Spur and Helical Gears

It is appropriate at this point to outline some of the different methods used to calculate maximum root stresses in helical gears. The American Gear Manufacturers Association have published a standard, AGMA 218.01 [1] for rating the bending strength of spur and helical gears. According to this standard the first step for analyzing a helical gear is to find the equivalent spur gear. The equivalent spur gear is a gear whose teeth in a transverse section closely approximate the shape of a normal section of a tooth belonging to the helical gear. In this way AGMA 218.01 converts the problem of finding a stress in a helical gear to finding a stress in a spur gear. Since all transverse sections of a spur gear are the same, it is assumed that it can be treated as a two-dimensional problem. The spur gear is approximated by a rectangular beam. Simple beam theory is used to calculate the tensile bending stress and the radial compressive stress after the point of application of the load has been slid to the centerline of the tooth and the load has been resolved into components (see Figure 1.4). These stresses are combined after the bending stress has been modified by a factor which takes into account the fact that on the helical gear the load does not run parallel to the tip of the tooth but at an oblique angle (see Figure 2.1). The resulting stress is multiplied by a stress concentration factor which is a function of the minimum radius of curvature of the tooth fillet. The value of the

stress concentration factor is based on experimental results of photoelastic tests done in 1942 by Dolan and Broghamer [9]. The process would end here if it could be assumed that the pair of gears is accurately cut from an appropriate material, the load intensity along the contact lines is uniform, and the loads are static. Only the first of these assumptions can be usually granted. Since the other two assumptions cannot be granted, relevant factors further modify the value of the maximum stress. Though the importance of these factors in the real world of design is undeniable, a consideration of them is beyond the scope of this thesis and they will henceforth be ignored.

It is unnecessary to present in detail the equation given in AGMA 218.01 for calculating the maximum root stress. This equation consists of many mathematical expressions which may be arbitrarily arranged in many ways. A possible arrangement of the equation is to form two groups of expressions. One group gives the stress caused by the application of a load intensity of unity and the other group represents load intensity. Obviously, the product of these two groups yields the stress due to the applied load. This arrangement is sensible in light of the fact that the AGMA is attempting to convert a three-dimensional problem into an equivalent two-dimensional problem. In this context it would not make sense to take the load on the three-dimensional helical gear and try to apply it to the two-dimensional section of the equivalent spur gear. It does make sense to

apply the same load intensity to the equivalent spur gear. The idea of load intensity as being an important parameter is clearly reflected in the title of Colbourne's paper [5], "Critical Load Intensity and Load Position on Helical Gear Teeth." Colbourne's method of calculating stresses is based on the ideas found in the AGMA standard. Colbourne uses the same idea of an equivalent spur gear, the same simple beam theory, and the same stress concentration factor. Colbourne's primary disagreement with the AGMA is with the question of what load intensity should be applied and where it should be applied for producing the maximum root stress.

In this study three-dimensional finite elements are used to calculate stresses. There is no conversion to a two-dimensional equivalent spur gear. Although the concept of load intensity appears in the finite element programs it does not take on central importance. The finite element programs load the helical gear tooth with the total load on the gear and the root stress σ_w is calculated. This stress is then multiplied by the fraction of the load F_L shared by the tooth to yield its fillet stress σ. Figure 2.7 summarizes the definitions of the variables L, L_{tot}, W, and W_1 and shows how the load on the single tooth may be expressed as either $W_1 L_A$ or WF_L.

This chapter has defined some new terms, introduced the reader to a typical contact region for a pair of helical gears, and broadly described two basic approaches to

L = the length of a contact line. Only that part of the line within the boundary of the contact region is measured. A contact line that does not intersect the contact region has a length of zero.

L_{tot} = the sum of the lengths of all the contact lines.

L_{min} = the minimum value of L_{tot}.

L_{max} = the maximum value of L_{tot}.

W = the magnitude of the net force being transmitted from the driving gear to the driven gear. The line of action of W will be normal to the tooth surfaces and so will lie in the plane of action and be perpendicular to the contact lines. The component of W that produces torque on the gears is $W \cos \psi_b$.

$W_l = \frac{W}{L_{tot}}$ = the load intensity acting on the lines of contact within the contact region. This definition assumes that W is uniformly distributed on the contact lines.

$F_L = \frac{L_A}{L_{tot}}$ = the fraction of the total load W acting on contact line A.

The magnitude of the net force acting on contact line A

$$= F_L W = \frac{L_A}{L_{tot}} W = \frac{W}{L_{tot}} L_A = W_l L_A$$

Figure 2.7. A summary of some important definitions and relationships.

calculating root stresses. It has been stated that the manner in which the variables W_i and F_L change as the gears rotate depends on the face contact ratio. These variables are important for the calculation of root stresses. To clearly understand the relationship between these variables and the face contact ratio a sequence of contact regions will be closely examined in the next chapter. The first contact region will have a very small face contact ratio. Successive contact regions will have larger and larger face contact ratios.

Chapter 3: Detailed Analysis of Helical Gear Pairs

3.1 $m_c \leq 2$

Figure 3.1a shows a contact region in which the total contact ratio is less than 2, which means that during some parts of the meshing cycle there will be only one pair of teeth in contact. The first position shown is that of a corner loading for CL A. Each of the contact lines extends across the contact region and has equal length. Assuming a uniform load intensity, it follows that $F_L = 0.5$. As the gears rotate in a positive direction, the contact lines move downward until they reach the position shown in Figure 3.1b. During this movement neither of the contact lines changes in length, so L_{tot}, F_L, and W_i will all remain constant.

As the gears continue to rotate, L_B will steadily decrease until CL B leaves the contact region completely. Figure 3.1c shows the position, known as the highest point of single tooth contact, where CL B has just left the contact region. The corresponding value of S is indicated on the drawing. During the motion that causes CL B to leave the contact region, L_A remains constant and no other contact lines enter the contact region. Therefore, the load intensity and F_L will both increase. At the point of single tooth contact $L_{tot} = L_A$ and F_L will be equal to 1, the highest value it can attain. The total length of the lines of contact will be a minimum, so the load intensity will be a maximum. As the gears continue to rotate, the values of F_L

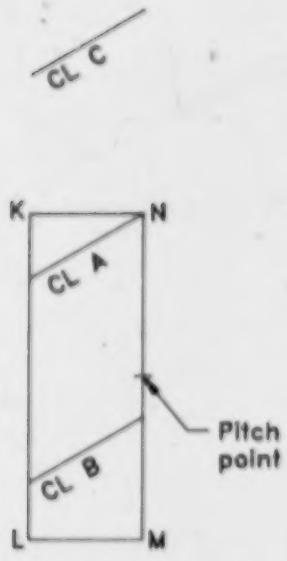

Corner loading

(a)

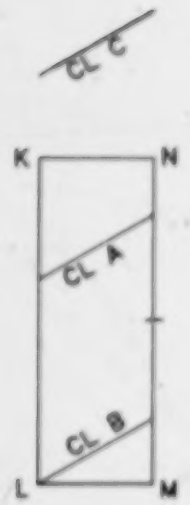

CL B will begin to leave the contact region

(b)

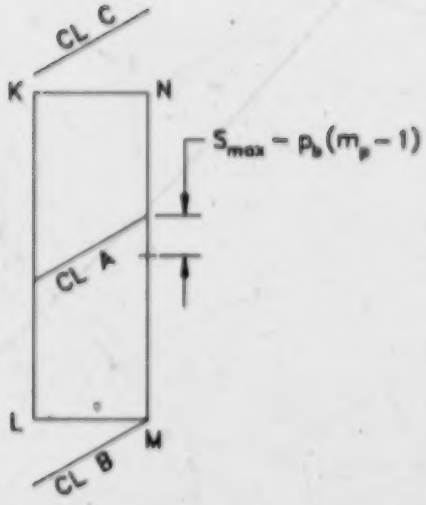

Highest point of single tooth contact

(c)

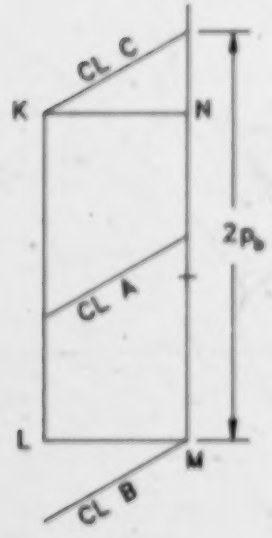

Face width increased until $m_c = 2$

(d)

Figure 3.1. Contact regions for helical gears with $m_c < 2$ and $m_c = 2$.

and W_i will remain constant until CL C begins entering the contact region and L_{tot} begins to increase.

In Figure 3.1d the face width of the gear pair has been increased so that CL C will begin entering the contact region at exactly the position of highest single tooth contact. As indicated, the value of the total contact ratio m_c is equal to 2 for this face width. Under these circumstances the value of F_L will still reach a maximum value of 1, but will then immediately decrease with continued rotation.

Figure 3.2 shows a type of a graph that will be seen two more times in this chapter. The variation of three dimensionless variables are shown as S changes from S_{max} to zero. Discussion of these graphs will assume that S begins with a value of S_{max}, the value corresponding to a corner loading, and then decreases as the gears rotate in what has been defined as the positive direction. In other words, the graph will be viewed from right to left rather than the usual left to right manner. The curve showing the variation of F_L follows exactly the description given above. It has been explained that after F_L reaches its maximum value of 1, it is usually constant for a short time before decreasing. For the particular pair of gears corresponding to the curves in Figure 3.2, the value of F_L is still 1 at S = 0. A pair of gears with a total contact ratio closer to 2 would show the F_L curve beginning to decrease somewhere in the region

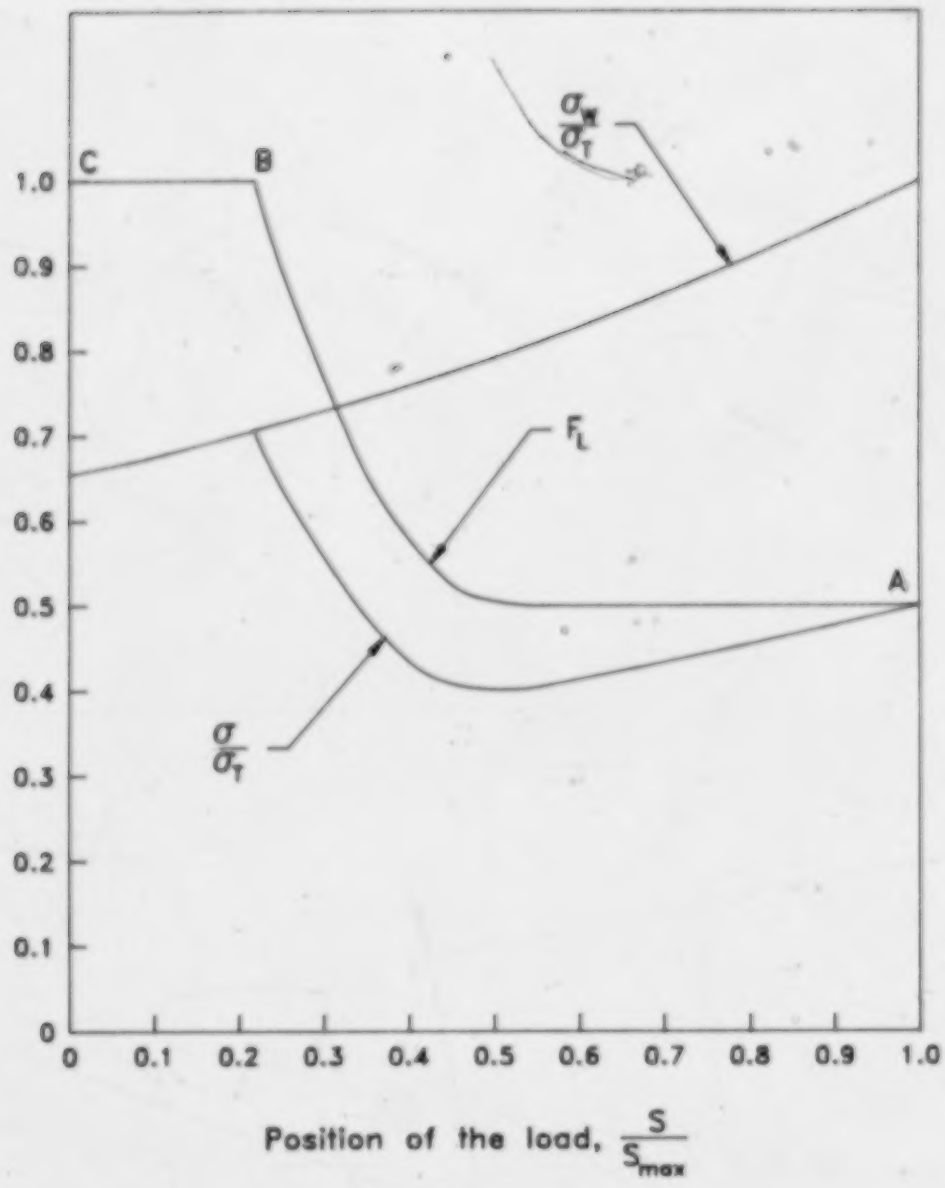

Figure 3.2. Fillet stress parameters versus load position for $m_c < 2$.

between the points B and C. As previously stated, if the total contact ratio is exactly 2, then the value of F_L will begin to decrease immediately at point B as S decreases.

A second curve in Figure 3.2 shows the variation of σ_w, the fillet stress due to a constant load W applied to the tooth. A dimensionless expression has been created by dividing σ_w by σ_T, where σ_T is the stress in the fillet when W is applied to the tooth in the corner position. By definition, σ_w/σ_T will be equal to 1 when $S = S_{max}$. As expected, as S decreases and the contact line moves towards the root, the stress due to a constant load decreases. The curve showing the variation of σ_w/σ_T is derived from the results of the finite element analysis. Since stress will vary directly with load, the product of F_L and σ_w/σ_T represents the tensile stress in the fillet when two gears are in mesh and the constant load W is being transmitted to the driven gear. Under these circumstances, the load W will be shared between one or more pairs of teeth, depending on the value of S. Since F_L is the fraction of the load acting along CL A, it is appropriate to define σ as the tensile stress in the fillet of the tooth being loaded by CL A. It follows that $\sigma = F_L\sigma_w$.

The curve representing σ provides the necessary information for determining S_c, the value of S that corresponds to maximum fillet stress. Figure 3.2 shows clearly that S_c is the value of S corresponding to the

highest point of single tooth contact. The critical value of F_L, F_{LC}, is 1. Although Figure 3.2 is only a single example of a pair of helical gears with $m_c \leq 2$, it may be regarded as typical. The generalization that S_c for such gears is the value associated with the highest point of single tooth contact is uncontroversial and is consistent with what is known about spur gears. For helical gears with $m_c \leq 2$ and $1.5 \leq m_p$, F_L is always 0.5 for the corner loading position. As S decreases, F_L is first constant, then rises with an increasing rate to a value of 1. So, like spur gears, F_L doubles as S varies from S_{max} to the highest point of single tooth contact. The variation of σ_w over this range is much less. While F_L doubles, σ_w is reduced by only 30%. Of the many gear pairs tested in this study, none shows σ_w decreasing by more than 40% as S varies from S_{max} to zero. If $m_c \leq 2$ and $m_p < 1.5$, circumstances can be created in which F_L is slightly greater than 0.5 for the corner loading position. Though F_L does not quite double under these circumstances, its increase is still proportionally much greater than the decrease in σ_w. It is sensible to say that in the product $F_L\sigma_w$, F_L is the dominant factor. When F_L is a maximum, σ is a maximum.

Three points on the F_L curve in Figure 3.2 are labelled. As will be seen in following sections, if m_c is less than 1, then F_L will be constant or increasing as S decreases in the portion of the curve between points A and

B. As S decreases past point B, F_L may be constant for a short time but will eventually decrease. Point B is at the largest value of S for which F_L is a maximum. All sections of the graph show σ_w decreasing with decreasing S. Results from the finite element programs show σ_w decreasing as S decreases, as long as CL A intersects side KL of the contact region. However, in many cases where CL A passes through the bottom of the contact region, decreasing S causes σ_w to increase. Under such circumstances the load intensity is increasing because the entire load W is being distributed along a contact line whose length is decreasing. Load sharing is not taken into account when calculating σ_w. The increase in load intensity more than compensates for the reduction in stress due to the decrease in distance between the load and the fillet. For gear pairs with a face contact ratio less than 1, this behavior occurs at low values of S. At such positions, F_L is both relatively low and decreasing as S decreases. Furthermore, it can be shown that another contact line will be entering the contact region, so the load intensity will, in fact, be constant. The value of σ decreases despite the fact that σ_w is increasing. It follows from these comments that between points B and C the product $F_L\sigma_w$ will always be decreasing. Therefore, the maximum value of σ must occur somewhere along the section of the F_L curve between points A and B. This conclusion applies to all helical gear pairs with m_f less than 1. Since this study is interested primarily in the maximum value of σ, future

graphs of the type shown in Figure 3.2 will show only the curves between $S = S_{max}$ and the highest value of S corresponding to the maximum value of F_L.

Additional information on figures that present quantitative results in this chapter and later chapters may be found in Appendix A.

3.2 $2 - m_p < m_t \leq m_p - 1$

Figure 3.3 shows a series of contact regions for which the total contact ratio m_c is greater than 2. Since $m_c = m_p + m_t$, it follows that $2 - m_p < m_t$. These contact regions also satisfy the condition that m_t is less than $m_p - 1$. These inequalities have several implications. Since m_p is a number between 1 and 2, $m_p - 1$ is a number less than 1. In fact, the expression $m_p - 1$ is the fractional part of m_p. The inequality $m_t < m_p - 1$ therefore implies both that m_t is less than 1 and that the fractional part of m_t is less than the fractional part of m_p. This last implication combined with the condition that m_c is greater than 2 implies that m_p must be greater than 1.5. If the profile contact ratio is less than 1.5 for a pair of gears then the corresponding contact region will not look like those shown in Figure 3.3.

By adding 1 to each side, the inequality $m_t < m_p - 1$ becomes $m_t + 1 < m_p$. Figure 3.3a shows that to satisfy this inequality, CL B must intersect side KL of the contact region when CL A is in the corner position. Under these circumstances the lengths of CL A and CL B will be equal and so the value of F_L will be 0.5. Furthermore, as the gears rotate, F_L will be constant until the position in Figure 3.3b is reached. As CL B then leaves the contact region, as shown in Figure 3.3c, both F_L and the load intensity will increase. The condition $m_c > 2$ implies that

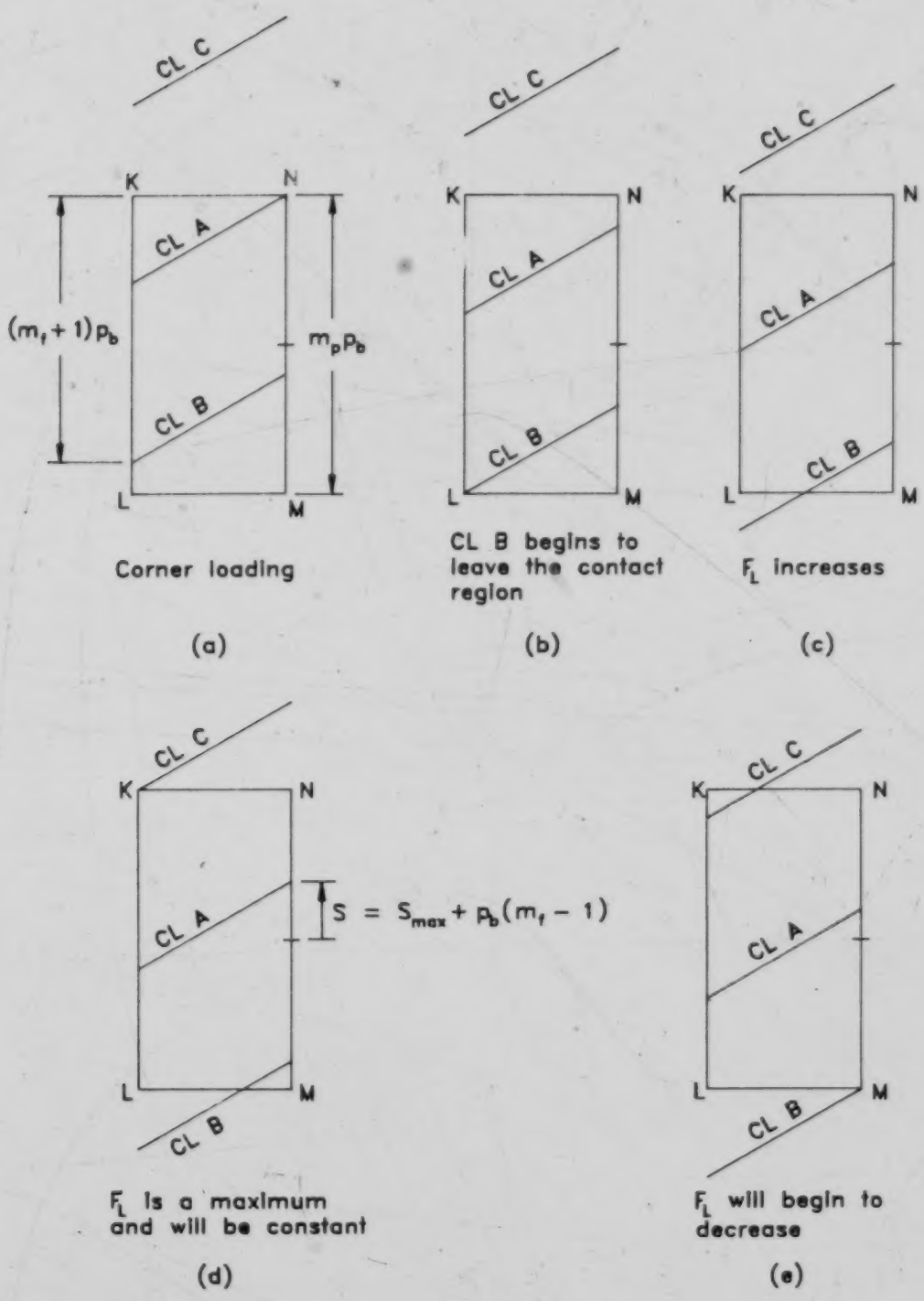

Figure 3.3. Contact region for a pair of helical gears with $m_c > 2$ and $m_f < m_p - 1$.

before CL B completely leaves the contact region CL C will begin entering the region. Figure 3.3d shows the position where CL C is about to enter the contact region and gives the corresponding value of S. As the gears rotate a small amount past this position, L_{tot} will remain constant because one contact line will be entering and one contact line will be leaving the contact region. The load intensity and F_L will also be constant. Finally, as the gears rotate past the position shown in Figure 3.3e, L_{tot} will increase and F_L and W_i will decrease.

According to the preceding discussion, as the gears rotate from the corner loading position, F_L will reach its maximum value at the position shown in Figure 3.3d. This is also the position where the load intensity will be a maximum because L_{tot} will equal L_{min}. The value of S associated with this position is a function of only S_{max}, p_b, and m_t. The value of p_b must be the same for each of the gears in the gear pair, otherwise they simply would not mesh. The value of the face contact ratio is determined by the gear with the smaller face width since this determines the width of the contact region. In this study it is assumed that both gears have the same face width. The value of S_{max} is determined by the tip circle radius of the driven gear and the operating pressure angle of the gear pair. If the operating pressure angle is given then it follows that S_{max}, p_b, and m_t are determined only by the characteristics of the driven gear. Changing the number of teeth of the driving gear will not

affect the value of S associated with the position shown in Figure 3.3d.

The graph in Figure 3.4 shows the variation of F_L, σ_w/σ_T, and σ/σ_T as a function of S as S varies from S_{max} to its value at the position where F_L reaches a maximum. Because $2 < m_c$ the load is always shared between at least two pairs of teeth and F_L does not reach a value of 1. As in the case of spur gears and helical gears with $m_c \leq 2$, the graph shows the dominance of F_L in determining the maximum value of σ. The maximum value of σ occurs when F_L is a maximum.

It should be appreciated that it is not obvious that F_L will necessarily dominate the factor σ_w in determining S_c. Although Figure 3.4 suggests the hypothesis that σ is maximized when F_L is maximized, much more evidence must be produced before such a hypothesis is regarded as proved. The value of F_L can no longer double from 0.5 to 1 as it can when $m_c \leq 2$. On the graph in Figure 3.4 it increases by 80%. It may be the case that for some gear pairs the increase in F_L will not offset the decrease in σ_w as S is reduced from S_{max}. The question of whether such gear pairs exist will be considered at the end of this chapter.

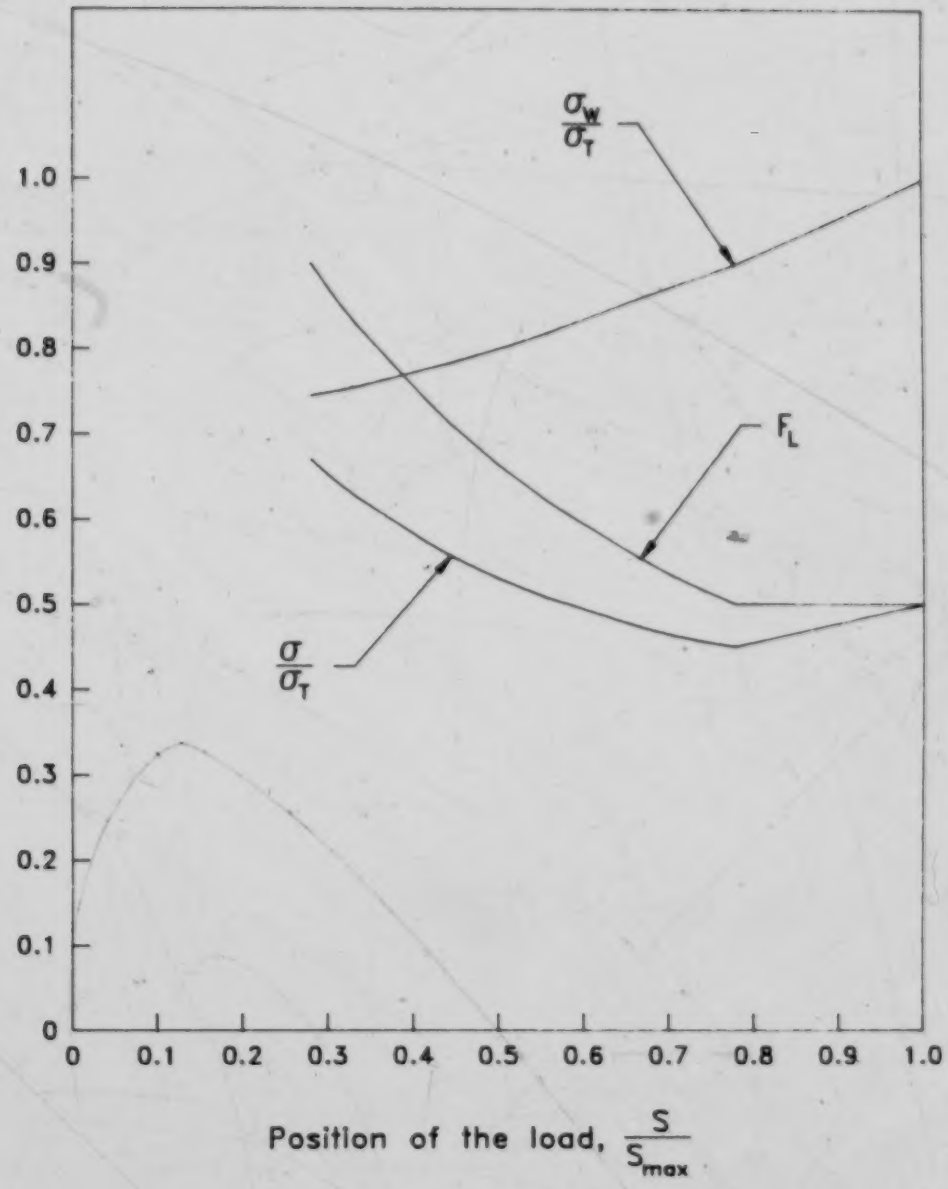

Figure 3.4. Fillet stress parameters versus load position for $m_e > 2$ and $m_f < m_p - 1$.

3.3 $m_p - 1 \leq m_f < 1$

Figure 3.5 shows a series of contact regions subject to the conditions that $m_c > 2$ and $m_p - 1 < m_f < 1$. As mentioned in the last section $m_p - 1$ is the fractional part of m_p. Since it is stipulated that m_f is less than 1, the inequality $m_p - 1 < m_f$ means that the fractional part of m_f is now greater than the fractional part of m_p. Figure 3.5a shows why this last inequality means that CL B must pass through the bottom side LM of the contact region. The proof that the distance betwen points Q and M is equal to $(m_p - 1)p_a$ is not included but is based on the same argument from similar triangles used in Figure 2.6.

Since CL B is already in the process of leaving the contact region in the corner loading position shown in Figure 3.5a, the value of F_L will be greater than 0.5. As the gears rotate L_B and L_{tot} will both decrease and F_L and W_i will increase. Again, both F_L and W_i will reach a maximum value in the position shown in Figure 3.5b in which CL C is on the verge of entering the contact region. Continued rotation will cause CL C to enter the contact region. The values of L_{tot}, F_L, and W_i will all be constant until CL B leaves the contact region completely. The load intensity and F_L will then decrease as L_{tot} increases. The value of S that maximizes F_L is shown in Figure 3.5b. This expression is identical to the one found in the last section. Both are based on the same condition that CL C be on the verge of

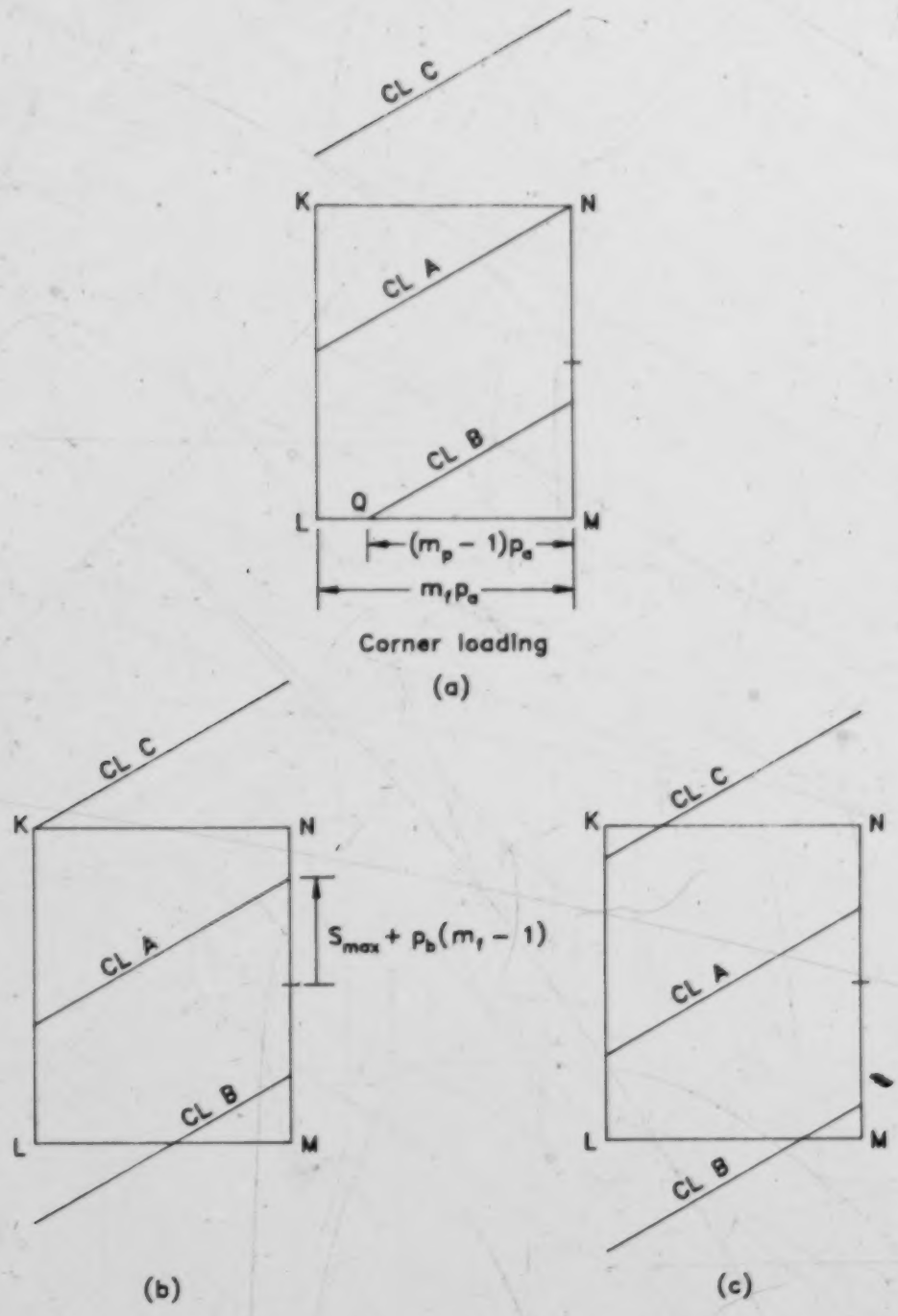

Figure 3.5. Contact region for a pair of helical gears with $m_e > 2$ and $m_p - 1 < m_f < 1$.

entering the contact region.

The graph in Figure 3.6 shows an F_L curve that varies even less than that shown in the last section. F_L no longer begins at 0.5 at $S = S_{max}$ and certainly does not reach a value of 1. The value of F_L increases by 29% from its value at the corner loading position. Compensating for this loss in variation is the fact that F_L begins its increase immediately and reaches its maximum value at a relatively high value of S. Therefore, during the interval that F_L grows to its maximum, the amount by which σ_w has decreased is less. Figure 3.6 again shows the maximum stress σ occurring at the point where F_L reaches its maximum value. Again the question arises as to whether some change in the gear pair will create a situation where σ_w will proportionally decrease more rapidly than F_L increases.

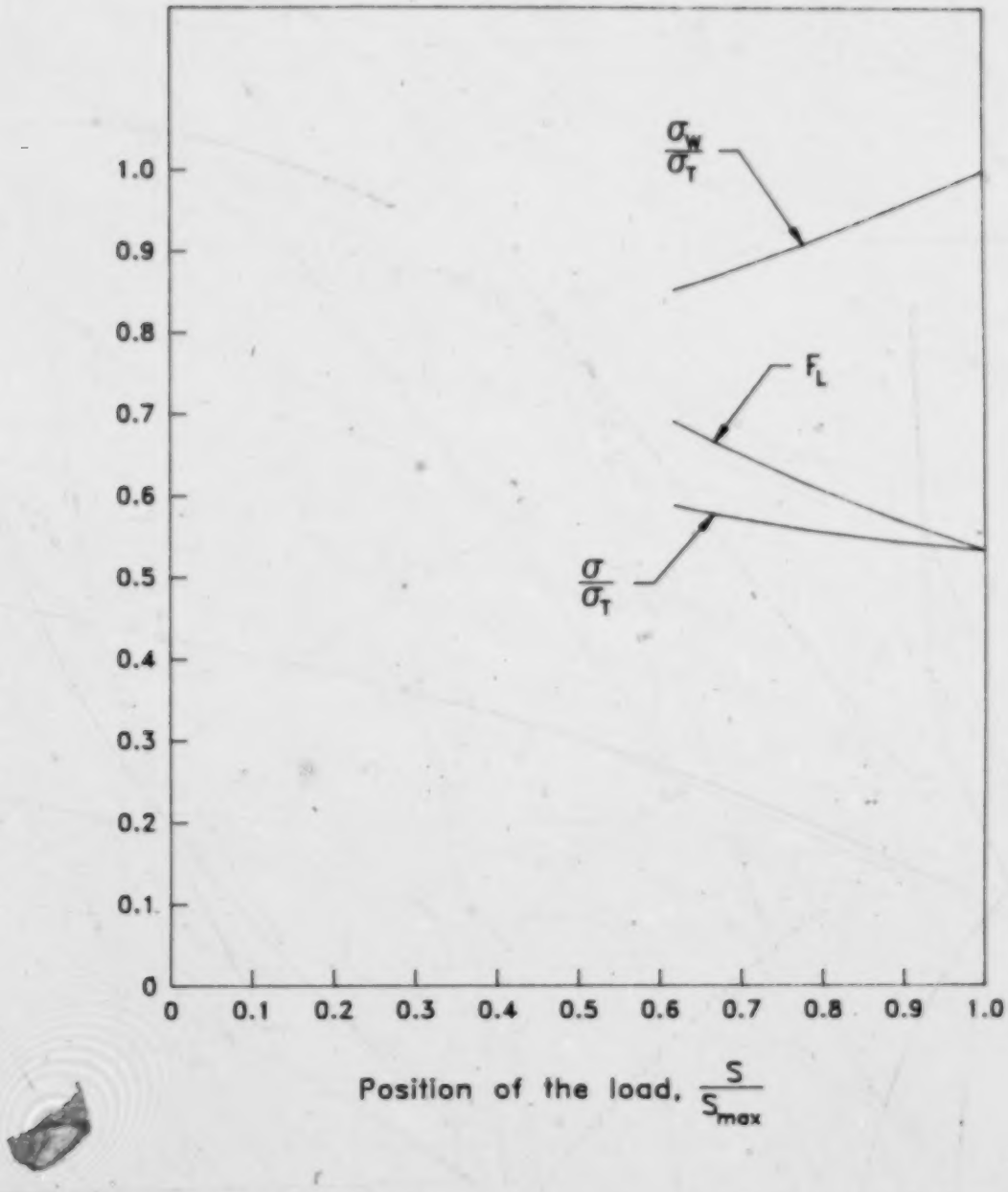

Figure 3.6. Fillet stress parameters versus load position for $m_e > 2$ and $m_p - 1 < m_f < 1$.

3.4 $1 \leq m_f$

Figure 3.7 shows the contact region of a helical gear with a face contact ratio of 1.0. In the corner loading position in Figure 3.7a CL C is just about to enter the contact region and CL B is leaving the contact region. Because one contact line is entering and one is leaving, rotation of the gears to the position in Figure 3.7c will cause no change in L_{tot} or the load intensity. In Figure 3.7a, b, and c the length of CL A is constant so F_L will also be constant. In Figure 3.7c CL B has completely left the contact region and CL A is just about to begin leaving. Again, as the gears rotate one contact line will be entering, one will be leaving, and L_{tot} will not change. Since L_A is now decreasing, the value of F_L will decrease. Eventually CL C will finish entering and will pass through corner N. The situation is then the same as that shown in Figure 3.7a. At no time during this cycle does L_{tot} change. The load intensity also will not change. No stresses need to be calculated to find S_c. At the corner loading position F_L is a maximum and the load line is in its best position for creating stress in the fillet. The critical value of S is S_{max}.

If m_f were increased to a value of 2 or 3 or any whole number, similar observations to those in the last paragragh could be made. So long as m_f is a whole number, the total length of the contact lines is constant, the load intensity

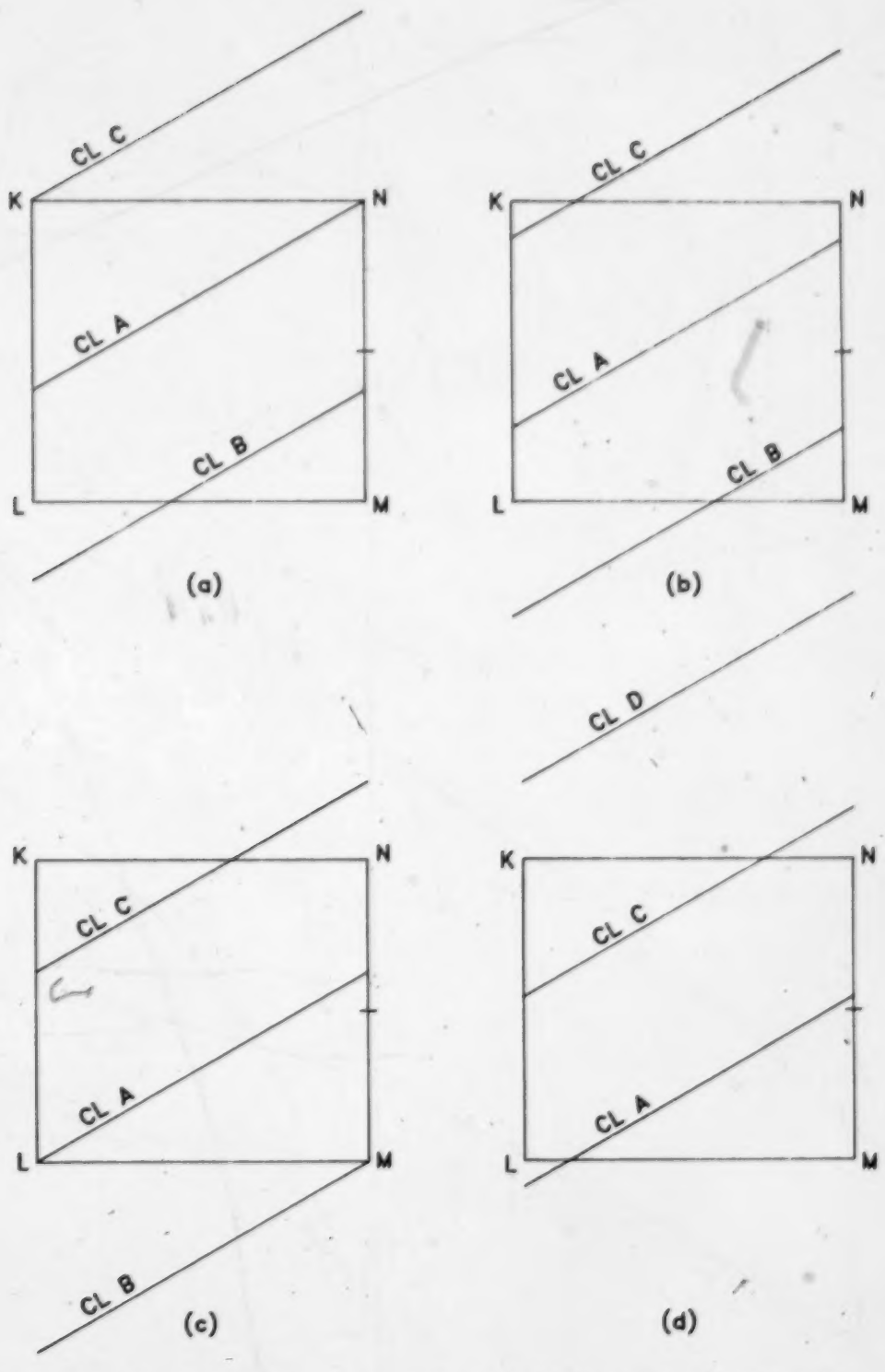

Figure 3.7. Contact region for a pair of helical gears with $m_f = 1$.

is constant, and the maximum fillet stress occurs with a corner loading.

Figure 3.8 shows a typical contact region for helical gears satisfying the inequality $1 < m_f \leq m_p$. Figure 3.8a shows that this inequality implies that CL A must pass through side KL. Because m_p is a number between 1 and 2 this inequality also implies that that fractional part of m_f is less than the fractional part of m_p.

As the gears rotate from position in Figure 3.8a to the position in 3.8b, CL C is entering the contact region, CL B is leaving the contact region, the length of CL A is constant, and therefore L_{tot}, F_L, and W_i will all be constant. As the contact lines move past the position in Figure 3.8b, a process not yet examined occurs. For a short time both CL A and CL B are leaving the contact region and CL C is entering. The effects on L_{tot} due to CL B and CL C may be cancelled. The net effect on L_{tot} is then the effect of CL A leaving the contact region. Obviously, L_{tot} will decrease at the rate that L_A decreases. Anytime L_{tot} decreases the load intensity increases. What is the effect on F_L in this case? In previous sections a decrease in L_{tot} also corresponded to an increase in F_L because, by definition, $F_L = L_A/L_{tot}$ and it was also the case that L_A was constant. Now, both L_A and L_{tot} are decreasing. The definition of F_L implies that F_L may range in value between 0 and 1. It is easily proven that if a fraction between 0

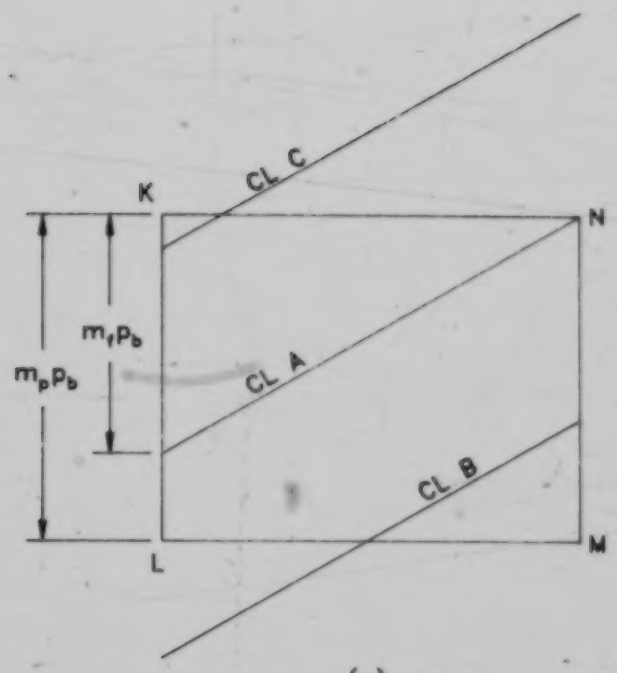

(a)

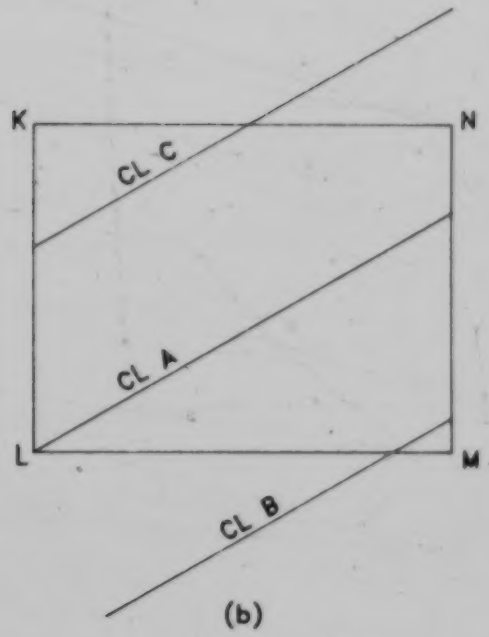

(b)

Figure 3.8. Contact region for a pair of helical gears for $1 < m_f \leq m_p$.

and 1 has both its numerator and denominator decreased by a small amount, the resulting fraction will be less than the original fraction. For example, if the numerator and denominator of the fraction 7/9 are reduced by 2 the resulting fraction is 5/7. The fraction 5/7 is less than 7/9. It follows that an equal reduction in L_A and L_{tot} will result in a decrease in F_L. As the gears rotate past the position shown in Figure 3.8b the load intensity will increase and F_L will decrease.

It was noted in the discussions of helical gears with $m_f < 1$ that the maximum value of F_L coincided with the maximum load intensity. In the case under discussion the load intensity is a minimum when F_L is a maximum. Because CL A passes through side KL of the contact region, σ_w will decrease as S decreases from S_{max}. Since F_L is a maximum at the corner loading position, it follows that this position creates maximum fillet stress.

In Figure 3.9 the fractional part of m_f is larger than the fractional part of m_p. In the corner loading position CL A now passes through the bottom side LM. Because $m_f < 2$, CL D has not yet entered the contact region. As the contact lines move from the position in Figure 3.9a to the position in Figure 3.9b, CL A and CL B will be leaving and CL C will be entering the contact region. It has just been explained that in such a situation F_L will decrease and the load intensity will increase. Since CL A passes through the

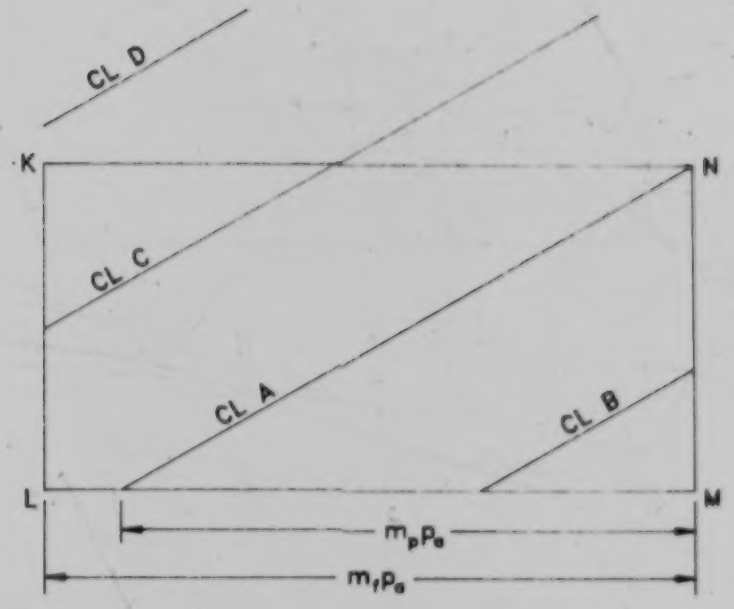

(a)

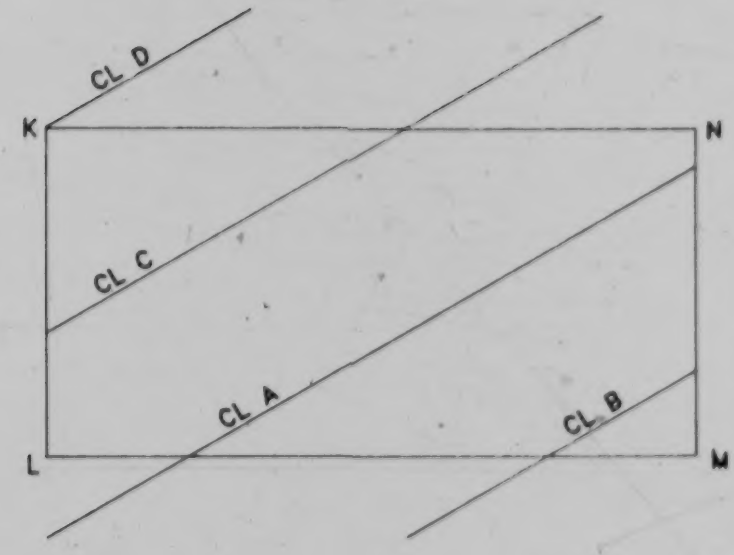

(b)

Figure 3.9. Contact region for a pair of helical gears with $m_p < m_f \leq 2$.

bottom side of the contact region, it cannot be assumed that σ_w will decrease as S decreases. If σ_w decreases then clearly the maximum fillet stress will occur during the corner loading position. For those cases where σ_w increases the question is not so easily settled. According to AGMA 218.01, the corner loading position ($S/S_{max} = 1$) causes maximum fillet stress whenever $1 \leq m_t$. In this study an exception was found. Using a gear pair with a 30° helix angle and with m_t just slightly greater than m_p, it was found that the maximum stress occurs at the position of maximum load intensity at $S/S_{max} = 0.39$. The stress at this position was found to be 7.0% higher than the stress caused by the corner loading. It was reasoned that decreasing the helix angle should reduce the variation of load intensity and tend to move the position of maximum stress back to the corner position. Pairs of gears were tested with helix angles of 25° and 20° and with m_t again just slightly greater than m_p. For the gear pair with a 25° helix angle, σ was just 1% higher at the position of maximum load intensity compared to σ for the corner loading. For the gear pair with a 20° helix angle, σ began decreasing immediately as S was reduced from S_{max}. It was also reasoned that increasing face width would decrease the variation in load intensity and the position of maximum stress would again move toward the corner position. The gear pair with the 30° helix angle had its face width increased from $m_t/m_p = 1.06$ to $m_t/m_p = 1.29$. As S decreased from S_{max} the value of σ was constant to

within 0.2% for a short interval before beginning a steady decrease. A thorough examination of the circumstances under which the corner loading position is not the position causing maximum stress was not undertaken. From the tests performed it appears that cases where the position of maximum load intensity causes a significantly higher stress than the corner position are relatively rare. A helix angle greater than 25° and m_f/m_p close to 1 appear to be necessary conditions.

If m_f is increased to a value greater than 2, CL D will pass through the contact region in the corner loading position shown in Figure 3.10a. So long as the fractional part of m_f is less than the fractional part of m_f, CL C will pass through the side KL of the contact region. When the fractional parts are equal, CL C will pass through point L and when the fractional part of m_f is greater than the fractional part of m_p, CL C will pass through the bottom side LM as shown in Figure 3.10b. CL E will not intersect the contact region in the corner loading position until m_f is increased to more than 3.

In the contact region shown in Figure 3.10a a small rotation of the gears will cause L_{tot} and W_i to remain constant since two lines are entering and two lines are leaving the the contact region. F_L will decrease immediately since CL A is leaving the contact region. When CL B completely leaves the contact region, L_{tot} will begin to

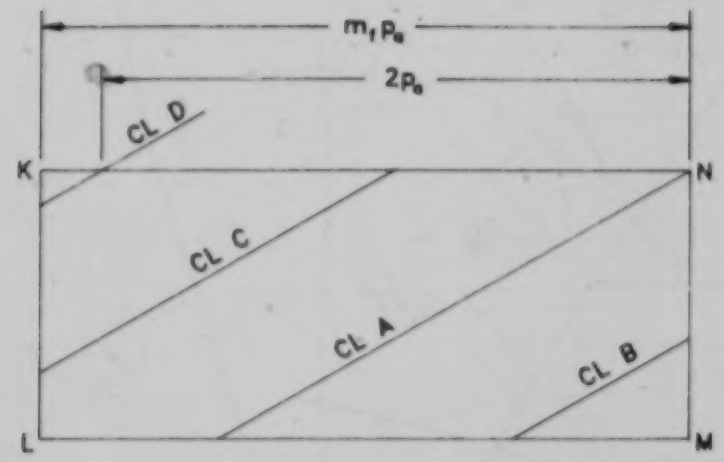

$2 < m_f \leq m_p + 1$

(a)

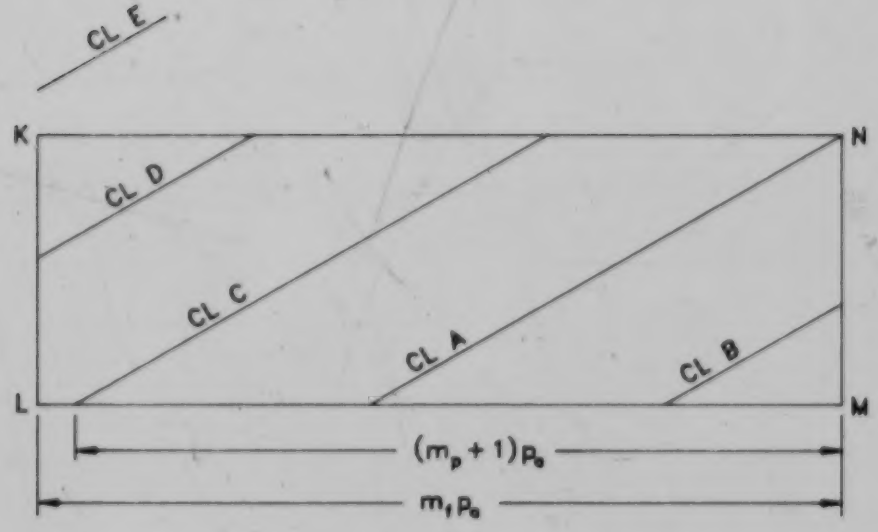

$m_p + 1 < m_f \leq 3$

(b)

Figure 3.10. Contact regions for helical gears with large face contact ratios.

decrease and the load intensity will increase. F_L will continue to decrease. In light of the previous discussions it is clear that the maximum fillet stress will occur when CL A is in the corner loading position where F_L is a maximum and W_i is a minimum. In Figure 3.10b the corner loading position has two lines leaving and one line entering the contact region. CL C is neither entering nor leaving the region. Rotation will cause L_{tot} and F_L to decrease and W_i to increase. Because L_{tot} is relatively large the variation in W_i will be small. The maximum fillet stress will occur in the corner position where F_L is a maximum and W_i is a minimum.

3.5 The Position Causing Maximum Fillet Stress

A number of observations can be made regarding the sequence of detailed discussions just completed. It is clear that for helical gears with a total contact ratio less than 2, the maximum fillet stress will occur at the position of highest point of single tooth contact. This conclusion is consistent with what is known about spur gears. For gears with a face contact ratio greater than 1, the maximum fillet stress usually occurs at the corner loading position, though some exceptions exist. In both cases the critical position is the position where F_L is a maximum. For those gears which have a total contact ratio greater than 2 and a face contact ratio less than 1, there is evidence that suggests that the maximum fillet stress again corresponds to the position that maximizes F_L. At this point this evidence consists of the graphs shown in Figure 3.4 and Figure 3.6. Both these graphs show the dominance of F_L over σ_w in determining where σ reaches its maximum value. The question is whether these graphs are typical or if cases can be found where the decrease in σ_w is proportionally greater than the increase in F_L as S decreases from S_{max}. In other words, the hypothesis to be tested is the assertion that σ always reaches its maximum value when F_L reaches its maximum value.

The discussion of how this hypothesis was tested will be easier if some new symbols are defined. First, the maximum value of F_L and the value of F_L for the corner

loading position will be denoted F_{LM} and F_{LT} respectively. A mathematical formulation of the hypothesis is then simply $F_{LC} = F_{LM}$. Second, the ratio of σ at $F_L = F_{LT}$ to σ at $F_L = F_{LM}$ will be denoted R_σ. Please note that in those cases where $F_L = F_{LM}$ for a range of positions, the position being specified is that which has the largest value of S. The hypothesis $F_{LC} = F_{LM}$ implies simply that R_σ is always less than 1.

Initially, a sensible way of testing the hypothesis is to calculate F_L, σ_w, and σ curves for a wide variety of gear pairs. Since the analysis of a single pair of gears with the finite element programs requires approximately one hour of computing time, limitations had to be placed on the variety of gear pairs tested. With a few exceptions the gears tested in this study had the following characteristics: they were assumed to be cut by a rack cutter with a tip round of $0.3m_n$ and pressure angle of 20° in the normal section, the profile shift was set to zero, the addendum and dedendum of both gears was set equal to m_n and $1.25m_n$ respectively, the gears were mounted at the standard center distance, and a Poisson's ratio of 0.3 was assumed for the material of the gears. Under these circumstances the amount of backlash is equal to zero. The helix angle, the number of teeth on each gear, and the face width were allowed to vary. The value of the helix angle in these early tests was varied between 15° and 30°.

The results from the finite element analysis supported the hypothesis. Investigations were then undertaken to gain a better understanding of how the σ_w and F_t curves were affected by changes in helix angle, numbers of teeth, and face width. The aim of such understanding would be increased efficiency in the search for examples which would disprove the hypothesis. It was noticed that plots of σ_w/σ_T versus S/S_{max} were similar for many gear pairs. Further testing showed that the amount of variation in such plots was primarily a function of helix angle. Figure 3.11 shows plots of σ_w/σ_T for helix angles ranging from 0 to 30°. These plots are all for gears with a face width of $4m_n$ and 40 teeth. Clearly, increasing helix angle corresponds to decreasing variation in stress for a constant tooth load. Since all the curves in Figure 3.11 must by definition pass through the point (1,1), the variation in σ_w/σ_T can be assessed on the basis of the value of σ_w/σ_T at $S = 0$. By definition, V_σ will equal $1 - \sigma_w/\sigma_T$ at $S = 0$. A large value of V_σ means the fillet stress decreases a relatively large amount as a constant tooth load moves from $S = S_{max}$ to $S = 0$. In Figure 3.11 the value of V_σ is 0.207 for the tooth with the 30° helix angle. The value of V_σ increases by 92% to 0.397 when the helix angle is reduced to zero.

Changing the number of teeth and changing the face width affect V_σ less than a change in helix angle. When the number of teeth is doubled from 20 to 40 for a gear with a

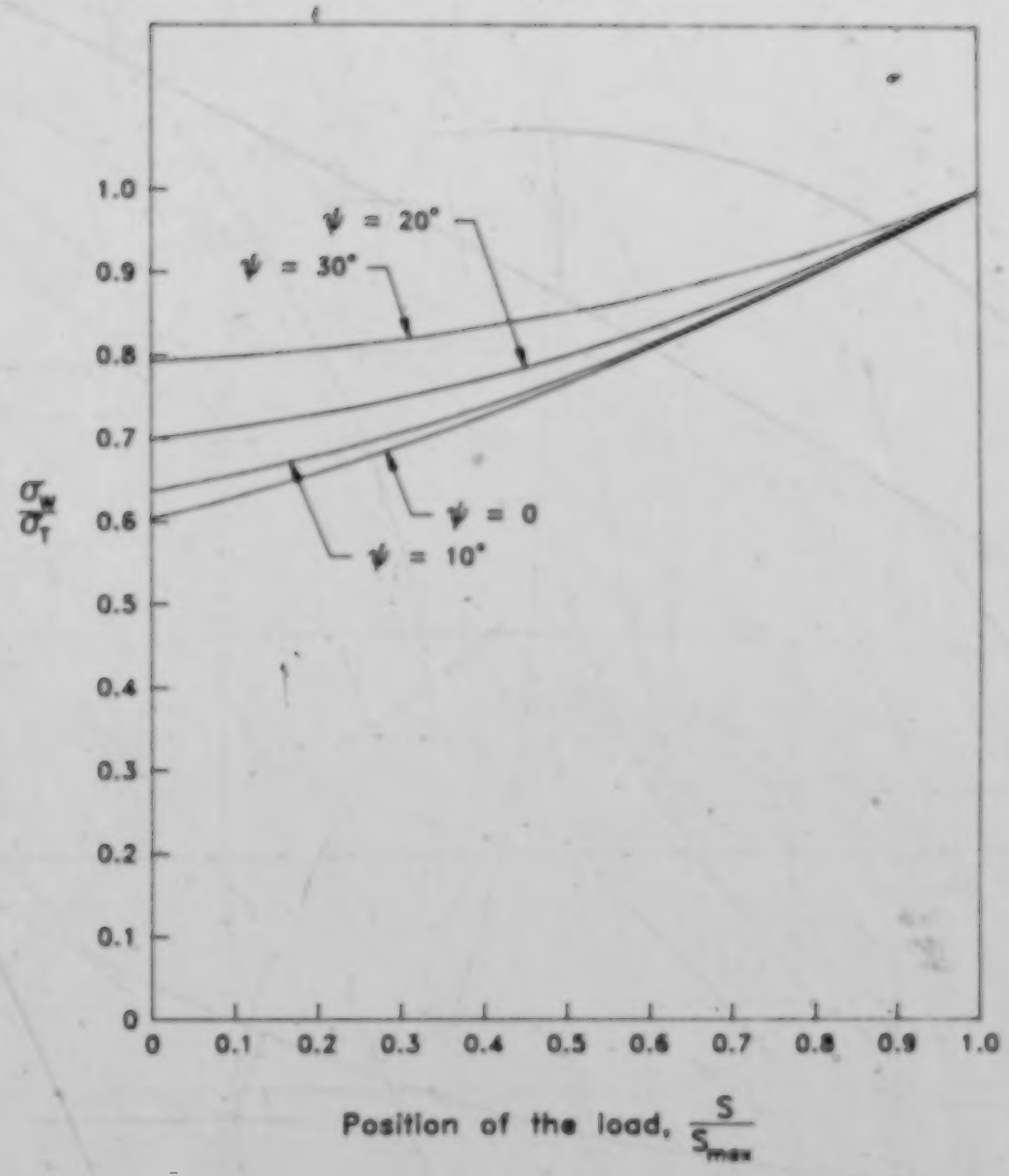

Figure 3.11. Fillet stress versus load position for different helix angles.

helix angle of 20°, V_σ increases by 15% from 0.263 to 0.302. Doubling the number of teeth again to 80 teeth causes V_σ to increase by only 5% to 0.318.

An explanation for the effect of tooth number on V_σ can be obtained by looking again at Figure 1.4 in the first chapter of this study. Figure 1.4 shows three loads on the tooth profile. As described before, the loads may be resolved into a tangential component and a radial compressive component. The radial compressive stress tends to reduce the tensile stress caused by the bending load. As the load moves from the tip of the tooth towards the root, the load vector rotates, the radial component decreases in magnitude, and the tangential component increases in magnitude. Decreasing the radial component and increasing the tangential component tends to increase the tensile fillet stress. This tendency partially counteracts the reduction in stress caused by moving the load closer to the root and, therefore, contributes to a lessening of V_σ. This counteracting tendency will be strongest for teeth with a small radius of curvature. For teeth with a straight profile the components of the load will be constant, the counteracting tendency will not exist, and V_σ will be relatively large. Increasing the number of teeth on a gear causes a straighter tooth profile and, therefore, also causes V_σ to increase. The greatest change in the curvature of a gear tooth's profile occurs when the number of teeth is low. This fact explains why doubling the number of teeth

from 20 to 40 causes a much greater change in V_σ than doubling from 40 to 80 teeth.

Increasing the face width of a spur gear with 40 teeth from $4m_n$ to $6m_n$ causes V_σ to increase 1.2%. Increasing the face width of a helical gear with 40 teeth and a helix angle of 20° from $4m_n$ to $6m_n$ causes a decrease in V_σ of 8%. An increase to $7m_n$ for the helical gear causes an additional 1.6% decrease in V_σ. Finally, increasing the face width of a helical gear with a 10° helix angle from $4m_n$ to $6m_n$ causes a 3.5% decrease in V_σ. The effect of face width on V_σ was not thoroughly explored. However, the evidence collected shows that the effect of increasing face width is relatively small and that this small effect rapidly decreases as the face width increases.

The curves in Figure 3.11 form the basis of a set of programs which will be called the HTEST programs. The HTEST programs assume that the σ_w/σ_T curve for a gear with a face width of $4m_n$, with 40 teeth, and with some helix angle is representative of all gears with that same helix angle, as long as m_t is less than 1. As has been stated in a previous section, when m_t is large enough to cause CL A to pass through the bottom side of the contact region, σ_w increases as the load moves towards the root. By stipulating that m_t is less than 1 these circumstances are avoided. A fourth degree polynomial was fitted to each of the σ_w/σ_T curves for gears with helix angles of 0, 10°, 15°, 20°, and 30°. Values

of σ_w/σ_T for helix angles between those just listed are found by linear interpolation. One version of the HTEST program varies the number of teeth on the driven gear from 20 to 80 teeth in 10 tooth increments, varies the number of teeth on the driving gear from 20 to 300 teeth in one tooth increments, varies the helix angle from 0 to 30° in 2.5° increments, and varies the face contact ratio from $2 - m_p$ to 1 in increments of 0.05. In this way over 250000 pairs of teeth are considered. HTEST calculates R_σ for each pair and records those circumstances, if any, which yield a value of R_σ that is greater than 1. Many examples were indeed found where R_σ is greater than 1. Strictly speaking, the hypothesis is therefore disproved. However, the practical usefulness of the hypothesis is still to be considered. Before making this evaluation several other points need to be presented.

As explained in section 3.2, the value of S corresponding to the maximum value of F_L is not influenced by the number of teeth on the driving gear if the operating pressure angle is kept constant. Therefore, once the driven gear is specified, the amount by which σ_w decreases as F_L reaches its maximum value is fixed. If $2 - m_p < m_t \leq m_p$, then F_{LM} is $m_t/(m_p + 2m_t - 2)$. The value of F_{LT} is either 0.5 or $m_t/(m_t + m_p - 1)$, depending on which of the fractional parts of m_t and m_p is greater. The ratio of F_{LM} to F_{LT} is therefore either $2m_t/(m_p + 2m_t - 2)$ or $(m_t + m_p - 1)/(m_p + 2m_t - 2)$.

Obviously, for a given value of m_t, the only parameter that affects these values and ratios is m_p. Increasing m_p causes F_{LM} to decrease and also causes F_{LM}/F_{LT} to decrease. Increasing the number of teeth on the driving gear causes m_p to increase. Therefore, once a pair of gears is found for which R_σ is equal to 1, any increase in the number of teeth on the driving gear will increase R_σ to more than 1. A decrease in the number of teeth on the driving gear will make R_σ less than 1.

A more sophisticated version of HTEST finds the number of teeth required on the driving gear to make R_σ greater than each of the numbers 1.00, 1.01, 1.02, and 1.03 in turn. The maximum number of teeth allowed on the driving gear was limited to 300. As an example of the results from HTEST, consider a driven gear with 40 teeth and a helix angle of 10°. Meshing this gear with a driving gear having 79 teeth will yield a value of 1.0001 for R_σ when m_t is equal to 0.95. If the driving gear has 103 teeth and m_t is equal to 0.55 then R_σ has a value of 1.01. To obtain a value of R_σ equal to 1.02 requires 122 teeth on the driving gear and again a face contact ratio of 0.55. R_σ will be greater than 1.03 if the number of teeth on the driving gear is increased to 149 teeth and m_t is 0.55. If the helix angle is increased to 12.5°, then a 40 tooth driven gear must be meshed with driving gears with 207 and 293 teeth to give values of R_σ greater than 1.01 and 1.02 repectively. In both cases the

value of m_t must again be equal to 0.55.

The results of the HTEST programs make sense. If the value of V_σ is small and the ratio F_{LH}/F_{LT} is large then it is unlikely that R_σ will be greater than 1. Increasing helix angle is the primary cause of decreasing V_σ. Increasing helix angle also tends to reduce m_p and, therefore, causes an increase in the ratio F_{LH}/F_{LT}. One would expect values of R_σ greater than 1 to be increasingly rare as helix angle is increased. With the number of teeth on the driven gear limited to 80 and the number of teeth on the driving gear limited to 300, no cases were found where R_σ was greater than 1.01 for gears with a helix angle of 17.5° or greater.

According to the reasoning just presented, the highest values of R_σ will occur with small helix angles. Using an interactive version of HTEST, circumstances were found which yielded a value of R_σ of 1.25. The gears that produced this result each had 200 teeth, had a helix angle of 1°, and a face contact ratio of 0.3. In practice such a gear pair would never be designed.

Figure 3.12 and Figure 3.13 show F_L curves for a range of face contact ratios. Figure 3.12 is for a pair of gears with a helix angle of 20°, 40 teeth on the driven gear and a profile contact ratio of 1.6. Figure 3.13 is for a pair of gears with a helix angle of 2.5°, 80 teeth on the driven gear and m_p = 1.8. The differences between these graphs are

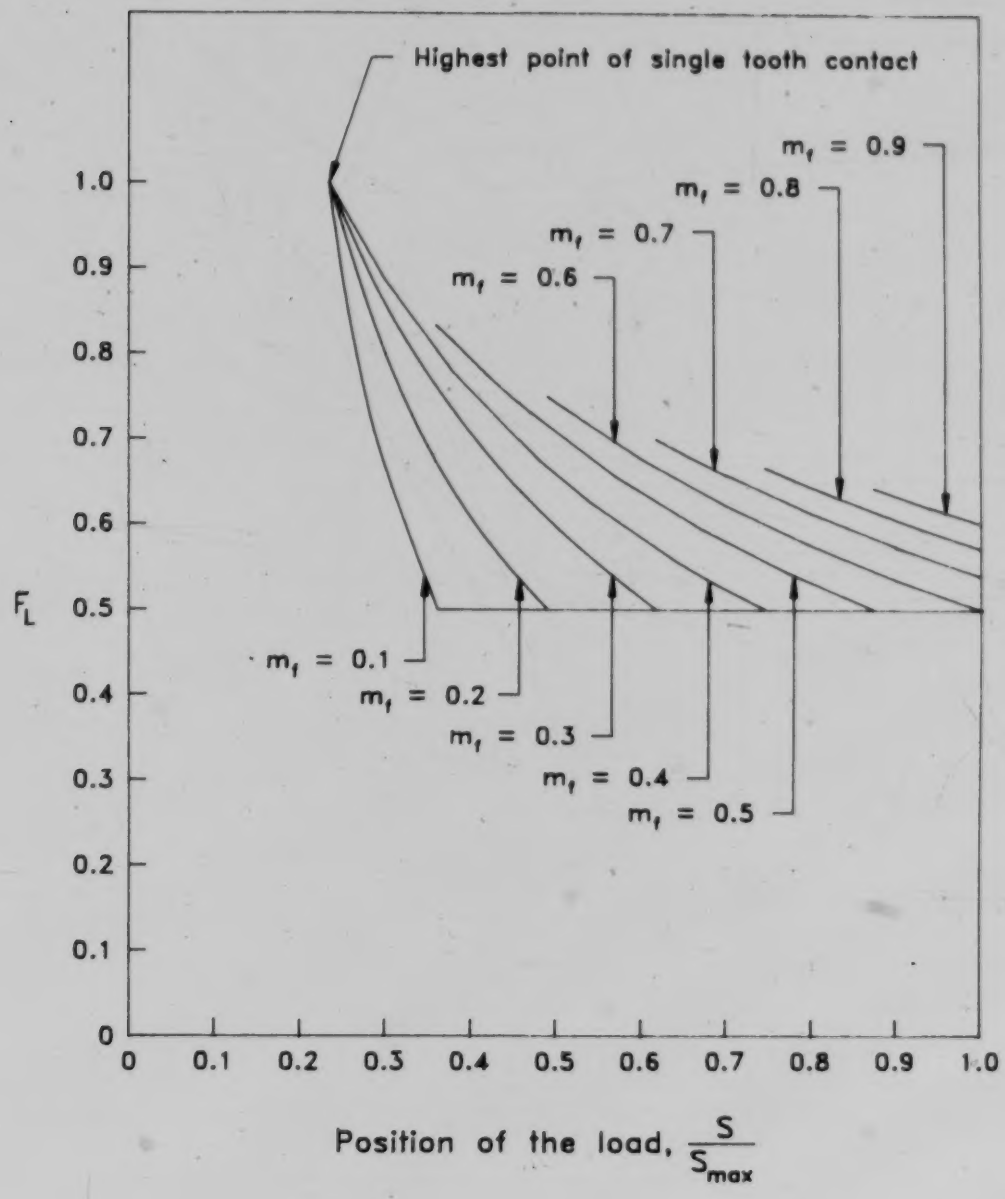

Figure 3.12. Fraction of the load versus load position for different face contact ratios with a helix angle of 20°.

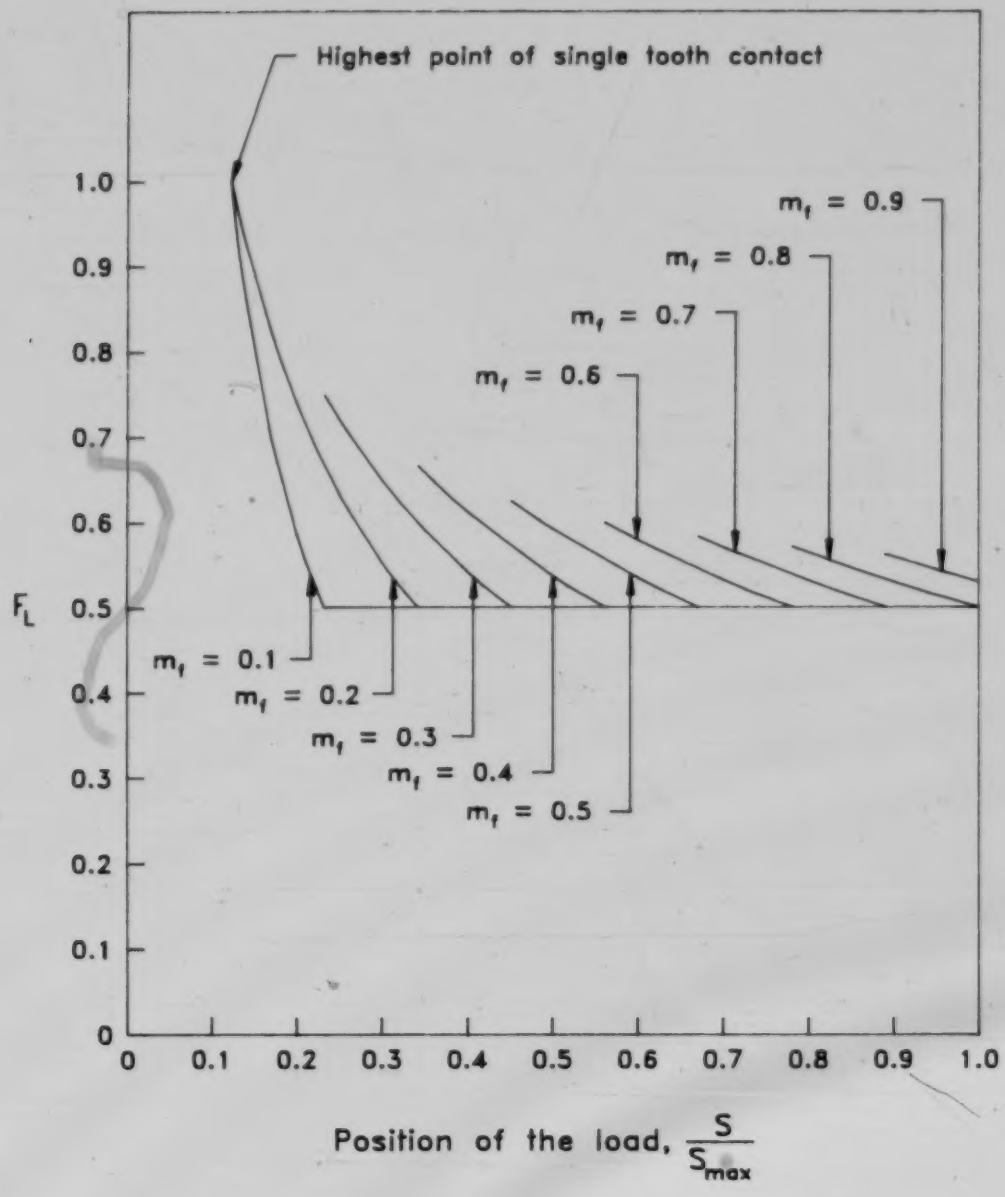

Figure 3.13. Fraction of the load versus load position for different face contact ratios with a helix angle of 2.5°.

easily seen. The rate at which F_{LM} decreases for increasing m_t is much greater in Figure 3.13. Also, F_{LM} tends to occur at lower values of S in Figure 3.13 as compared to Figure 3.12. Having relatively low values of F_{LM} at low values of S are precisely the conditions which would cause high values of R_σ.

The hypothesis that $F_{LC} = F_{LM}$ has been shown to be false. However those cases which disprove the hypothesis would be rarely encountered in the real world. A value of R_σ of 1.02 means that σ for a corner loading will be 2% higher than σ at the position of F_{LM}. In this case, mistakenly calculating the maximum stress at the position of F_{LM} has little practical significance. If a value of R_σ of 1.02 is regarded as a tolerable error and if the numbers of teeth on the driven and driving gears are limited to 80 teeth, then the hypothesis $F_{LC} = F_{LM}$ is valid for helix angles greater than or equal to 12.5°. If the numbers of teeth are restricted to 70 on each gear then the hypothesis is valid for helix angles greater than or equal to 10°. Gear pairs outside these limits are relatively rare so the hypothesis has in fact a large scope of validity. It should be emphasized that for gear pairs outside the limits just given it does not follow that the maximum stress will necessarily occur in the corner loading position rather than the position of F_{LM}. Only for some values of m_t will R_σ be greater than 1.02. Usually the required value of m_t is near 0.55.

The work of J.R. Colbourne [5] has been mentioned in the first two chapters of this thesis in connection with the issue of the position producing maximum fillet stress. Colbourne's conclusions are stated in terms of load intensity. He claims that the position of maximum stress occurs when the load intensity is a maximum for helical pairs with $m_f < 1$. For helical gears with $1 \leq m_f$, he claims the position of maximum stress occurs in the corner loading position where the load intensity is a minimum. As was pointed out in earlier sections, F_L is a maximum when W_i is a maximum for $m_f < 1$, and F_L is a maximum in the corner loading position where W_i is a minimum. The assertion that fillet stress is maximized when F_L is maximized is identical in substance to the conclusions reached by Colbourne. In the last section it was reported that a case was found where $1 \leq m_f$ and the maximum stress occurred at the position of maximum load intensity. It was remarked that the few tests done suggested that exceptions such as the one found would be rare. In this section the hypothesis was investigated for $2 - m_p < m_f < 1$. Again, exceptions were found. However, the exceptions of significance ($R_\sigma > 1.2$) are created by gear pairs that would rarely, if ever, be used in a practical design problem.

Figure 3.14 lists sets of equations that give critical values of S and F_L for various face contact ratios. These equations assume $F_{LC} = F_{LM}$. Equations (3) and (4) give F_{LC}

Critical values of F_L

(1) $m_c \leq 2$ $\qquad F_{LC} = 1$

(2) $2 - m_p < m_f \leq m_p$ $\qquad F_{LC} = \dfrac{m_f}{m_p + 2(m_f - 1)}$

For $n = 2, 3, 4, \ldots$

(3) $m_p + n - 2 < m_f \leq n$ $\qquad F_{LC} = \dfrac{m_p}{m_f + n(m_p - 1)}$

(4) $n < m_f \leq m_p + n - 2$ $\qquad F_{LC} = \dfrac{m_p}{2m_f + n(m_p - 2)}$

Critical values of S

(5) $m_c \leq 2$ $\qquad S_C = S_{max} - p_b(m_p - 1)$

(6) $2 - m_p < m_f < 1$ $\qquad S_C = S_{max} + p_b(m_f - 1)$

(7) $1 \leq m_f$ $\qquad S_C = S_{max}$

Figure 3.14. Critical values of F_L and S.

for $m_p < m_f$. The inequality specifying the validity of equation (3) is equivalent to the statement that the fractional part of m_f is greater than the fractional part of m_p. If the fractional part of m_f is less than the fractional part of m_p, then equation (4) is used. Understanding the inequalities in this way makes programming these equations for a computer very easy.

Chapter 4: The Finite Element Programs

4.1 Introduction

Two complete and autonomous sets of programs were written for two-dimensional (2D) and three-dimensional (3D) finite element analysis. The 2D program uses eight node quadrilateral elements and the 3D program uses twenty node brick elements. In each case the elements are isoparametric. The 3D programs will be described in some detail. The basic structure of both sets of programs is identical. For the remainder of this chapter any reference to finite element programs can be taken as a reference to the 3D programs unless otherwise indicated.

The finite element programs can be separated into three distinct parts. The first part generates information pertaining to the nodes, elements, and loads, and will be called the mesh generation program. The second part creates the stiffness matrix, solves the equilibrium equations, and outputs displacements. This part will be called the finite element program. The third part uses the displacements outputted from the finite element program to compute stresses at specified locations and outputs these stresses in a convenient format. This part will be called the stress output program.

4.2 Introduction to the Mesh Generation Program

The mesh generation program originally outputted nodal and element information in a format that could be used by ADINA, a commercial finite element program bought several years ago by the Department of Civil Engineering. ADINA proved to be inflexible, inconvenient, and expensive. It was decided that the author of this thesis would write his own programs. As a result of this decision the mesh generation program was expanded so that it now computes much of the information normally computed by a finite element program. For example, the mesh generation program numbers the equilibrium equations and creates the arrays that specify the structure of the stiffness matrix. Having these calculations done in this section means that information concerning the number of degrees of freedom and the size of the stiffness matrix is available before submitting the job to the finite element program. It is then known whether the arrays in the finite element program are sufficiently large and estimates can be made as to how long the finite element program will run.

The mesh generation program creates meshes for spur gears, helical gears, and cantilever beams with uniform rectangular cross-section. Figure 4.1 shows an oblique drawing of a spur gear and Figure 4.2 shows an oblique drawing of a cantilever beam. A close look at these two figures will show that they have identical basic element

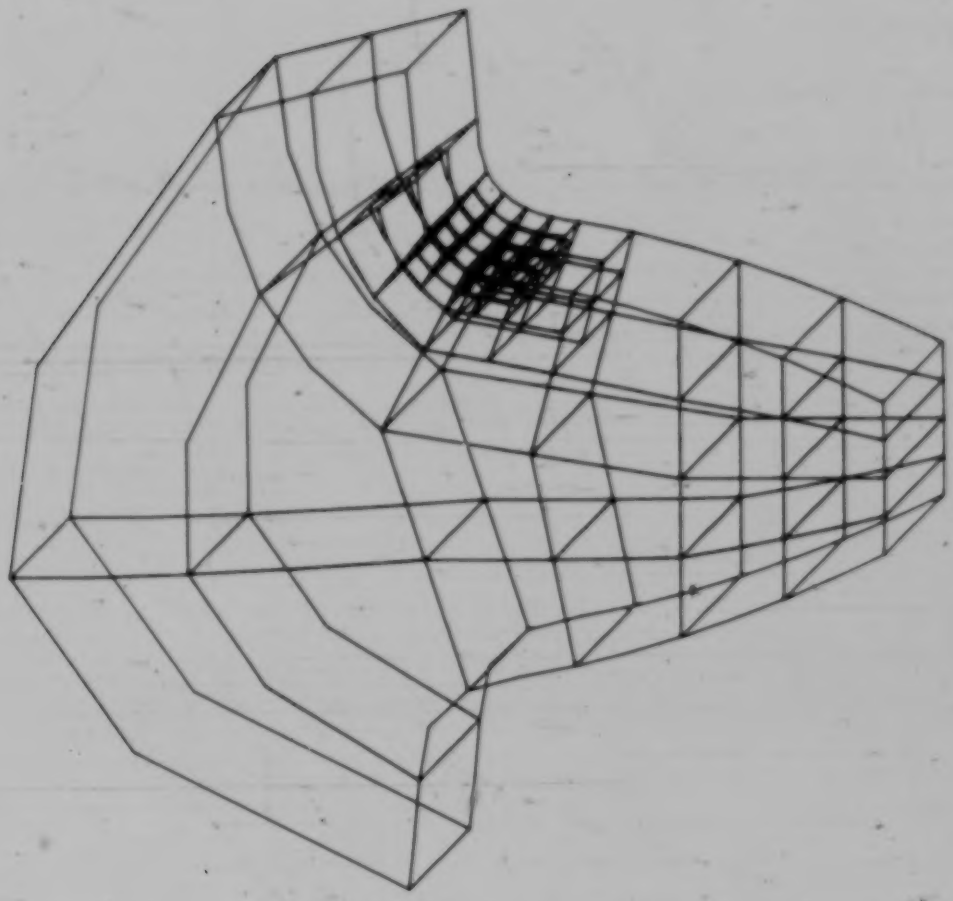

Figure 4.1. A 3D drawing of a finite element mesh for a spur gear.

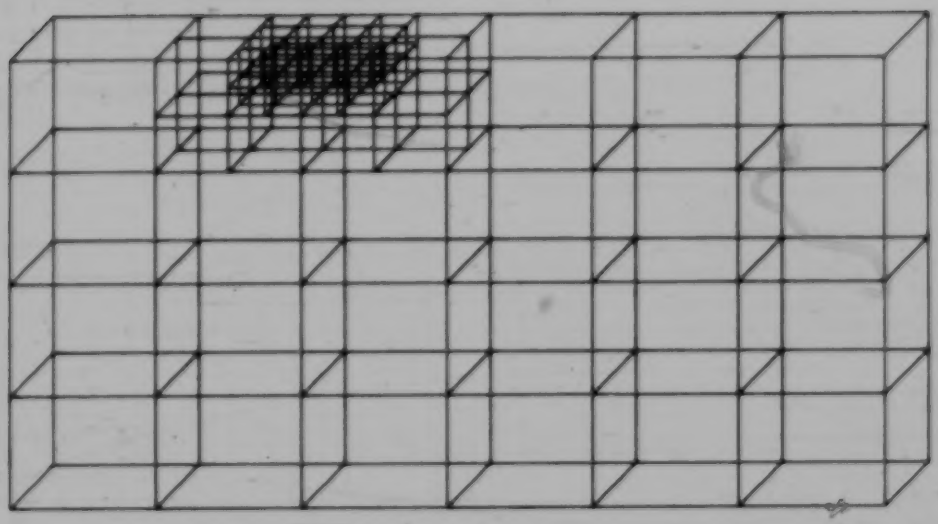

Figure 4.2. A 3D drawing of a finite element mesh for a rectangular cantilever beam.

structure. Basic element structure refers to the numbers of elements of different size and how these elements are arranged in relation to one another. Basic element structure is independent of the actual shape of the elements. Because they are much easier to draw, rectangular beams will usually be used to describe basic element structure. To further clarify these statements Figure 4.3 shows the z = 0 transverse sections of the gear tooth in Figure 4.1 and the rectangular beam in Figure 4.2.

Figures 4.4 and 4.5 use side and top views of a rectangular beam to show two examples of basic element structures that were actually used in this study. Figure 4.4 shows the four different sizes of elements that are available. As indicated, the smallest elements are A size elements and the largest elements are D size elements. The D elements are used only to extend the face width of the tooth. Type C elements cannot be nested into the D elements in the way that the B and A elements are shown to be nested into the C and B elements. The basic element structure shown in Figure 4.4 contains 272 elements and 1673 nodes. Since some of the nodes are fixed or constrained, the total number of degrees of freedom is only 3552. The storage of the stiffness matrix for this basic element structure requires a one dimensional array which will hold 1542684 double precision numbers. The basic element structure in Figure 4.5 has slightly fewer elements and degrees of freedom but requires slightly more space for the stiffness matrix

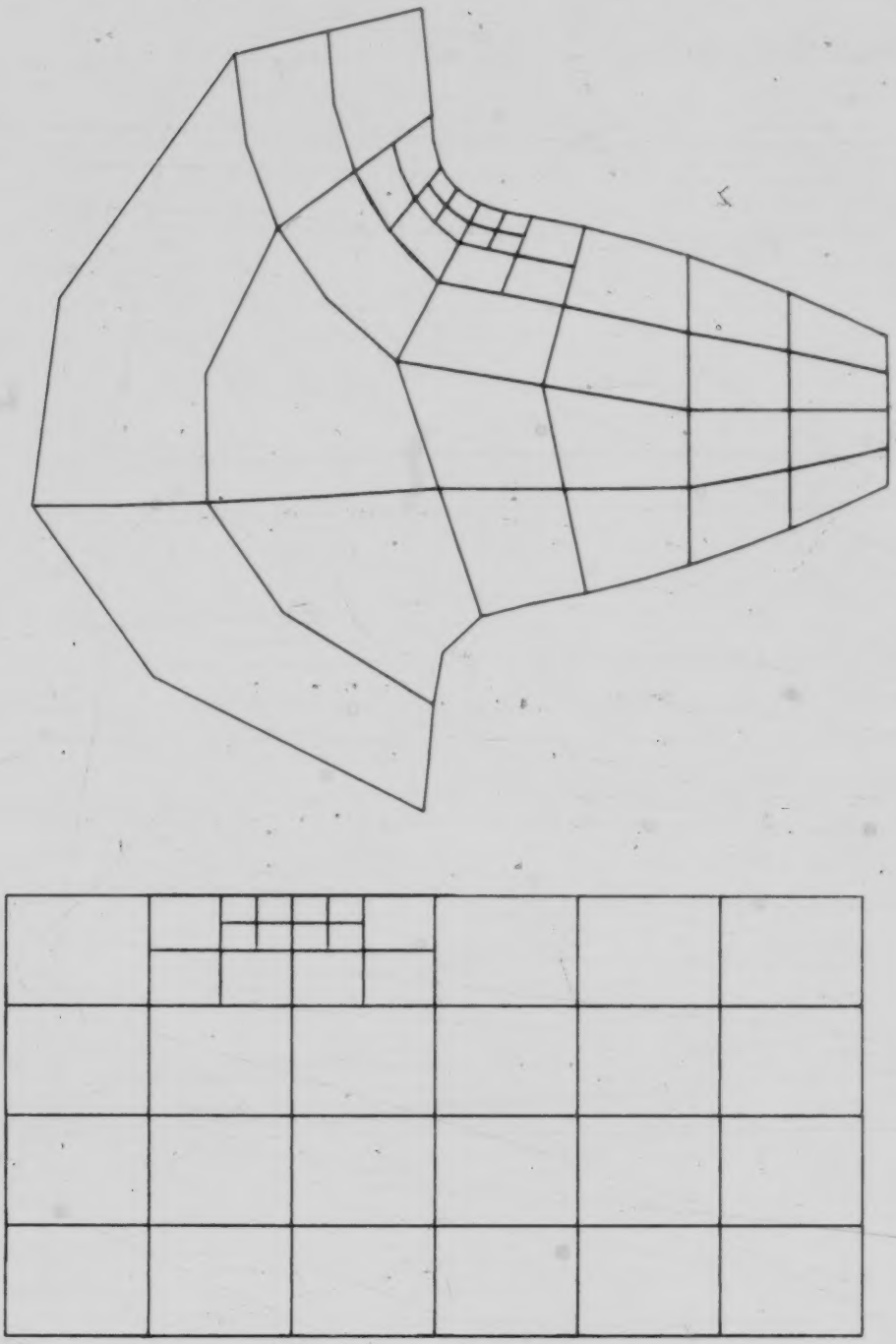

Figure 4.3. Side views of the 3D meshes shown in Figure 4.1 and Figure 4.2.

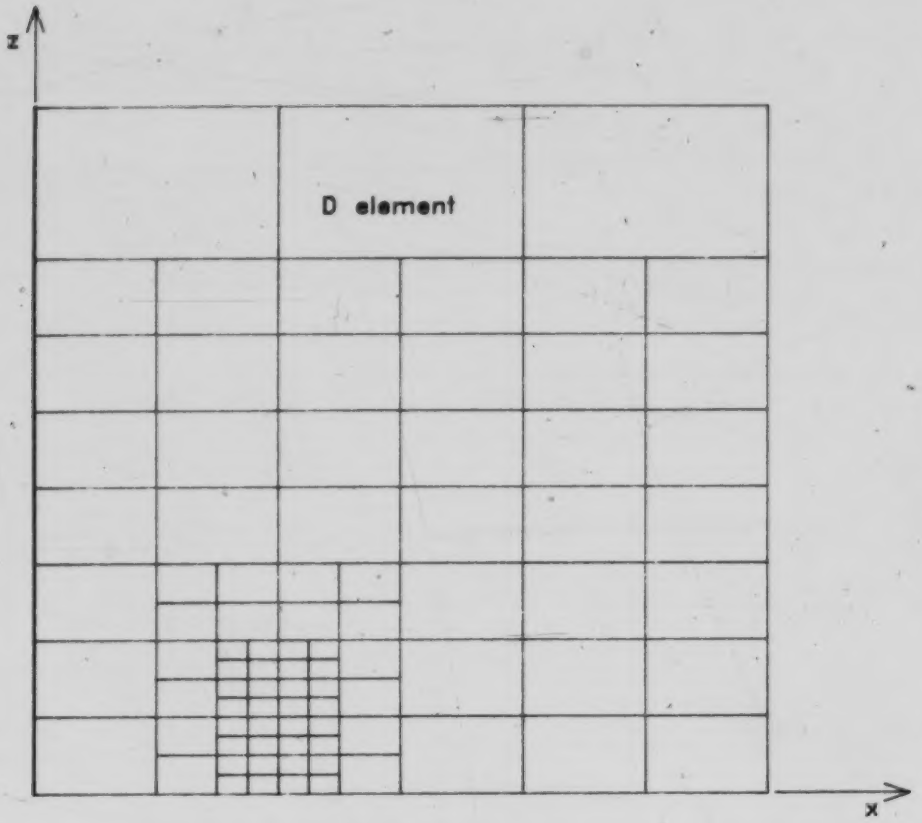

Top view

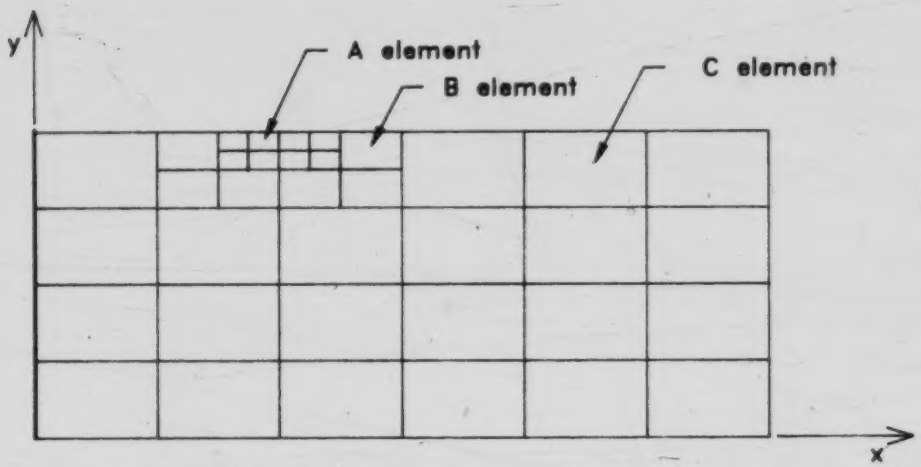

Side view

Figure 4.4. A basic element structure used for a gear tooth with a large face width.

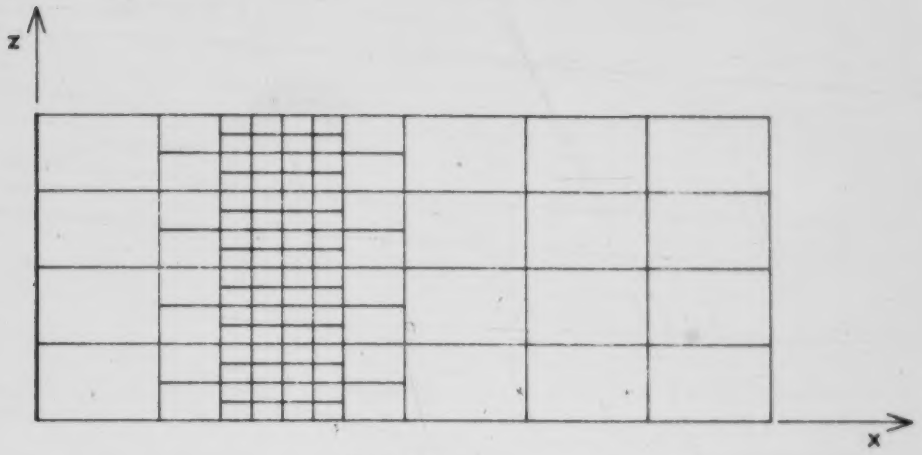

Top view

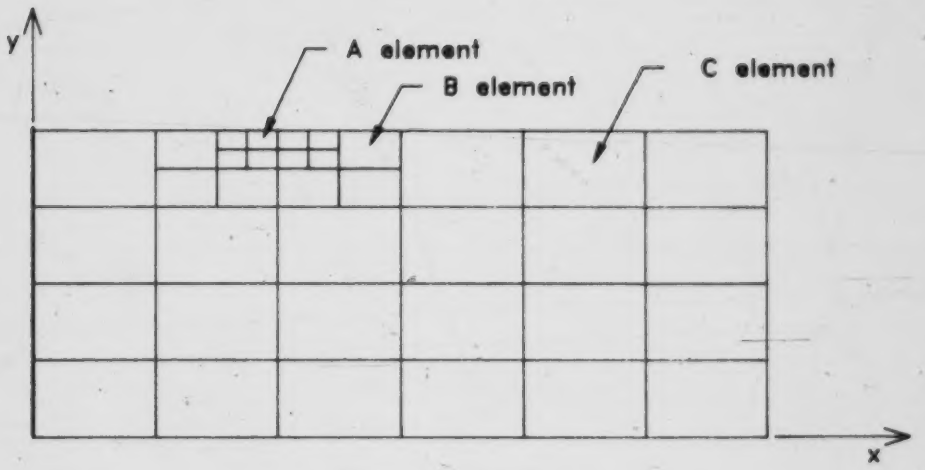

Side view

Figure 4.5. A basic element structure used for a gear tooth with a small face width.

because of greater band width.

In Figures 4.4 and 4.5 some of the lines are thickened. When the top and side views are considered together, these thickened lines represent a surface at the end of the beam or gear tooth. All the nodes in this surface are fixed. This boundary condition was used for all the finite element analysis.

The first step in the mesh generation program is to create a matrix of points in the xy plane. The names of subroutines which perform this task are MSHGNG and MSHGNR. The subroutine NODE then uses the information generated by MSHGNG or MSHGNR as the basis for generating nodes in the direction of the z axis. Subroutine CEQGEN generates equations which constrain the displacements of some nodes to the displacements of other nodes. The need for these equations will be explained later. After CEQGEN has created the constraint equations, a series of seven subroutines called ELGEN1, ELGEN2, assign the nodes to elements. The final major task is to generate the loads to be applied to the nodes. This task is performed by either LOADG or LOADR. A variety of small tasks such as numbering equations and specifying the structure of the stiffness matrix are then done by the MAIN program. Finally, the information generated by the mesh generation program is written into a file.

4.3 The Mesh Generation Subroutines MSHGNG and MSHGNR

Figure 4.6a shows the side view of a 3D mesh for a rectangular cantilever beam. Figure 4.6b shows a plot of the 2D information that is created as a basis for forming the 3D mesh. Figure 4.7 shows a plot of the 2D information that is created as a basis for forming the 3D mesh for the gear tooth shown in Figure 4.1. MSHGNR creates 2D information for rectangular cantilever beams and MSHGNG creates 2D information for gears.

The formation of the 2D information for rectangular cantilever beams is very simple, requiring about a dozen lines of programming. The formation of the 2D information for a gear tooth is more complex and will be briefly outlined.

The first major task is to generate the profile of a tooth. The exact shape of this profile is specified by providing information about the radius of the gear blank, the number of teeth to be cut, the dimensions of the cutter, the helix angle, and the amount of profile shift. MSHGNG assumes the gear is cut by a rack cutter. To specify the dimensions of the cutter teeth, the following information is input: the normal module, the normal pressure angle, the addendum of the rack teeth, and the shape of the round at the tip. In the normal section, rack cutter teeth usually have a circular round at the tip with a radius equal to

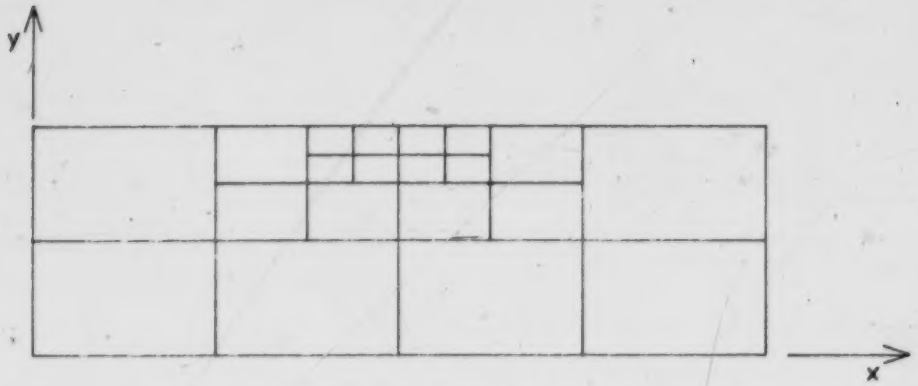

Side view of a three-dimensional mesh

(a)

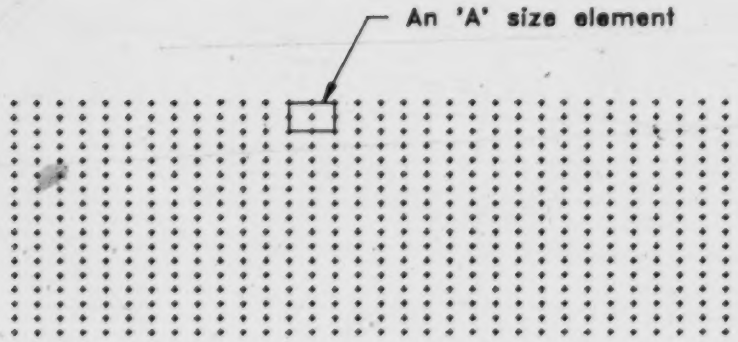

Matrix of points created by MSHGNR

(b)

Figure 4.6. Data created by MSHGNR for rectangular cantilever beams.

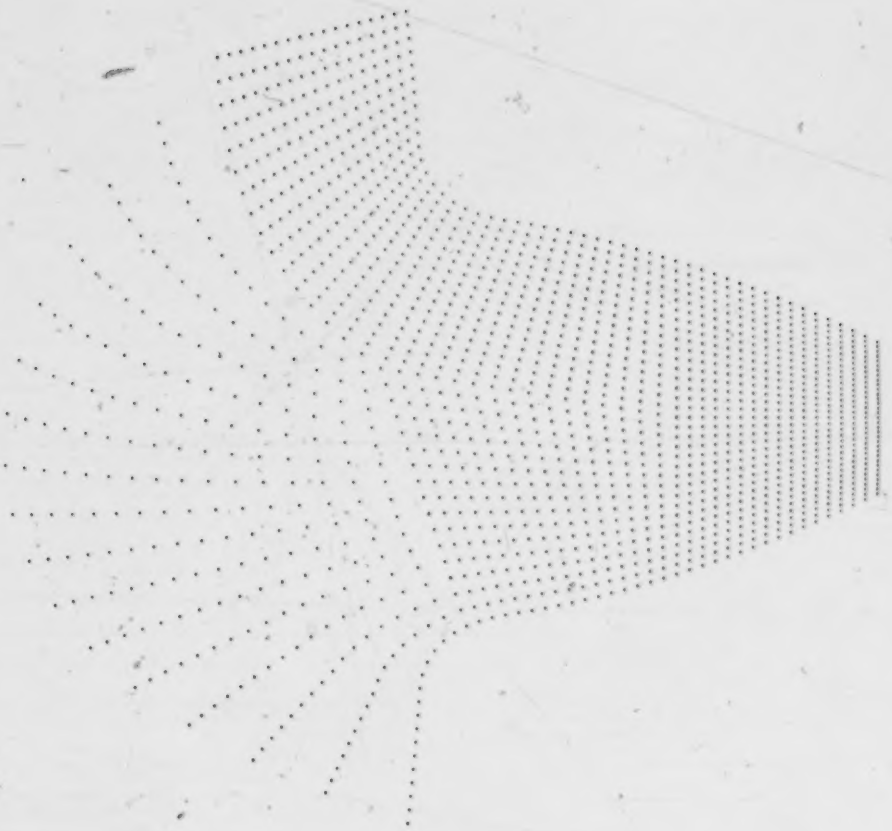

Figure 4.7. Data created by MSHGNG for the gear tooth mesh shown in Figure 4.1.

about 0.3 of the normal module. MSHGNG is more general and allows the specification of an elliptical round by inputting the lengths of the major and minor axes. Knowing the shape of the normal section of a rack cutter tooth allows MSHGNG to calculate the shape of the rack tooth in the transverse section. A circular round at the tip in the normal section will become elliptical in the transverse section. Once the shape of the profile of a rack cutter tooth is known in the transverse section, the profile of the gear tooth is easily determined. Given the coordinates of any point on the rack tooth profile and the slope of the normal through this point, a subroutine called XGYG calculates the coordinates of the corresponding point. The words "corresponding point" refer to the point on the gear tooth which comes into contact with the given point on the rack tooth. The details of the subroutine XGYG follow from an understanding of the concept of a conjugate pair which the reader will find explained in any basic text on the geometry of gear teeth. If requested, MSHGNG will provide the user with detailed information about the gear profile such as the coordinates of points on the profile, the slope of the normal at these points, and the radius of curvature between adjacent points.

Since the transverse section of the gear tooth is symmetrical about its center-line, only half of the entire tooth profile needs to be generated with XGYG. For this half of the profile MSHGNG uses a trial and error method to generate over 200 equally spaced points. These points on the

profile provide the basis for forming a matrix of points that is much denser than those plotted in Figure 4.7. The surplus of points is provided to make manual adjustment of the mesh easier. These adjustments are done by a subroutine MSHCH which is called by MSHGNG. In practice the mesh automatically generated by MSHGNG needs very little adjustment by MSHCH.

Out of the very fine matrix just described, MSHGNG selects the points shown in Figure 4.7. The location of the interior points is further modified in ways that minimize the additional adjustment that must be made in the CEQGEN program.

NODE

Subroutine NODE generates the nodes of the elements. The information from MSHGNG or MSHGNR supplies the starting points of lines of nodes that run parallel to the negative z axis for spur gears and cantilever beams. In the case of helical gears these nodes lie along helices which wind around the gear axis. The nodes belonging only to the D elements are generated first. Then nodes belonging only to the C elements are generated. Nodes for the B elements and finally the nodes for the A elements are generated. The only complication in the programming of NODE comes in leaving holes in the large elements into which the smaller elements can be nested. NODE numbers the nodes with global node

numbers.

CEQGEN and ELGEN

Although the CEQGEN subroutine precedes the generation of the elements by the seven ELGEN subroutines, the function of CEQGEN will be more easily understood if the elements are discussed first. Figure 4.8a shows a typical element with its nodes labeled with numbers from 1 to 20. These numbers are the local node numbers for the element. The task of the seven ELGEN subroutines is to find the corresponding global node numbers. This author did not find or invent a compact and elegant procedure for this task. The ELGEN routines are exceptionally tedious.

It is important that the results of the ELGEN be seen. During the course of development of the mesh generation programs, several plotting routines were written. The most useful of these reads the output of the mesh generation programs and plots the elements in either two or three dimensions. The user has control over which elements are plotted and even which parts of the elements are plotted. Visually inspecting the mesh is a very important part of using the mesh generation programs. It is the only way the user can know how to adjust the parameters that control where the A type elements are in relation to the fillet. Only by inspecting the mesh can the user make intelligent modifications through MSHCH.

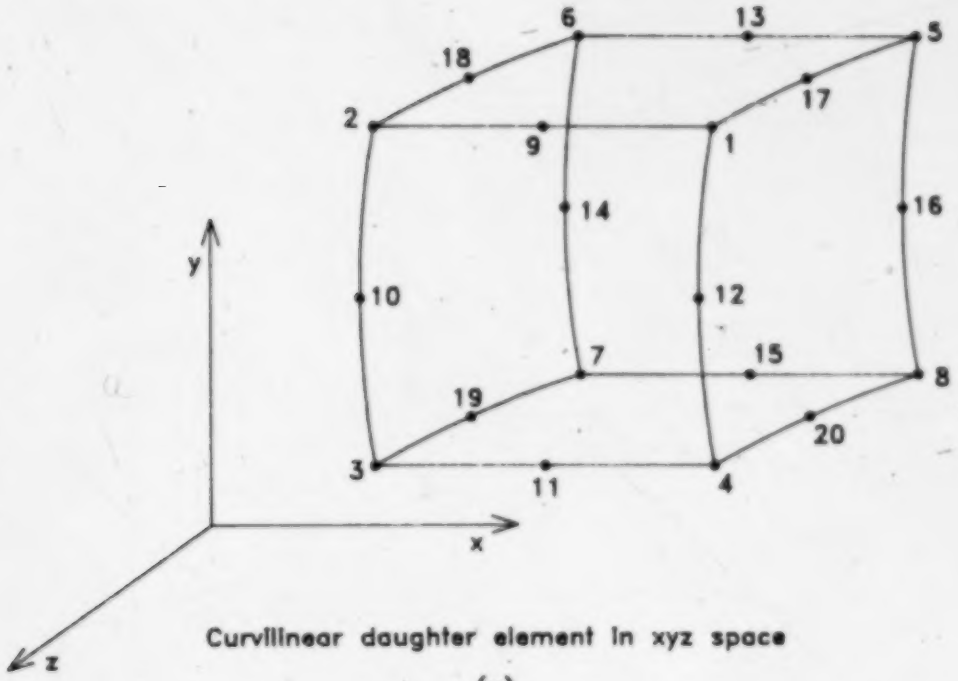

Curvilinear daughter element in xyz space

(a)

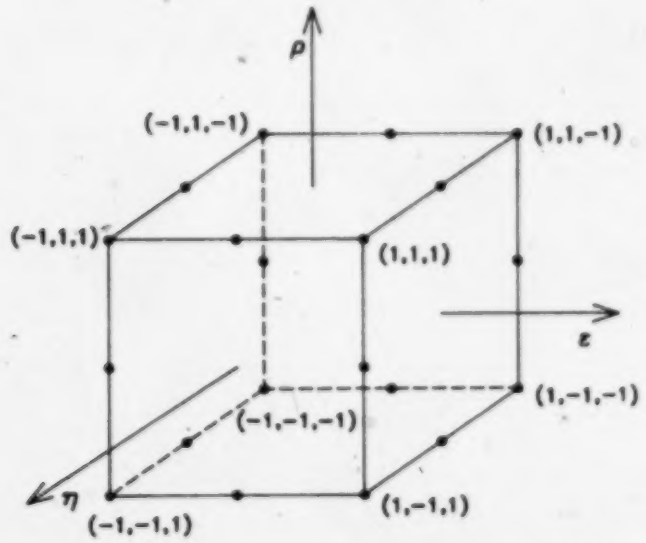

Parent element in $\varepsilon\rho\eta$ space

(b)

Figure 4.8. A curvilinear daughter element and its parent.

Before moving on to the CEQGEN subroutine a few pertinent facts about isoparametric elements will be reviewed. The element in Figure 4.8a is a curvilinear element that exists in space defined by the xyz coordinate system. This element may be called a daughter element. The parent element is the cube shown in Figure 4.8b. The parent element exists in a space defined by a $\epsilon\rho\eta$ coordinate system whose origin is at the center of the cube. The daughter element may be regarded as a mapping from the parent element of the form $\langle x\ y\ z\rangle = \langle\phi\rangle[x_i\ y_i\ z_i]$, where $\langle x\ y\ z\rangle$ is a row vector containing the x, y, and z coordinates of a point in the daughter element; x_i, y_i, and z_i are column vectors containing the coordinates of the nodes of the daughter element; and $\langle\phi\rangle$ is a row vector of shape functions whose values are determined by specifying ϵ, ρ, and η. There will be twenty shape functions since one is needed for each node of the element. If ϕ_i is the shape function for local node i, then examples of typical shape functions for corner and midside nodes would be $\phi_1 = 0.125(1 + \epsilon)(1 + \rho)(1 + \eta)(\epsilon + \rho + \eta - 2)$, and $\phi_8 = 0.25(1 - \epsilon^2)(1 + \rho)(1 + \eta)$, respectively. Elements are said to be isoparametric by definition if the same set of shape functions is used to find internal displacements of the element from the displacements of the nodes. The equation for the displacement at a point is $\langle u\ v\ w\rangle = \langle\phi\rangle[u_i\ v_i\ w_i]$, where u, v, and w are the displacements of the point in the x, y, and z directions,

respectively; u_i, v_i, and w_i are the vectors containing the displacements of the nodes; and $\langle\phi\rangle$ is the same vector of shape functions mentioned above.

Figure 4.9a shows a drawing of four smaller elements attached to one large element. Figure 4.9b shows the surface that is the boundary between the two different sizes of elements. The numbering of the nodes in this figure has nothing to do with the numbering shown in Figure 4.8. The nodes that are numbered from 1 to 8 in Figure 4.9b are nodes that belong to both the large and the small elements. These nodes present no special problem. The other nodes belong only to the small elements and do present a problem. If these nodes are left to themselves, a continuous displacement field over the boundary will not be ensured. In other words, the requirement of compatibility will not be satisfied. The displacements of these nodes must be constrained. From the point of view of the large element, the displacement of a particular point on the boundary surface is a function of the displacements of nodes 1 to 8. To ensure compatibility it is necessary to make the displacements of points 9 to 21 match the displacements of the surface of the large element. CEQGEN creates the constraint equations that ensure compatibility wherever there is a boundary between elements of different size.

The generation of the constraint equations is made easier if the $\xi\rho\eta$ coordinates of nodes 9 to 21 in

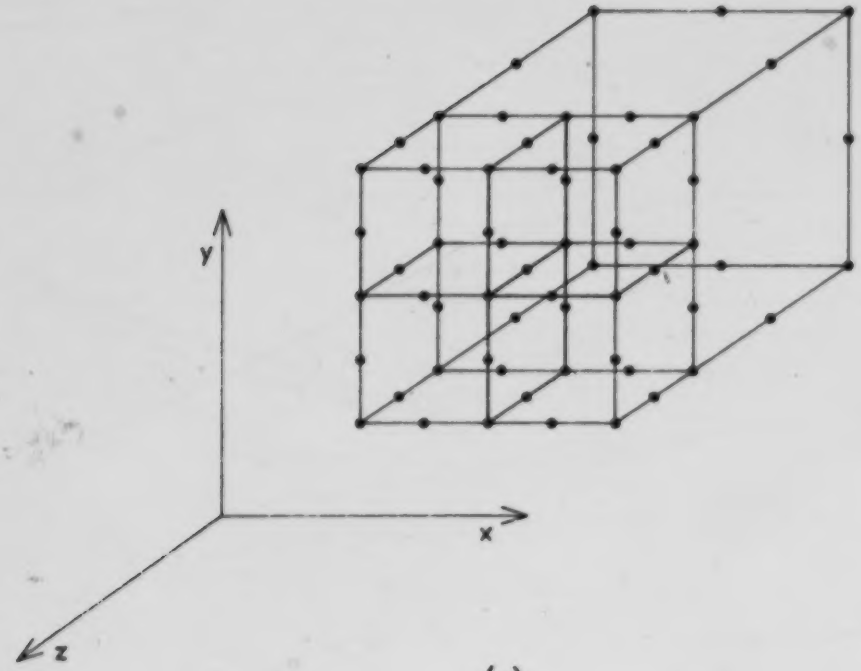

(a)

(b)

Figure 4.9. The boundary between elements of different size.

Figure 4.9b are known and constant. Assume the boundary surface in the figure is the result of mapping from the plane $\eta = 1.0$. If node 9 corresponds to a mapping from the point in the parent element where $\epsilon = 1$ and $\rho = 0.5$, then the displacement of node 9 along the x axis will be $u_9 = 0.375u_1 + 0.75u_8 - 0.125u_7$. If node 17 has coordinates of (0.5,0,1) in the parent element, then $u_{17} = au_1 + bu_2 + au_3 + cu_8 + au_5 + bu_8 + au_7 + du_8$, where $a = -0.1875$, $b = 0.375$, $c = 0.25$, and $d = 0.75$. Part of the job of the MSHGNG subroutine is to locate node 9 and node 17 so that their coordinates are close to those just mentioned. In any event, as CEQGEN moves over the boundaries, the nodes are moved to the desired locations. The amount of movement is minimized if MSHGNG has done its job well.

LOADG and LOADR

As their names suggest, these subroutines generate load information. In the case of gears, LOADG takes the load W and uniformly distributes it along the contact line. This line loading must then be represented by an equivalent set of nodal loads. The concept of virtual work is used to determine the correct nodal loads.

An example of a contact line on a helical gear is shown at the beginning of Chapter 2 in Figure 2.1. This line lies in the surface of the tooth. Load intensity vectors along the contact line would be normal to this surface. LOADG

finds the elements over which the contact line passes. The line will not necessarily lie in the surface of the element because the actual surface of the tooth is being approximated by the curvilinear element. It is assumed that the contact line will be very close to the element surface. It is necessary to find points in the parent element which correspond to points that are very close to the contact line in the daughter element. Since it is impossible to solve for ϵ, ρ, and η in the equation $\langle x\ y\ z\rangle = \langle\phi\rangle\langle x_i\ y_i\ z_i\rangle$, a subroutine was written that uses a trial and error procedure to map from (x,y,z) to (ϵ,ρ,η). After the contact line on the daughter element has been mapped onto the parent element, one of the nodes on the surface of the element is given a displacement of 1. The displacements along the contact line can then be calculated using the equation $\langle u\rangle = \langle\phi\rangle[u_i]$. Simpson's rule is then used to integrate the work done by the line load. This work is numerically equal to the equivalent load for the node that was moved. One by one each of the eight nodes on the surface of the element is given a displacement of 1 and its nodal load calculated.

To test the LOADG subroutine an exact solution was found to the problem of an oblique line passing through a flat eight-node rectangle. The LOADG subroutine was applied to this problem and the results were compared to the exact solution. Another type of check can be done every time LOADG is run. The moments of the line load about each of the x, y, and z axes are calculated and outputted as well as the sum

of the moments of the nodal loads. These two sets of moments can then be compared. The performance of LOADG is poorest in this last test. The sum of the moments of the equivalent nodal loads agree with the exact value to five significant digits. This degree of accuracy is more than sufficient. Part of the reason LOADG works so well is that it uses only double precision numbers. During the development of LOADG it was found that the subroutine that maps from xyz to $\epsilon\rho\eta$ would not work well unless double precision numbers were used. Since that time all parts of the finite element programs have been converted or written so that only double precision numbers are used.

LOADR creates load information for rectangular cantilever beams. Several types of loadings can be applied. The beam can be put into pure tension or a bending load at the end can be applied. An oblique line load running across the top surface of the beam can also be applied. In this last case the exact solution for a line running across a rectangular element is used to calculate the equivalent nodal loads.

Neither LOADG or LOADR takes into account the fact that constrained nodes cannot have loads applied to them. One of the tasks of the MAIN program is to find any constrained nodes with loads and redistribute these loads to unconstrained nodes in a way that is consistent with the requirements of virtual work.

4.4 The Finite Element Program

There exist many books on the theory of finite elements. The purpose of this section is not to review the basic theory of finite elements but to give some detail about the finite element program that was written by the author of this thesis. This finite element program will be called FEAP. FEAP creates a set of simultaneous equations, known as equilibrium equations, having the form $\{Q\} = [K]\{q\}$, where $\{Q\}$ is a column vector containing the loads placed on the nodes, $[K]$ is the global stiffness matrix of the gear, and $\{q\}$ is a column vector containing the displacements of the nodes of the gear. Since $\{Q\}$ is known and $[K]$ can be found, the displacements can be solved for. From the displacements, stresses can be calculated. FEAP does not in fact calculate any stresses; its sole output is displacements.

FEAP was written so that it could be compiled to run in the Single Job Executive mode on the FPS-164 Scientific Computer. Two of these computers are attached to the University of Alberta's mainframe computer, the Amdahl. The FPS-164 is specially designed to do jobs involving large arrays and large numbers of computations. The FPS-164 has 2 megawords of 64-bit memory. Because all numbers, including integers, are stored in one of these 64-bits words, they are approximately equivalent in accuracy to double precision on the Amdahl.

At present, FEAP will accomodate a problem involving 2000 nodes, 300 elements, 4000 degrees of freedom, 500 constraint equations, 10 different load sets, and a stiffness matrix that will fit into 1.7 million words of memory space. It is usually the limit on the size of the stiffness matrix that determines whether a problem can be done.

The mesh generation program calculates almost everything up to the point where the stiffness matrix must be formed and puts this information into a single data file. Almost immediately after reading this data, FEAP begins forming the global stiffness matrix [K]. To do this the stiffness matrices of the individual elements are formed one by one. The formation of an element stiffness matrix involves an integration that can be done only by numerical means. FEAP uses a 3 x 3 x 3 Gaussian quadrature for this integration. Because each of its nodes has three degrees of freedom the element stiffness matrix for a 20-node brick will be 60 x 60. Because it is symmetric it can be stored in an array with a length of 1830. Each of these 1830 numbers is then added to appropriate locations in the global stiffness matrix. Because of the presence of constraint equations the movement of numbers from the element stiffness matrix to the global stiffness matrix is not as simple as it would be otherwise. This topic is examined more thoroughly in the next section of this study. The global stiffness matrix is finished when the contributions from all the

elements have been made. The global matrix [K] is an n x n matrix where n is equal to the number of degrees of freedom. A typical value for n in this study is about 3600. To store such a matrix would require a memory with a capacity for 12.96 million numbers. However, like the element matrices, [K] is symmetric and so the memory requirement is immediately cut almost in half. Over 6 million numbers is still three times the space available. Fortunately, besides being symmetric, [K] is banded and therefore contains many zeros which do not need to be stored. To take full advantage of this bandedness, [K] is stored column by column in a one-dimensional array. The columns are stored only up to the point of the last non-zero number. This method, sometimes known as the "skyline" method, makes the storage of [K] much more compact. The size of this one-dimensional K array and the locations of the columns within the array are all calculated by the mesh generation program and are part of the data read by FEAP.

With the global stiffness matrix completed, FEAP uses Gaussian elimination to solve for the displacements. These displacements are written into a file that is then transferred to the Amdahl.

4.5 Creating the Constrained Stiffness Matrix

If $\{q'\}$ is the vector of displacements before the constraint equations are applied, and $\{q\}$ is the vector after the constraints are applied, then the relationship between these two vectors can be written $\{q'\} = [T]\{q\}$. If $\{q\}$ contains 3600 numbers and there are 1200 constraint equations, then $\{q'\}$ will contain 4800 numbers and $[T]$ will be a 4800 x 3600 matrix. A typical row of $[T]$ will either contain all zeros except for a single 1, or will contain all zeros except for the coefficients of a linear constraint equation. If $[K']$ is the stiffness matrix that would be formed if there were no constraints being applied, and $[K]$ is the stiffness matrix after the constraints have been applied, then it is easily shown that $[K] = [T]^T[K'][T]$. Unfortunately $[K]$ cannot in practice be easily formed through these simple matrix multiplications. The first reason is that $[K']$ is too large to store in the available space. Even if $[K']$ can be squeezed in, there would be no space to perform the multiplications and to store $[K]$. So, instead of using the equation $[K] = [T]^T[K'][T]$, an algorithm was developed that would take the numbers in the element stiffness matrix and appropriately modify and then move them directly into the constrained stiffness matrix. This algorithm was tested by using it on a relatively small problem and then comparing the stiffness matrix obtained with that obtained by actually finding the product $[T]^T[K'][T]$. Ultimately, the algorithm is verified by the

final results of the finite element program.

It was the experience of the author of this study that most of the many available books on finite element analysis provide little useful advice to one faced with the job of actually writing a finite element program. One book which is very useful is Finite-Element Method: Basic Technique and Implementation by Tong and Rossettos [16]. Even this book provided no help with the problem of forming the constrained stiffness matrix directly from the element stiffness matrices. Although such procedures must exist, they do not appear to be readily available. A description of the algorithm used by FEAP has therefore been included in Appendix B of this study.

4.6 The Stress Output Programs

The stress output programs consist of a set of relatively small MAIN programs which call various subroutines stored in a separate file. Each of the MAIN programs first reads in the mesh data from the mesh generation program and the displacement data from the finite element program. Subroutines are then called which calculate stresses at any point in any element. Another subroutine finds principal stresses. One of the MAIN programs has been designed for use with cantilever beams. It outputs the finite element stresses alongside stresses calculated according to simple beam theory so comparisons can be easily made. Altogether, about 14 MAIN stress output programs have been developed for 2D and 3D analysis.

Chapter 5: Evaluation and Results of the Finite Element Programs

5.1 Assessing the Performance of the Finite Element Programs

This section addresses the question of whether the finite element programs provide accurate information about fillet stresses in gear teeth. No attempt will be made to describe the multitude of tests used to make sure various subroutines work properly. Neither will the many checks performed during each run be described. Instead, a few arguments and comments will be presented which, taken together, provide good reason to believe that the finite element programs correctly perform their intended tasks and output useable information.

Both the 2D and 3D finite element programs can be used to find stresses in cantilever beams with rectangular cross-sections. These beams may have either bending or tensile loads applied. If Poisson's ratio is set to zero, then the finite element programs should give results that are close to the results of simple beam theory.

Both the 2D and 3D elements in this study have one midside node on each edge. For the sake of simplicity, consider just the 2D elements for a moment. The shape functions for the 2D elements contain a complete set of quadratic terms (ϵ^2, $\epsilon\rho$, and ρ^2), as well as some cubic terms ($\epsilon^2\rho$ and $\epsilon\rho^2$). The first partial derivatives of the shape functions are used to find the strain and stress

distributions within the element. These first partial derivatives contain linear terms and quadratic terms. If the derivatives of the shape functions are inspected one at a time, it becomes apparent that none of them contains a full set of quadratic terms. It is no surprize that these elements have no difficulty producing linear stress distributions, but are incapable of producing some parabolic stress distributions. A cantilever beam constructed of a single line of elements and loaded with a bending load at the end will produce very accurate results for tensile and compressive stresses, which vary linearly in the beam. According to beam theory, the shear stresses should vary parabolically along a cross-section and should be constant along the length of the beam. The finite elements give the opposite result. Along the length of the beam the shear stresses vary parabolically and along the cross-section they are constant. Only at the points used in a 2 x 2 Gaussian quadrature do the shear stresses from the finite elements agree with beam theory.

Many basic element structures were used to model a cantilever beam. In the following discussion all numerical values are taken from results which used the basic element structure shown in Figure 4.5 for 3D elements. Stresses were calculated in the region of the A size elements. In the case of a uniform tensile load at the end of the beam, the load is calculated to produce a stress of exactly 9. The output from the finite element program gives the stress as

9.00000000. In the case of a bending load the difference between the 3D finite element solution and simple beam theory is sensitive as to how the load at the end of the beam is applied and how far from the loaded end the stress is calculated. If the load is distributed over a line on the top surface of the beam, the difference between simple beam theory and the finite element solution may be as much as 1.5%. If the stress is calculated at exactly the same point, but the load is distributed over the surface at the end of the beam, the difference between theory and the finite element solution drops to 0.13%. At other locations this difference is much less. All of the percentage differences just given refer to comparisions between tensile stresses caused by the bending load. One does not expect comparisons between shear stresses to be as good because, as explained above, the elements are incapable of producing the correct parabolic stress field. To give the reader an idea of how well the shear stresses are approximated some numerical results will be given. In a case where beam theory gives the tensile stress as exactly 8.25 and the shear stress as exactly zero, the finite elements give the stresses as 8.253 and -0.00225 respectively. At another location beam theory gives stresses of 7.387 and -0.147, while the finite element program outputs 7.397 and -0.144. At this point one could reasonably claim that it has been proved that the finite element programs work properly for rectangular cantilever beams with Poisson's ratio set equal to zero.

As stated in Chapter 4, the boundary condition at the fixed end of the beam is that all the nodes are fixed. When the value of Poisson's ratio is increased from 0 to 0.3, the boundary condition at the end of the beam has a significant effect on the stresses, especially in the case of the 3D analysis. One would expect this effect to become smaller as the distance from the fixed end increases. Also, since the rectangular cross-section of the beam has two lines of symmetry, one would expect the stress distribution in such a section to be symmetrical about these lines. All of these expectations were fulfilled by the finite element results. There is no reason to believe the programs do not also run correctly for non-zero values of Poisson's ratio.

The production of a mesh for a gear tooth involves many subroutines not used to produce a simple cantilever beam. As well, the elements produced for a gear tooth are curvilinear and are oriented at a great variety of angles. It is entirely possible that programming errors could exist that would not affect the performance of the finite element programs when applied to simple cantilever beams, but affect the analysis of gear teeth. One way of checking this possibility is to produce a spur gear tooth with a very small pressure angle and a very large number of teeth. Such a tooth would look like a cantilever beam with circular shoulder fillets. Figure 5.1 shows such a tooth produced with the 2D finite element mesh generation program. The 2D loading subroutines can apply either a tensile load or a

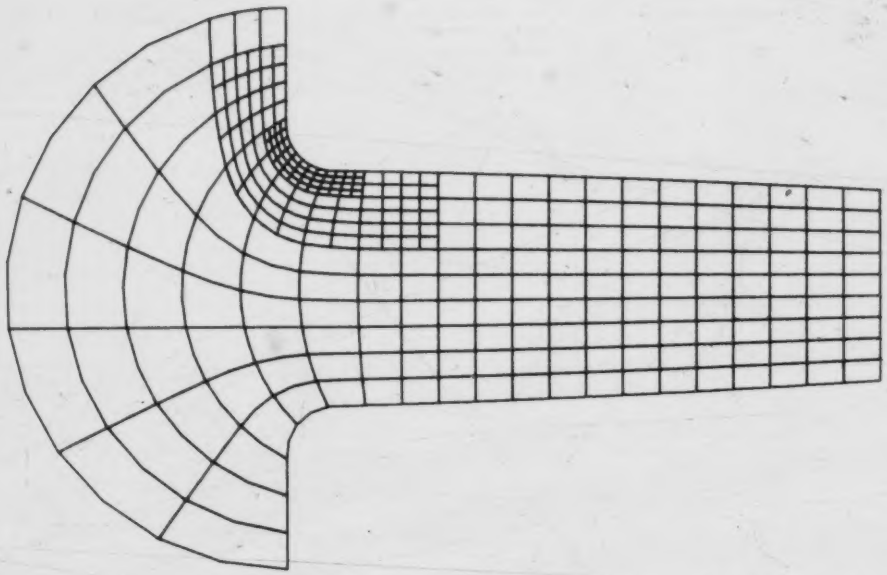

Figure 5.1. A mesh used for the 2D finite element analysis of a rectangular bar with circular shoulder fillets.

bending load at the end of the tooth. In the regions away from the fillet, the 2D finite element analysis gives the expected results of simple beam theory. In the fillet region stress concentration factors were calculated and compared with published values [14]. In the case of a tensile load the calculated value is within 2% of the published value. In the case of the bending load, the calculated value is 12% higher than the published value. The published values are based on photoelastic tests and certainly not to be regarded as exact solutions. The comparisons just described were done as a check. They show that the finite element programs are not producing absurd results. The comparisons with published values were done only with the 2D finite element programs.

As Figure 5.1 shows, the mesh in the fillet area is very fine. Figure 5.2 shows a similar 2D mesh for a typical gear tooth. This mesh has 308 elements. Continuity of displacements between elements is guaranteed by the shape functions. These shape functions do not, however, guarantee continuity of stresses. In fact, the degree to which stresses are continuous between boundaries is an indicator of whether the mesh is fine enough to accurately approximate the stress gradients at a particular location. In the very fine meshes such as those shown in Figure 5.1 and 5.2, stresses on the fillet at points between elements differ from one another by at most 0.3%. In many instances the difference is less than 0.1%. Such close agreement is evidence that the elements are more than sufficiently small.

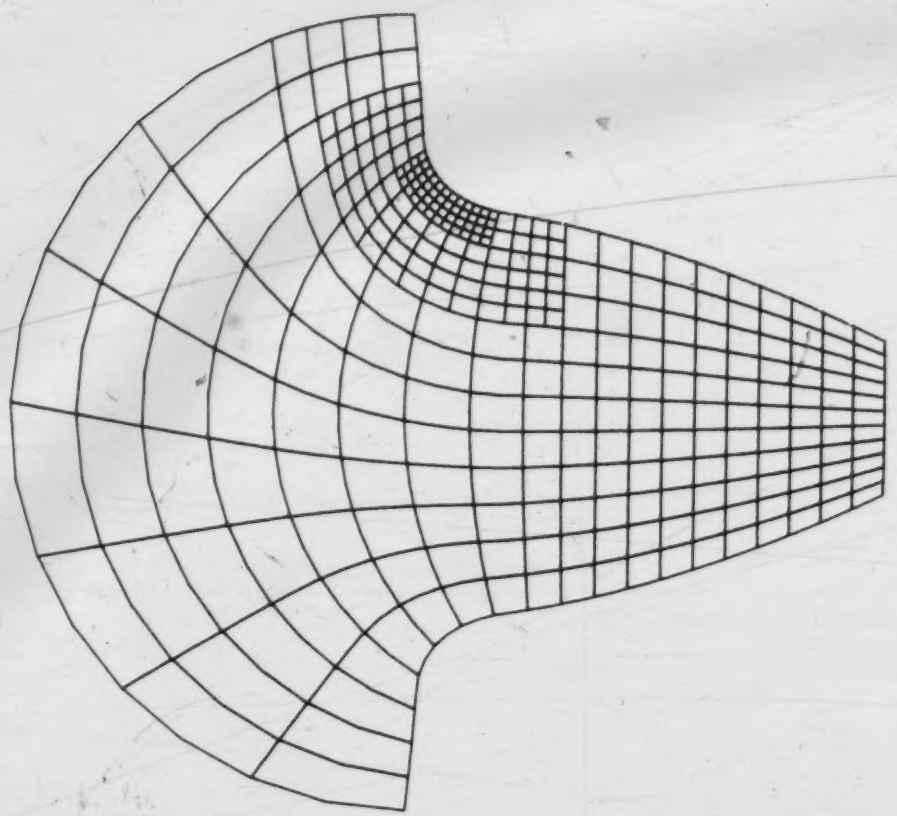

Figure 5.2. A mesh used for the 2D finite element analysis of a spur gear.

A mesh with only 189 elements gives a maximum fillet stress that differs by only 0.002% from the value from the 308 element mesh.

At this point it would seem very likely that the 2D finite element programs are working correctly. If the 3D programs are working properly, they should reproduce the results of the 2D programs within reasonable limits. It was stated above that, in the case of rectangular cantilever beams, Possion's ratio has an especially large effect on the stresses outputted by the 3D programs. This is the case with gear teeth as well. Changing Poisson's ratio from 0 to 0.45 causes the maximum fillet stress outputted by the 2D programs to change by only 0.36%. The maximum fillet stress from the 2D analysis is affected by less than 0.1% by changing from plane stress to plane strain analysis. The only reasonable comparison that can be made between the 2D and 3D analysis is in cases where Poisson's ratio is set to zero. Identical spur gear teeth were subjected to ten constant loads ranging in position from $S = S_{max}$ to $S = 0$ in equal intervals. With Poisson's ratio set to zero the tooth was analyzed by both the 2D and 3D finite element programs. The fine mesh shown in Figure 5.1 was used for the 2D analysis and a basic element structure like that in Figure 4.5 was used for the 3D analyis. Maximum fillet stresses for each of the load positions were compared. At $S = S_{max}$ the 3D stress is 2.0% lower than that from the 2D analysis. At $S = 0$ the 3D stress is 2.1% lower than that

from the 2D analysis.

The stresses along the fillet in the direction of the z axis should be symmetrical about the plane z = -F/2 for spur gear teeth, regardless of the value of Poisson's ratio. This was indeed the case. For basic element structures that are also symmetrical about the z = -F/2 plane, stresses at corresponding positions on either side of the plane agreed to every one of the eight digits outputted. Comparisons between different basic element structures were made. These comparisons support the claim that the 3D finite element programs do provide meaningful information about fillet stresses in spur gear teeth.

It is evident that the 3D analysis works for spur teeth. The only difference between spur teeth and helical teeth as far as the programming is concerned is in regard to the node generation subroutine NODE and the load generation subroutine LOADG. Checks by plotting and checks by various calculations verified the operation of these routines when applied to helical gears.

It has already been explained with reference to the 2D analysis that an important criterion for evaluating the performance of finite element results is the degree of continuity of stress over element boundaries. Two typical types of output from the 3D stress output programs are stresses along the fillet in a given transverse section and stresses along some curve running from z = 0 to z = -F. The

curves used for this last type of output are either a helix running along the surface of the fillet or a curve that joins points of maximum fillet stress in successive transverse sections. In all cases, stresses at boundaries between elements are calculated using one element, and then the other element, so comparisons can be easily and frequently made. When stress values are given along the fillet in a given transverse section, differences across boundaries in the vicinity of the point of maximum stress are about 7%. When stresses are given along a curve running from z = 0 to z = -F, differences across boundaries typically range from 0.7% near the sides of the tooth to 0.05% in the middle of the tooth. As will be shown in the next section, the stress gradients tend to be much larger on the sides of the tooth than in the middle.

The isoparametric elements created by the finite element programs in this study are standard elements. Their ability to simulate the behavior of loaded structures is not a matter of controversy. The degree to which this simulation is accurate is largely a function of the number of elements used. If round-off errors in the numerical computations have a negligible effect then increasing the number of elements increases the accuracy of the result. However, increasing the number of elements also increases memory space requirements and computational time. The 2D mesh shown in Figure 5.2 requires an array with a length of 159572 to store the stiffness matrix and takes about 225 seconds of

computer time. The much coarser 3D meshes shown in the last chapter require an array with a length of over 1400000 and take over 3000 seconds of computing time. Given the limitations imposed by the F164 Scientific Computer and the manner in which FEAP is programmed, it is impossible to substantially increase the fineness of the 3D mesh. The evidence presented above indicates that the basic element structures used for the 3D analysis of gear teeth are sufficient to yield results that are within a few percent of the actual values.

5.2 Results of the Finite Elements Programs

Some results of the finite element programs have already been presented in Chapter 3 in the form of σ_w/σ_T versus S/S_{max} curves. The aim of this section is to give a more detailed presentation and discussion of some of the results of the 3D finite element programs.

It was stated in the last section that the value of Poisson's ratio ν has a substantial effect on stresses. Figure 5.3 shows how fillet stress is affected by Poisson's ratio for a spur gear with 36 teeth and a face width of $4m_n$. Clearly, increasing ν tends to decrease the fillet stress on the sides of the tooth and increase stress in the middle of the tooth. This trend makes sense when it is realized that the sides of the tooth will be in a state of plane stress while the middle of the tooth will approach a state of plane strain. The elements in plane strain will be stiffer than elements in plane stress and so will carry more of the load. The ratio of the maximum stress at $z = -F/2$ to the maximum stress at $z = 0$ is 1.47 for the curve with $\nu = 0.3$ and the load at $S/S_{max} = 1$. This ratio decreases slightly to 1.44 when the load is moved to $S/S_{max} = 0.333$. The substantial variation in stress across the width of this particular tooth suggests an inadequacy in the assumption of uniform load intensity along the contact line.

The comparisons in the last paragraph were between stresses at different values of z on the curves with

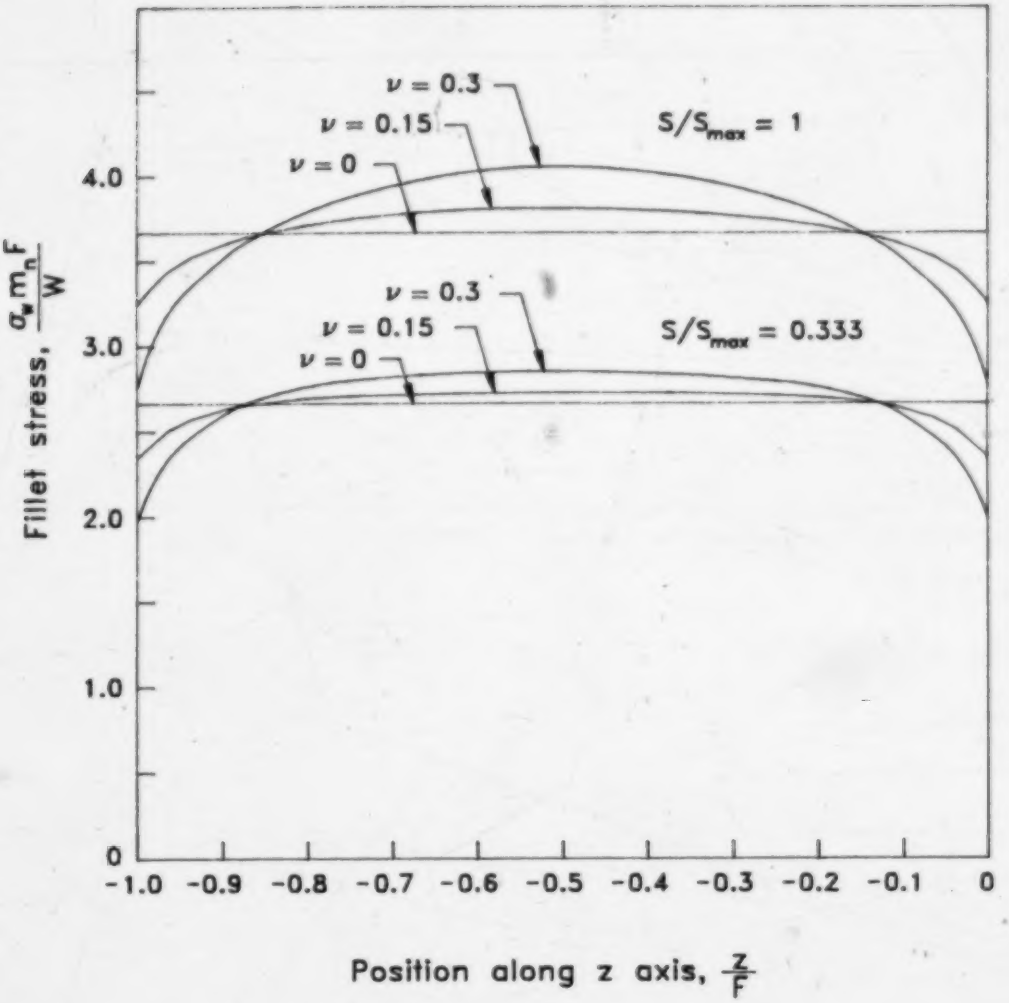

Figure 5.3. Maximum fillet stress along the face width for a spur gear with different values of Poisson's ratio.

ν = 0.3. Comparisons can also be made between stresses at identical values of z, but on curves corresponding to different values of ν. The most relevant value of z is z = -F/2, since this is where the fillet stress is at its maximum. At load position S/S_{max} = 1 the maximum stress at z = -F/2 with ν = 0.3 is 10.4% higher than the stress calculated for the tooth with ν = 0. At load position S/S_{max} = 0.333 this percentage difference is 7.1%. For the tooth under consideration the effects caused by changing Poisson's ratio are not negligible. In the last section it is stated that varying Poisson's ratio has a very small effect (less than 1%) on stresses when 2D finite element analysis is used. The significant changes in stress caused by changes in ν in the 3D analysis show the fundamental inadequacy of modelling a spur gear tooth as a two dimensional object.

Figure 5.4 shows the effect of varying Poisson's ratio with a helical gear tooth having 40 teeth, a helix angle of 20°, and a face width of $6m_n$. The reader may be surprized that even with ν set to zero the maximum fillet stress does not occur in the section z = 0. An example of an attempted explanation is to recognize that the load on the tooth will produce a bending moment not only around the z axis but also about the y axis (see Figure 2.1). The moment about the y axis will tend to put the fillet in compression in the z = 0 section and in tension in the z = -F. This explanation may be somewhat satisfactory for the reduction in stress on the

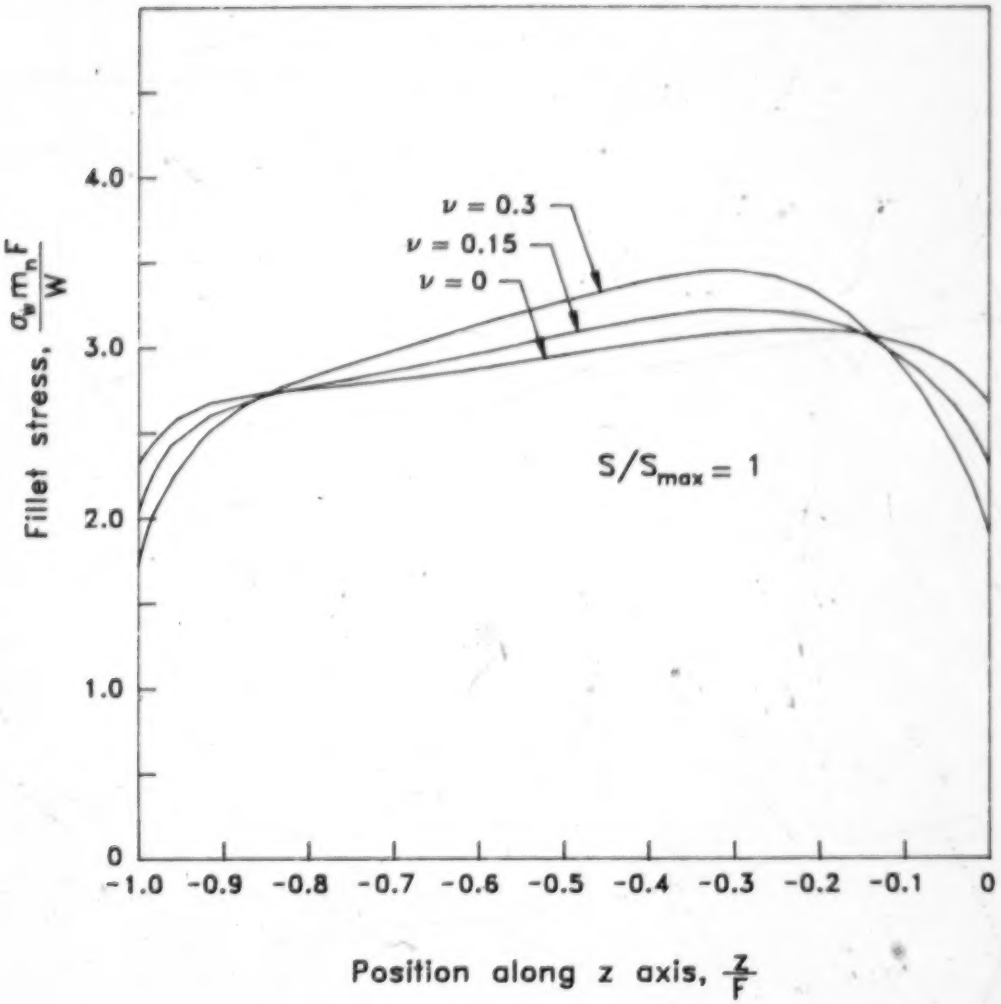

Figure 5.4. Maximum fillet stress along the face width for a helical gear with different values of Poisson's ratio.

z = 0 side of the tooth. It fails completely to explain the sudden reduction in stress near z = -F.

As expected, Figure 5.4 shows that increasing Poisson's ratio reduces the stresses on the sides of the tooth and increases the stress in the middle section of the tooth. The maximum stress moves towards z = -F/2 as ν increases. The maximum stress on the ν = 0.3 curve is 11.1% higher than the maximum stress on the ν = 0 curve. Again, this significant change in stress caused by varying Poisson's ratio cannot be predicted by a 2D model of the tooth.

The last figure in this study, Figure 5.5, shows how the maximum stresses vary along the face width as the load position changes. As S decreases the location of the maximum value of the curves moves towards the z = 0 side of the tooth.

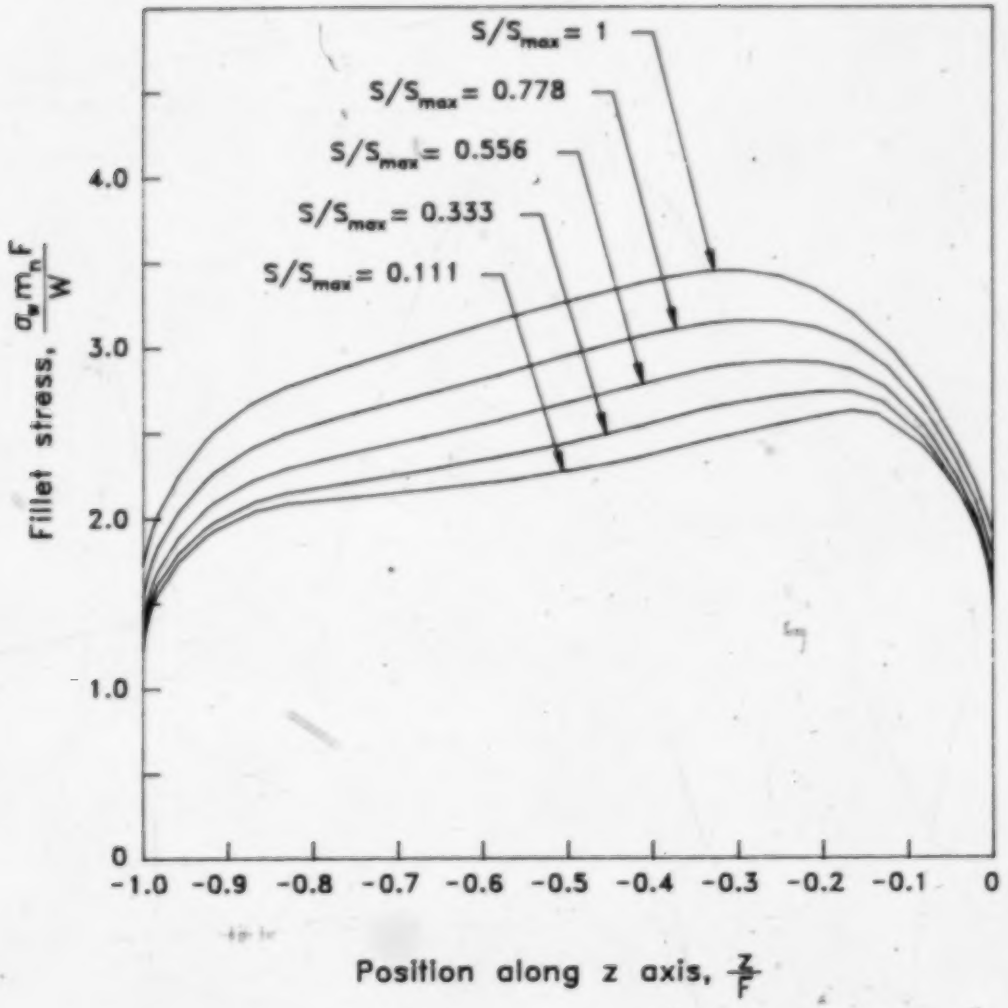

Figure 5.5. Maximum fillet stress along the face width for a helical gear at different load positions.

5.3 Conclusion

For most helical gear pairs the position of engagement that causes maximum fillet stress will be the position where the fraction of the load on the tooth first becomes a maximum as the load moves from a corner loading position. For gear pairs with a face contact ratio less than 1, this critical position coincides with the position of maximum load intensity. For gear pairs with a face contact ratio greater than 1, the critical position is that of a corner loading where the load intensity is a minimum.

Exceptions to the generalizations just stated exist in cases where the face contact ratio is less than 1 and also in cases where the face contact ratio is more than 1. If the face contact ratio is less than 1, significant exceptions tend to occur when the number of teeth on each gear exceeds 80, the helix angle is less than 10°, and the face contact ratio has a value near 0.55. In these exceptional cases the critical position is the corner loading position.

If the face contact ratio is greater than 1, then the position causing maximum fillet stress is normally the corner loading position where the load intensity is a minimum. An exception to this rule has been shown to occur for a helical pair with a helix angle of 30° and a face contact ratio slightly greater than the profile contact ratio. In this case, the critical position occurs at the position of maximum load intensity. Reducing the helix angle

or moving the value of the face contact ratio away from the value of the profile contact ratio moves the critical position back to the corner loading position.

Both spur gear teeth and helical gear teeth are three-dimensional objects. The stress distributions along the fillets of these gear teeth are complex and cannot be generated from two-dimensional models. Maximum fillet stress calculated using a 3D model may be as much as 10% higher than the maximum stress obtained from a 2D model. The results of the 3D analysis show a significant variation in stress along the face width of a tooth even in the case of spur gears. These results suggest an inadequacy in the assumption of uniform load intensity along the contact lines even in the best of circumstances.

The amount of computing time and the memory requirements of 3D finite element analysis are much greater than those required by 2D analysis. However, as large high-speed computers become more accessible this disadvantage of 3D analysis becomes increasingly unimportant.

Bibliography

[1] "AGMA Standard For Rating the Pitting Resistance and Bending Strength of Spur and Helical Involute Gear Teeth," AGMA 218.01, December 1982.

[2] Allison I.M. and Hearn E.J., "For the Bending Strength of Helical Gears," Engineering, October 1978, pp. 1055-1057

[3] Chabert G., "An Evaluation of Stresses and Deflection of Spur Gear Teeth Under Strain," ASME 72-PTG-27, October 1972.

[4] Colbourne J.R., "The Kinematics of Crossed Helical Gears," Journal of Mechanical Design, vol. 104, January 1982, pp. 83-89.

[5] Colbourne J.R., "Critical Load Intensity and Load Position on Helical Gear Teeth," Proceedings of the Second World Congress on Gearing, vol. I, Paris, March 1986, pp. 179-190.

[6] Colbourne J.R., "Effect of Oblique Loading on the Fillet Stress in Helical Gears," AGMA Paper No. 86 FTM 6, October 1986.

[7] Colbourne J.R., The Geometry of Involute Gears, Springer-Verlag, New York, 1987.

[8] Dawe D.J., Matrix and Finite Element Displacement Analysis of Structures, Clarendon Press, Oxford, 1984.

[9] Dolan T.J. and Broghamer E.L., "A Photoelastic Study of Stresses in Gear Tooth Fillets," University of Illinois Engineering Experiment Station Bulletin 335, March 1942.

[10] Gould P.L., Introduction to Linear Elasticity, Springer-Verlag, New York, 1983.

[11] Howes M.A.H., editor, Source Book on Gear Design, Technology and Performance, American Society of Metals, Metals Park, Ohio, 1980.

[12] Mabie H.H. and Ocvirk F.W., Mechanisms and Dynamics of Machinery, Third Edition, John Wiley and Sons, New York, 1975.

[13] Oda S. and Shimatomi Y., "Study on Bending Fatigue Strength of Helical Gears," Bulletin of the JSME, vol. 23, no. 177, March 1980, pp. 453-460.

[14] Peterson R.E., Stress Concentration Factors, John Wiley and Sons, New York, 1974.

[15] Shotter B.A., "A New Approach to Gear Tooth Root Stresses," Journal of Engineering for Industry, February, 1974.

[16] Tong P. and Rossettos J.N., Finite-Element Method: Basic Technique and Implementation, The MIT Press, Cambridge, Massachusetts, 1977.

[17] Trbojevic M.D., "Load Distribution on Helical Gear Teeth," The Engineer, August 16, 1957, pp. 222-224.

[18] Wilcox L.E., "Finite-element Analysis Pinpoints Gear-tooth Stresses," Machine Design, February 23, 1978, pp. 88-92.

Appendix A: Additional Information on Figures

There are several figures in this study which show graphs of various functions pertaining to gear teeth. For the interested reader, more detailed information on some of these graphs is given below. Unless otherwise indicated, the following statements summarize the settings used to generate and load the gear teeth.

- The normal module of the rack cutter is set to 10.
- The addendum of the cutter is set to 12.5.
- The tip round of the cutter has a radius of 3.
- The normal pressure angle of the cutter is 20°.
- The tip circle radius of the gear blank is set so as to yield an addendum of 10 for the gear.
- The profile shift is set to zero.
- The load on the tooth is made equal to 100F. A consequence of this load and the fact that m_n is equal to 10 is that m_nF/W is equal to 0.1. The value of the dimensionless stress $\sigma_w m_n F/W$ is found by multiplying σ_w by 0.1.
- Poisson's ratio is set to 0.3.
- The gears are mounted at the standard center distance.

Figures 3.2, 3.4, and 3.6

The number of teeth on the driven gear is 40, the number of teeth on the driving gear is 80 and the helix angle at the pitch circle is 20°. The face width increases from 18.37 to 40 to 65.

Figure 3.11

Fourth degree polynomials were fitted to the curves shown on the graph in this figure as well as a curve corresponding to helix angle of 15°. The polynomials for these curves in order of increasing helix angle are as follows:

$y = 0.02309x^4 - 0.08643x^3 + 0.2290x^2 + 0.2312x + 0.6031$

$y = -0.09074x^4 + 0.1416x^3 + 0.1273x^2 + 0.1859x + 0.6360$

$y = -0.1277x^4 + 0.2322x^3 + 0.06970x^2 + 0.1621x + 0.6638$

$y = -0.09308x^4 + 0.1958x^3 + 0.06695x^2 + 0.1320x + 0.6983$

$y = -0.05608x^4 + 0.1629x^3 + 0.03595x^3 + 0.06464x + 0.7926$

where $y = \sigma_w/\sigma_T$ and $x = S/S_{max}$.

Figure 5.3.

The face width is equal to 40.

$\nu = 0.3$

$S/S_{max} = 1$

$\sigma_w = 27.675$ at both $z = -40$ and $z = 0$

$\sigma_w = 40.587$ at $z = -20$

$S/S_{max} = 0.333$

$\sigma_w = 19.860$ at both $z = -40$ and $z = 0$

$\sigma_w = 28.565$ at $z = -20$

$\nu = 0.15$

$S/S_{max} = 1$

$\sigma_w = 32.502$ at both $z = -40$ and $z = 0$

$\sigma_w = 38.169$ at $z = -20$

S/S_{max} = 0.333

σ_w = 23.508 at both z = -40 and z = 0

σ_w = 27.313 at z = -20

ν = 0

S/S_{max} = 1, σ_w = 36.77

S/S_{max} = 0.333, σ_w = 26.663

Figure 5.4

The face width is equal to 60.

S/S_{max} = 1

ν = 0

σ_w = 23.254 at z = -F

σ_w = 31.010 at z = -13.75

σ_w = 26.802 at z = 0

ν = 0.15

σ_w = 20.396 at z = -60

σ_w = 32.159 at z = -17.5

σ_w = 23.089 at z = 0

ν = 0.3

σ_w = 17.266 at z = -60

σ_w = 34.472 at z = -20

σ_w = 19.046 at z = 0

Figure 5.5

The face width is equal to 60.

$S/S_{max} = 1$

$\sigma_w = 17.266$ at $z = -60$

$\sigma_w = 34.472$ at $z = -20$

$\sigma_w = 19.046$ at $z = 0$

$S/S_{max} = 0.778$

$\sigma_w = 15.423$ at $z = -60$

$\sigma_w = 31.525$ at $z = -16.875$

$\sigma_w = 17.630$ at $z = 0$

$S/S_{max} = 0.556$

$\sigma_w = 14.059$ at $z = 60$

$\sigma_w = 29.157$ at $z = -15$

$\sigma_w = 16.425$ at $z = 0$

$S/S_{max} = 0.333$

$\sigma_w = 13.175$ at $z = -60$

$\sigma_w = 27.342$ at $z = -10.625$

$\sigma_w = 15.435$ at $z = 0$

$S/S_{max} = 0.111$

$\sigma_w = 12.250$ at $z = -60$

$\sigma_w = 26.231$ at $z = -10$

$\sigma_w = 14.802$ at $z = 0$

Appendix B: An Algorithm for the Formation of the Global Stiffness Matrix

If [k] is the stiffness matrix for an element and [K] is the global stiffness matrix, then the question to be answered is how a specific number from [k], namely k_{mn}, is moved into the global stiffness matrix. In the algorithm about to be presented the subscripts m and n indicate generalized coordinates which exist in reference to an element. The number k_{mn} is found in row m and column n of [k]. Subscripts that are capital letters refer to generalized coordinates which exist in the global system. Since both the element and global stiffness matrices are symmetric only the numbers above and including the diagonal are stored. If k_{mn} and K_{MN} are numbers stored in the element and global stiffness matrices respectively, then it follows that $m \leq n$ and $M \leq N$. If the first subscript of K is not less than or equal to the second subscript, then the order of the subscripts must be switched.

Case 1: If m and n correspond to global generalized coordinates M and N, then k_{mn} is simply added to the existing value of K_{MN}.

Case 2: If m corresponds to global coordinate M but there exists no global coordinate for n, then n must refer to a node that is either fixed or constrained. If the node is fixed, then k_{mn} will not modify the global stiffness matrix.

If the node is constrained, a constraint equation can be found that gives the displacement of n in terms of generalized coordinates belonging to the global matrix. The constraint equation will have the form $u_n = \alpha_A u_A + \alpha_B u_B + \alpha_C u_C + \ldots$; where u_n, u_A, u_B, and u_C are the displacements of generalized coordinates n, A, B, and C; and α_A, α_B, and α_C are the relevant coefficients. The global stiffness matrix is then modified in the following way: $\beta\alpha_A k_{mn}$ is added to K_{MA}, $\beta\alpha_B k_{mn}$ is added to K_{MB}, $\beta\alpha_C k_{mn}$ is added to K_{MC}, etc., where β is equal to 1 if the two subscripts of K are not equal and β is equal to 2 if the subscripts are equal.

Case 3: If m = n and there exists no global coordinate corresponding to m, then $u_m = u_n = \alpha_A u_A + \alpha_B u_B + \alpha_C u_C + \ldots$. The number k_{mn} affects [K] in the following way: $\alpha_A \alpha_A k_{mn}$ is added to K_{AA}, $\alpha_A \alpha_B k_{mn}$ is added to K_{AB}, $\alpha_A \alpha_C k_{mn}$ is added to K_{AC}, $\alpha_B \alpha_B k_{mn}$ is added to K_{BB}, etc., until all combinations of A, B, C,. . . taken two at a time are used.

Case 4: If m does not equal n and neither m nor n corresponds to a generalized coordinate in the global system then two constraint equations are relevant, $u_m = \alpha_A u_A + \alpha_B u_B + \alpha_C u_C + \ldots$ and $u_n = \theta_R u_R + \theta_S u_S + \theta_T u_T + \ldots$. The number k_{mn} affects [K] in the following way: $\beta\alpha_A \theta_R k_{mn}$ is added to K_{AR}, $\beta\alpha_A \theta_S k_{mn}$ is added to K_{AS}, etc., for all combinations of the coefficients from

the first equations with the coefficients of the second equation. The value of β is 1 if the subscripts of K are unequal and β is 2 if the subscripts of K are equal.